GRS

Radionuclide transport and retention in natural rock formations

Heselbach site

**Gesellschaft für Anlagen-
und Reaktorsicherheit
(GRS) mbH**

Radionuclide transport and retention in natural rock formations

Heselbach site

Dagmar Schönwiese
Ulrich Noseck
Thomas Brasser

September 2006

Acknowledgments

Type and extent of the results from investigations at Heselbach site which are compiled in this report have only been enabled by close co-operation with the following partners (in alphabetical order of institution). Several contributions of these partners are included in the report.

Destinct details of investigation results (e.g. profiles of boreholes, compilation of results from XRD-measurements and chemical analyses) are available on request from the authors (ulrich.noseck@grs.de, thomas.brasser@grs.de)

Kazimierz Rozanski, Marek Dulinski
AGH - University of Technology
Faculty of Physics and Nuclear Techniques
al. Mickiewicza 30
30-059 Kraków, Polen
eMail: rozanski@novell.ftj.agh.edu.pl / dulinski@novell.ftj.agh.edu.pl

Johannes Fachinger
Forschungszentrum Jülich - ISR
52425 Jülich
eMail: j.fachinger@fz.juelich.de

Melissa Denecke, Horst Geckeis, Kathy Dardenne
Forschungszentrum Karlsruhe
Institut für Nukleare Entsorgung (INE)
76021 Karlsruhe
eMail: denecke@ine.fzk.de / geckeis@ine.fzk.de / dardenne@ine.fzk.de

Walter Pohl, Dieter Zachmann, Klaus-Peter. Schleicher
Technische Universität Braunschweig
Institut für Umweltgeologie
Pockelsstraße 3
38106 Braunschweig
eMail: walter.pohl@tu-bs.de / d.zachmann@tu-bs.de / k-p.schleicher@tu-bs.de

Peter Hardi
Technische Universität Braunschweig
Institut für Baustoffe, Massivbau und Brandschutz (iBMB)
Hopfengarten 20
38102 Braunschweig
eMail: p.hardi@tu-bs.de

Juhani Suksi
University Helsinki
Department of Chemistry
A. I. Virtasenaukio 1
00014 Helsinki
eMail: juhani.suksi@helsinki.fi

Janusz Janeczek
Uniwersytet Śląskii
Bankowa 12
40-007 Katowice, Polen
eMail: janeczek@us.edu.pl

Contents

1   Introduction

Radioactive wastes pose a significant hazard potential to nature and man and thus require a long-term safe disposal. In the Federal Republic of Germany, the concept of radioactive waste disposal in repositories in different deep geological formations is being pursued.

For the assessment of a potential repository site, the future behaviour of relevant geological formations is simulated by means of long-term safety models. These models are based on process assumptions which are to be verified specifically. Natural analogues are a suitable instrument for it. According to the definition of the German "Natural Analogue Expert Group", these are naturally occurring systems where physical and chemical processes take or took place over geological time scales as they are to be expected in repository systems or their subsystems, near field, far field, biosphere.

The identification and research of long-term processes in radionuclide-containing rock layers provides a useful supplement to short-term laboratory experiments. Conclusions on the leaching and migration behaviour of uranium in natural systems enhance the understanding of the behaviour of long-lived radionuclides and may also provide quantitative informations on the main processes occurring.

Main objective of the current project has been to investigate a natural occurring uranium enrichment in Tertiary sediments near Heselbach village (Upper Palatinate, Bavaria) - in co-operation with the Institute of Environmental Geology (IUG) of the Technical University of Braunschweig. A particular aim of the investigations was to assess the location with regard to its potential suitability as a natural analogue site. In this respect, special emphasis was placed on geological investigations. Besides drilling and evaluation of the lithologic layers, the hydrogeological situation of the location and the existing uranium phases have been subjected to a closer examination. Apart from that, radiometric analyses completed the results.

This report presents the relevant results of investigations performed at Heselbach. Since on-site experimental investigations formed an essential part of the work, these are described to the appropriate extent. Following this, model assumptions concerning possible processes of uranium enrichment at Heselbach and a 2D vertical groundwater flow model are presented.

2   Introduction to the investigation area

In the following chapter, the Heselbach investigation area in general and the array of drillings are delineated.

2.1   Geographical setting

The Heselbach investingation area is located 30 km N of Regensburg and about 6 km SE of the district town of Schwandorf bordering the former lignite opencast mining site *Wackersdorf-Nord*. It is directly located at the interstate road B85, W of the village of Heselbach (municipality of Wackersdorf) and is separated into a northern and southern section by the interstate road. At a distance of about 40 km E, the border to the Czech Republic passes.
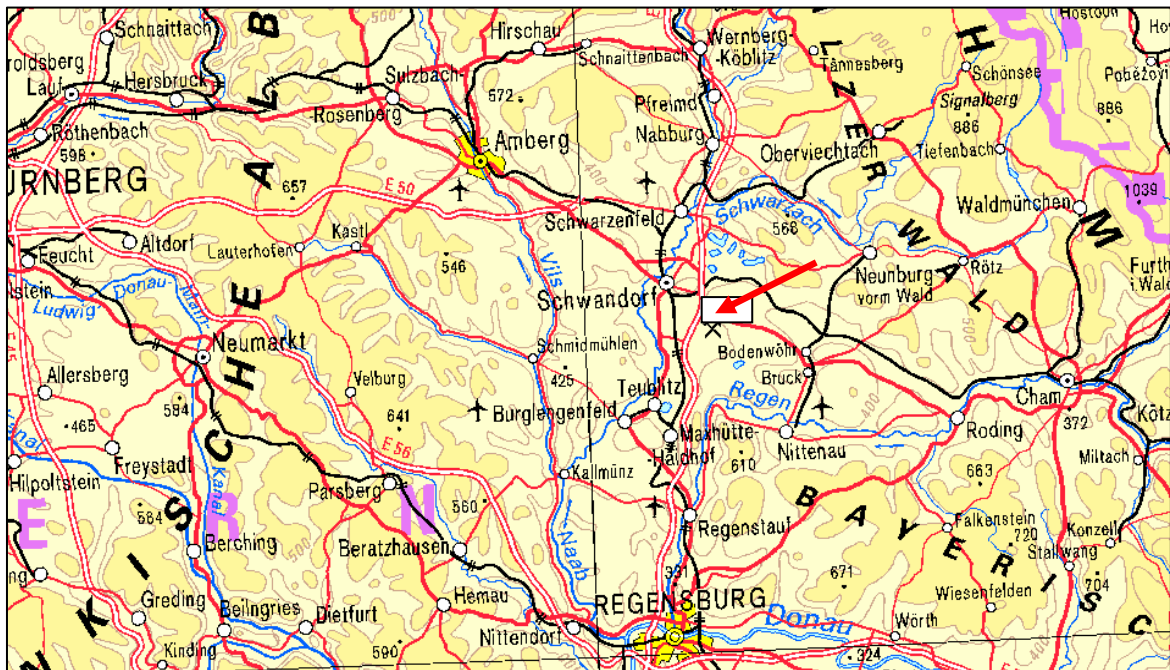
Fig. 1:   Location of Heselbach investigation area SE of Schwandorf (from TK-Bayern 1:1'000'000)

The outer limits of the investigation area are defined by the coordinates R 4513300-4514100 and H 5461800-5462300 in the Gauss-Krüger system. The area itself has a size of about 0.3 km² and the major part of the drillings was sinked along a profile line with a length of about 100 m that runs in W-E direction north of the B85.
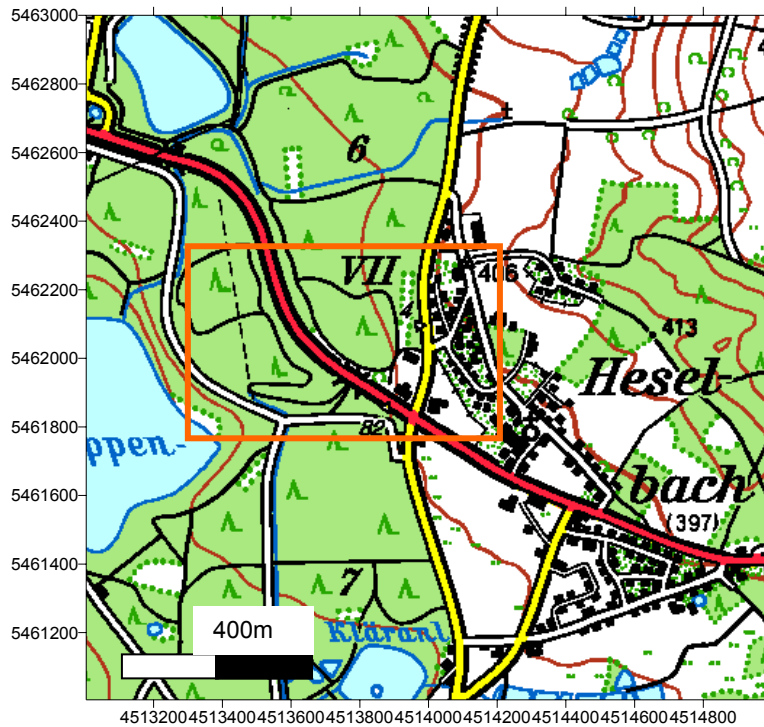
Fig. 2: Location of the investigation area W of Heselbach village (red frame); the dark red line plots the interstate road B85 (from TK-Bayern 1:50'000)

Fig. 3: Satellite view of investigation area. The village of Heselbach runs parallel to the right edge of the picture. Lake Knappensee is a result of recultivation of former open cast lignite mining [from *Google Earth*]

4

The topographic elevation within the investigation area varies between 393 m a.s.l. (Keuper sandstone elevation in the E) and 364 m a.s.l. in the down stream area close to lake *Knappensee*.

About 75 % of the total surface is covered by spruce forests that were afforested in the 1970's and 1980's within the scope of surface mining recultivation measures. The remaining 25 % represent village and company grounds. The major part of the drillings is located on the property of the car dealership "*Autohaus Lohbauer*". During the project, the expansion of this company led to sealing of former woodland areas with large-scale concrete composite paving.

2.2 Geology and hydrogeology

2.2.1 Geology

The investigation area is located amidst the Bodenwöhr basin, a half-rift structure filled with thick sediments, sharply limited in NE by the Pfahl fault zone. Along the Pfahl fault the crystalline basement (Bayerischer- und Oberpfälzer Wald – *Bavarian and Upper Palatinate forest*) is overthrusted to the foreland. There are no fault margins to the S so that the Mesozoic sediments of the Bodenwöhr basin rise constantly with 2°- 5° towards the town of Regensburg (Fig. 4).
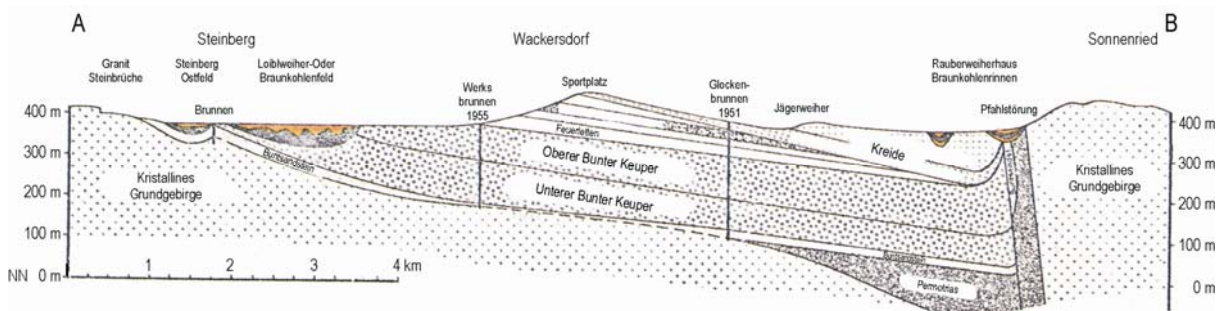
Fig. 4:   Geological cross section of the Bodenwöhr basin /KOR 94/

2.2.1.1 Geological evolution of the overburden

During the Permian period, pullapart basins were formed in the region of today's Bodenwöhr basin due to tectonic activities along the Pfahl fault zone. Today, the

sedimentary fills of these basins are found only locally and to a limited degree due to the following erosion. While the Trias was particularly characterised by large terrestrial Keuper fills with thickness up to 200 m, marine sediments were deposited for the first time in the Lias. At the beginning, these were wadden sands near the coast which, towards the end of Lias, altered to black clays and had their largest extension up to the Bohemian Massif in the Malm epoch. Due to the tilted block uplift of the Eastern Bavarian basement S of the Bodenwöhr basin during the Lower Cretaceous (Table 1), the sediments eroded continuously and the crystalline basement was uncovered.

Table 1: Overview of the geological development of the Bodenwöhr basin

Period My		Epoch	Facies	Lithology	Climate	Tectonic activity
Quater-nary 0-2.5		Holocene	erosion of younger Tertiary sands	mud	alternation of glacial and interglacial	
		Pleistocene		loam, gravel		
Tertiary 65-2.5	Neo-gene	Pliocene		sands		2nd uplift of the whole area
		Miocene		lignite		formation of the Ur-Naab canyon
	Palaeo-gene	Oligocene				main movement of the Pfahl
		Eocene				
		Paleocene				
Cre-taceous 146-65	Upper	Coniacian	erosion	hiatus		1st uplift of the whole area
		Turonian	continental	pebble, sandy-gravelly		depression of Bodenwöhr basin
		Cenomanian	marine			transgression beyond Pfahl fault
	Lower		erosion, karstification	hiatus	tropical	lifting of Eastern Bavarian basement
Jurassic 208-146	Upper	Malm	full marine	limestone, dolomite		
	Middle	Dogger	full marine	clayey marl, marine fine sand		
	Lower	Lias	Lias fullmarine	clayey marl		
Triassic 235-208	Upper	Keuper	continental limnic	Medium feldspar-rich, partly fine-grained sandstone	aride; semi-aride	

After a depression phase in the Upper Cenomanian, marine deposition conditions occurred again. The Cretaceous sea transgressed to the north beyond the Pfahl fault. At the beginning of the Upper Turonian, submarine depression took place and the

Bodenwöhr half-graben was filled. The younger Cretaceous deposits have been eroded by the strong uplifts in the older Tertiary so that a stratigraphic gap is characteristic today for this period. Also in the Tertiary (Paleogene) the main movement of the Pfahl and the associated thrusting affected the foreland. The uplift of the total area beyond the Pfahl led to uncovering of the crystalline. At the same time, a depression of the erosion basis within the Tertiary Molasse basin enabled a fast-regressing depression of the Ur-Naab basin system /TIL 54/. The main valley was filled with sands, but in the silted branches, moor-like swamps were formed which resulted later in lignite seams. Towards the end of Tertiary, sandy silts covered the basin filling before these, in parts, eroded again during the Quaternary. Today, covering takes place partly by debris and mud of the basement and partly by overlying Tertiary remains and siliceous remains of the Cretaceous /MEY 93/.

2.2.2   Climatic conditions

In general, cold winters and hot summers dominate in the Bodenwöhr basin. Climate data of the region show mean air temperatures of -2° to -3°C for January and +16° to +17°C for July. Data from Bavarian State Office for Water Management, LfW (annual values 1931-1960) demonstrate a mean annual precipitation of 757 mm for the area of the topographical map TK 6639 Wackersdorf (thereof 35.5 % during summer months June to August). The mean evaporation amounts to 527 mm/y, being app. 70 % of precipitation. This results in a mean discharge ($A_o + A_u$) of 230 mm/y.

2.2.3   Hydrogeology

The lithology of the Mesozoic sediments within the Bodenwöhr basin varies extremely and groundwater is bound to defined groundwater storeys. Between Cretaceous groundwaters and groundwaters from the Triassic a clear hydraulic separation exists. In the investigation area, the sandstone layers of the Burgsandstein (Keuper) represent an aquifer relevant for water supply (see Fig. 6).

Groundwater from investigation area flows towards the main receiving stream (Naab river in the west) with a gradient of about 3.5 %. In direct vicinity to the investigation area two lakes formed as a result of the recultivation measures in the worked out mining area: *Knappensee* and *Steinberger See*. Their water levels reach 364 m resp. 358 m a.s.l. and are connected with the groundwater system of the investigation area.
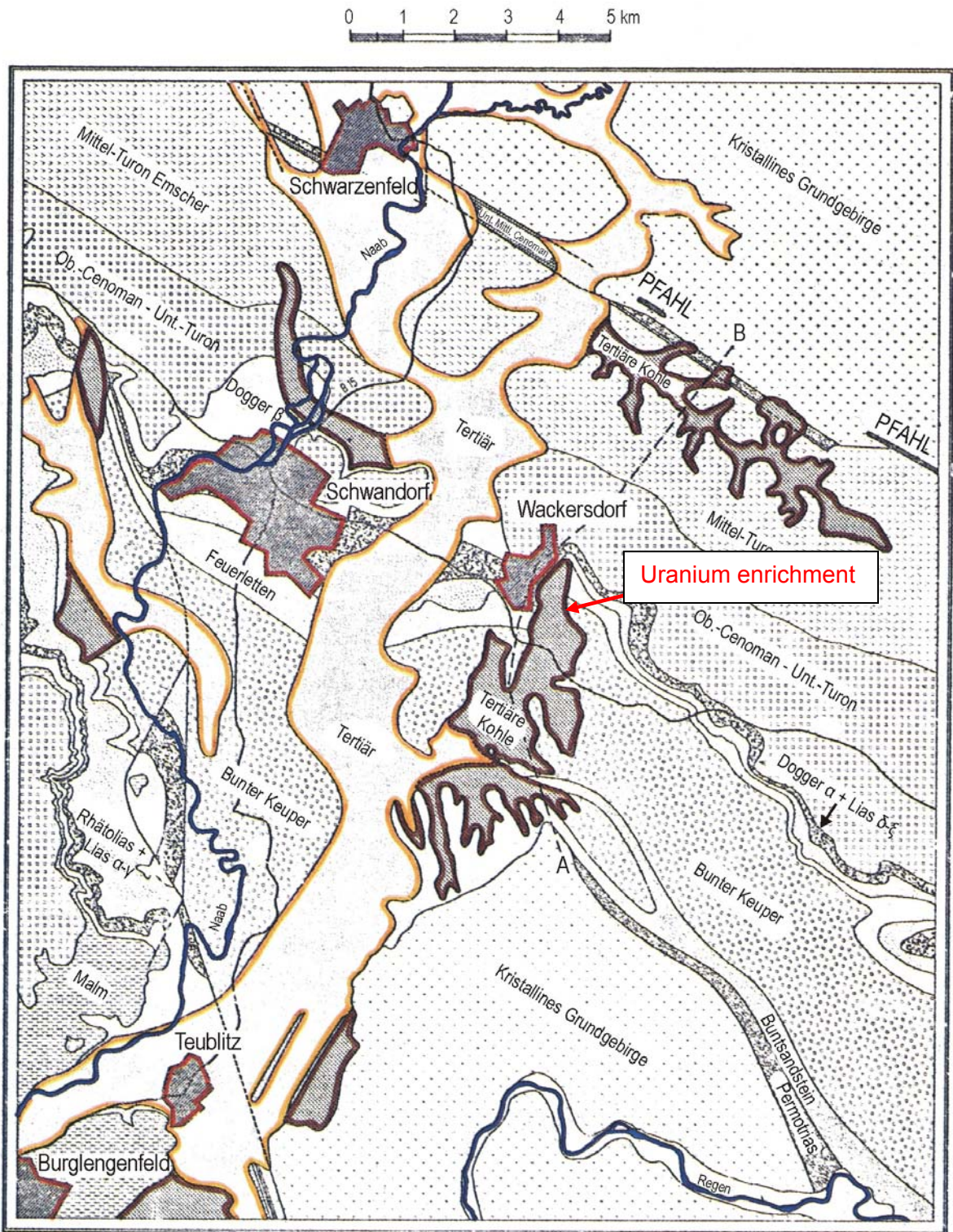
Fig. 5: Geological map of the Naab area with Miocene Naab river system /KOR 94/; location of U-enrichment is marked by the arrow

The high storage capacity of the Mesozoic sediments results in a general groundwater recharge rate of app. 4.5 l/s km^2 in the Bodenwöhr basin /MEY 93/. Within the project, a groundwater recharge rate is determined for the distinct investigation area (see below).
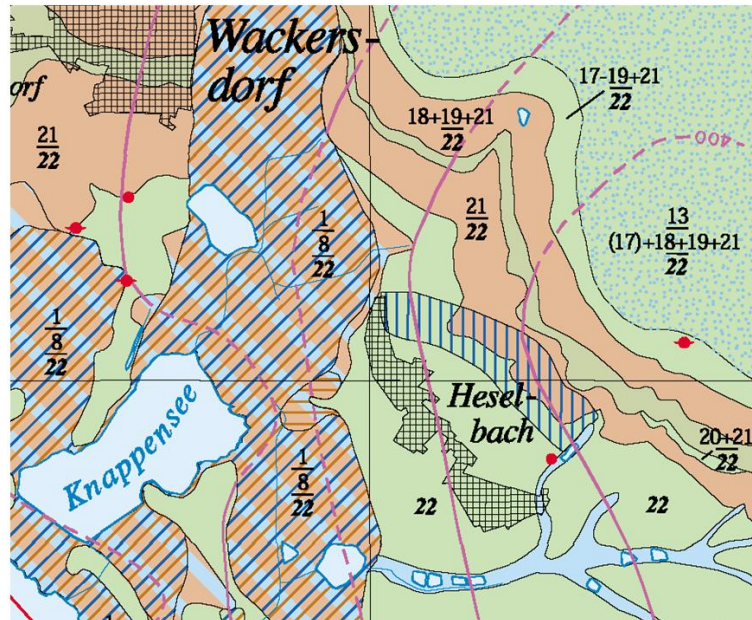
Legend: **1 = artificial accretion**: good-poor pore aquifer / **8 = Tertiary: sandy layers** = good, clayey-coaly layers = very poor pore aquifer / **13 = Cretaceous**: +/- good pore and joint aquifer / **17 = Jurassic (Dogger)**: intermittent joint aquifer / **18 = Jurassic (Opalinus clay)**: mostly impermeable / **19 = Jurassic (Lias)**: moderate-poor joint aquifer / **21 = Triassic** (**Keuper, clay and clayey sandstone**): mostly impermeable / **22 = Triassic (Keuper sandstone)**: good-moderate joint aquifer

Fig. 6: Cut-out of hydrogeological map of Wackersdorf-Heselbach area (from: Hydrogeological map, scale 1:50'000, sheet L6738 Schwandorf)

2.2.4 Stratigraphy

2.2.4.1 Keuper

In the surroundings of Wackersdorf, Keuper sediments have been drilled with a thickness of up to 175 m (research drilling K1). These are represented mainly by medium- to coarse-grained arkoses and sandstones. The Burgsandstein outcropping in the investigation area is particularly characterised by interbedded red/red-brown clay deposits.

2.2.4.2 Tertiary

At the beginning of the Palaeogene, a humid and warm climate has been prevailing together with extensive erosion. Starting with Lower Miocene, a sharp linear incision of the Ur-Naab basin system took place. Its basis near Schwandorf was about 100 - 150 m below today's Naab altitude /TIL 56/.

Fig. 7:   Drilling HB08-02: Cover (0 - 2.5 m); Burgsandstein below 2.5 m

Due to epeirogenic movements, the strong erosion activity declined with the beginning of the Middle Miocene and the uncovered valley system became a deposition area. According to the hydrographic/morphological situation, sands, clays ore biomasses deposited. The formation of lignite and clay layers ended with the second uplift of the foothills of the Bavarian Forest at the Danube and Keilberg rim fault zone. Beginning erosion removed parts of the soft humite layers again using the old discharge network. Isolated side valleys generally remained unaffected. An Upper Miocene depression of the region led to filling of the basin with sands, silts and clays of the so-called 'Hangendtertiär' (overlying Tertiary).

2.2.4.2.1 The Wackersdorf lignite

The Wackersdorf lignite seams were formed at the time of the Neogene in the Upper Miocene (18 - 20 My). The Ur-Naab, running from N to S, was at that time a flow system which had numerous branches. Within these shallow, trough-shaped basins marshy conditions with exuberant vegetation prevailed. In the Wackersdorf side bay, the most important lignite deposits of the whole Oberpfalz region occured. Alltogether

two seams, the lower and upper seam, are separated by a thick interbedded clay ('Tonzwischenmittel') /ZIE 61/. While the lower seam has a thickness of up to 15 m, the upper seam reaches thicknesses between 15 and 23 m. In the North field area, the Tertiary basin had a relatively small Tertiary thickness with a maximum of 40 m. The Tertiary sediments are separated from the underlying Keuper by an underlying green/gray, partly sandy clay layer. Facially, interbeds and underlying clay are almost identical. Therefore, differentiation is hardly possible.

Table 2:   Typical analysis from main interbedded clay sediment /MEY 93/

	Water content	Loss	SiO_2	Al_2O_3	Fe_2O_3	CaO	MgO	SO_3	Na_2O $+K_2O$
wt. %	28.00	13.59	56.88	34.90	3.41	0.28	1.28	0.59	2.66

The actual investigation area is located at the eastern margin of the Wackersdorf lignite opencast mining area. Lignite seam and underlying clay deposits crop out with small thicknesses and the transition to the Keuper sandstone is recorded.

2.2.4.3   Quaternary

In the Bodenwöhr basin, quaternary sediments were deposited in form of slope debris and mud. About 800'000 years ago, the climate cooled down to such a degree that in the following years four to five ice age cycles occurred /TIL 56/. In contrast to Northern Germany and the Alpine foreland in the south, the deposition planes in the investigation area were always glacier free but the landscape experienced a climatic overprint by molten snow masses.

2.3   Anthropogenic influences

The investigation area is located amidst a former lignite opencast mining region. It belongs to the former Schwandorf lignite district which comprised the mining areas Rauberweiher in the N and Wackersdorf SE of Schwandorf. For several decades, mining had a great influence on the whole region and changed the landscape significantly through open pit mining. In addition, during last years, the original bedding conditions at the Tertiary rim have been disturbed by new construction measures on the plot of land of Autohaus Lohbauer.

2.3.1 History of the lignite open pit mining at Wackersdorf

Important changes of the original geological and hydrogeological conditions (partly represented in Fig. 8) are the result of many decades of mining in the region. First lignite deposits were already discovered in the year 1800. Until 1845, however, only small amounts were extracted. After a 20-year interruption, mining was resumed in 1865. However, the Wackersdorf lignite did not increase in importance before foundation of the *Bayrische Braunkohle-Industrie AG (BBI)* in 1906, a successor company of the former "Bayerische Braunkohlen und Brikett-Industrie-Gewerkschaft Klardorf". In 1915, BBI decided to change from underground to open pit mining, and since 1930 the steam power plant in Dachelhofen had been supplied with Wackersdorf coal from the Bayernwerk AG. The coal mining rate continuously increased up to 1 million tons of lignite in 1945.

The economically important North field with 17 million tons of coal extended beneath the area of Alt-Wackersdorf. This led to the resettlement of the residents in the years 1951 to 1953. In the 1950's, it was possible to increase the mining rate again substantially due to the technical progress by means of bucket wheel excavators and conveyor belt systems (up to 3.9 million tons in 1960). Within the 76 years of BBI AG's mining history, a total of 189 million tons of lignite was mined. From 1974 until the cessation of lignite mining in 1982, the Wackersdorf lignite was mixed with Czech coal in the coal handling system before supply to the steam power plants Schwandorf and Frauenaurach. A major part of the open coal pits was backfilled with the coarse ash, a residual product from the power plants. In addition, electrostatic filter ashes and gypsum were deposited. Especially in the West field and in the region of Lake Knappensee, red muds from the 'Vereinigte Aluminium-Werke Schwandorf' were deposited. Today, pits that were not backfilled, form an extensive lake landscape after rise of the groundwater level which is used as a regional recreation area. The actual investigation area comprises areas of the former Central field and the northern East field. However, the major part, including uranium enrichment, is located in the former North field (Fig. 9).
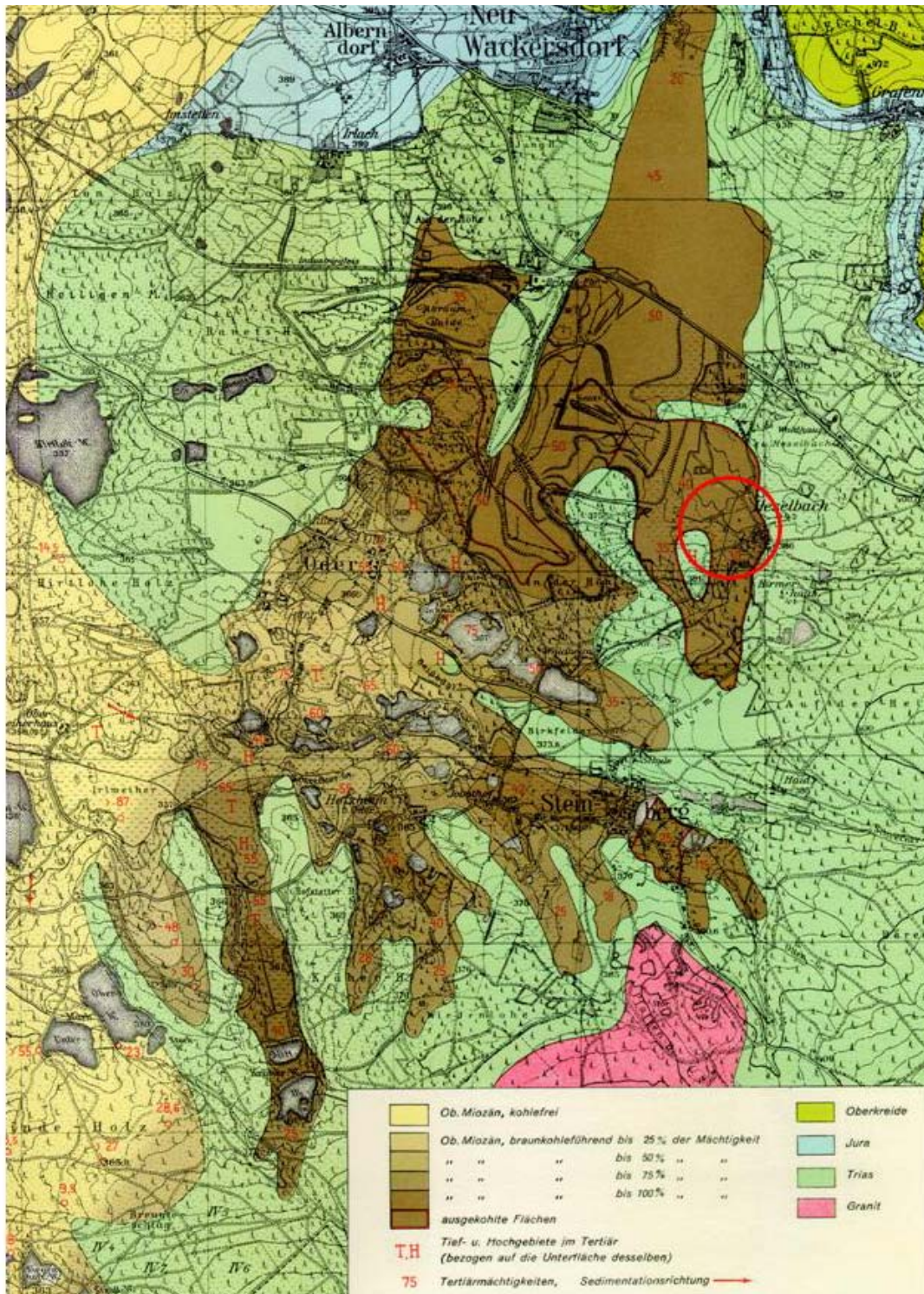
Legend: **yellow – brown** = Miocene with increasing lignite content; **olive-green** = Upper Cretaceous; **light-blue** = Jurassic; **green** = Triassic; **red** = Granite

Fig. 8: Geological situation before lignite mining. The investigation area is indicated by red circle.
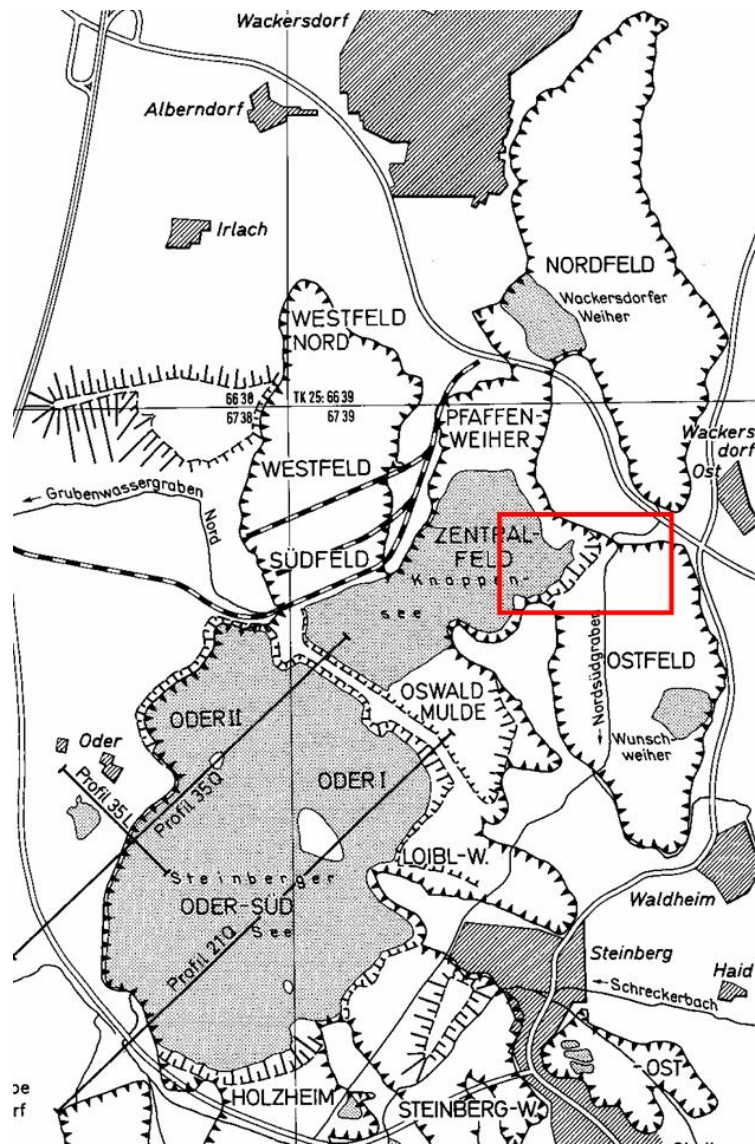
Fig. 9: Lignite fields near Wackersdorf of Bayrische Braunkohle-Industrie (BBI) after recultivation /MEY 98/ with boundary of extraction area; bolt frame = investigation area

2.3.2 History of the different mining fields within the investigation area

Surface mining in the North field

First plannings to extent lignite mining to the north field stem from 1938. In 1942, 28 exploration drills were performed to investigate seam thickness and extension.

The real exploratory work started in 1946 with the removal of the overburden and the construction of a flood protection channel (Grundwassergraben Nord) with a length of

5 km /KOR 94/. The first lignite was mined on 16th March 1948. In the same year, the municipality of Wackersdorf decided to resettle its residents to enable the extraction of another 17 million tons of lignite from the North field. So, the houses of Alt-Wackersdorf and the miners' colony Wackersdorf-Ost were torn down in the years from 1950 to 1953 and the families resettled to Neu-Wackersdorf. In the North field, the output increased rapidly and conveyer belts with a width of 800 m were used to replace the chain conveyers. In 1955, uranium enrichment was discovered in the peripheral zone of surface mining in the North field and Igelweiher whose extraction, however, was not taken into consideration due to the small amounts and the high processing costs associated with it. For the restoration of the natural receiving water conditions, the construction of the north-south channel (*Nordsüdgraben*) with a length of 3.3 km was started in 1963/1964 (Fig. 9). At this time, the North field was already worked out and backfilled in large areas. The last coal was mined in the North field in April 1969 after a mining history of 22 years. With this, the high-quality coal of the upper seam, well suited for briquette production with a maximum ash content of 8 %, was completely mined out /MEY 93/. Already in 1970, large parts of the North field were backfilled. The final backfilling was ended in October 1974.

Opencast mining in the East field

The first lignite mining in the East field started in 1928/1929 and extended to the year 1953; as of 1949, the East field was backfilled with mining debris.

Opencast mining in the Central field

From 1920 to 1932/1933, lignite had continuously been mined from the Central field. Only the upper seam was mined here because the lower seam was not suited for briquette production due to extensive argillation /KOR 94/. Large-scale backfilling of the worked out surface mines with ashes from the plants was performed since the construction of the ash washing bunker at the periphery of the Central field in 1952. A second mining phase in the Central field started in 1964 but ended already two years later.

2.3.3 Construction measures 2002 - 2003

At the plot of land of Lohbauer company, where the direct transition from Tertiary basin to Keuper sandstone formed a natural outcrop, extensive construction measures were

performed in the years 2002 and 2003. In the course of the company's expansion, the original terrain (Fig. 11) was covered with a layer of lime gravel (several decimetres in thickness) and paved with concrete-composite slabs (Fig. 12). As a consequence, more than 25 % of the investigation area's surface is now sealed and partly drained by a drainage system.

Fig. 10: Satellite images of change of use of main investigation areal directly W of Heselbach village: under construction in 2002 (top) and after completion (bottom). The total areal with lettering "Autohaus Lohbauer" has been woodland before which covered nearly all of preserved uranium deposit after opencast mining in this area. Some drillings are marked for orientation [figures imported from *Google Earth*]

Fig. 11: View from well no. B01-99 eastwards after wood clearing but before paving; in the foreground rim of Tertiary basin (flat surface), the backdrop cuesta is caused by Keuper sandstone

Fig. 12: Terrain of Autohaus Lohbauer (September 2003) after completion of pavement work, view from E to W, positions of drillings HB06-02 und HB05-02 are marked

2.4 Wells and measuring points network

2.4.1 Realisation of the 2002 and 2003 drilling campaigns

On the basis of the precedent investigations /NOS 02/, the drilling company Etschel & Meyer performed ten core drillings in January 2002, using a dry drilling method. The aim was to explore the uranium enrichment in the carboniferous sediments of the Wackersdorf lignite district, already identified in the North field, finally to acquire more detailed knowledge on uranium phases and their mobilisation and immobilisation processes within the Tertiary sediments. The drill cores were taken between the 16th and 22nd January 2002 under wintry conditions (-3° to 0°C and a snow cover of 10 cm, see Fig. 13). Three of the new wells (HB01-02; HB02-02 and HB08-02) characterise the upstream area of groundwater inflow from the Keuper sandstone, and well HB10-02 the down stream area to lake Knappensee. The major part of the wells is located in the immediate vicinity of the exploration drills already performed in 1999 and includes, with two parallel profile lines, the transition area of the outcropping Keuper sandstone in the E to the former opencast mining area in the W.

From 13th to 15th September 2003, the Institute of Environmental Geology (IUG) of the Technical University at Braunschweig drilled an additional borehole (HB11-03), also using a dry drilling method, and equipped as 4" groundwater-level measuring point. In addition to the extraction of new drill core material, the main objective of this drilling was to explore the hydrogeological regime within the Tertiary basin by means of a tracer test in more detail. Therefore, the installation of filter elements was limited to the uranium-bearing lignite layer, relevant for transport processes. In addition, the setup of a 4" tube allowed in-situ-probe descending.

Alltogether, a total of 14 groundwater measuring points was available with 112 drill core metres for analytic purposes.

Fig. 13:   Drilling of well HB02-02 in Keuper sandstone (16.01.2002)

All wells in the investigation area are shallow wells whose final depths are between 2.65 and 13 metres. The deepest well is HB10-02 in the down stream area. The basis of this well is at 363.63 m a.s.l. and thus reaches the level of the Lake Knappensee located in the immediate vicinity (364 m a.s.l.).

2.4.2   Recovery and storage of sediment cores

During the drilling campaigns, first in-situ gamma-spectrometric measurements were performed along the drill cores by means of a portable spectrometer. The measurements covered gamma radiation from daughter products of the uranium decay chain (mainly ^{214}Bi).

For the storage of sediment cores without uranium enrichment, common wooden boxes were used. The cores itself were covered with polyethene sheets to protect them against evaporation loss. The drill cores with redox-sensitive material (cores with high gamma peaks) were stored in PVC half-shells inserted into PVC cover tubes to protect the cores against dehydration and entry of oxygen (see Fig. 14).

Fig. 14: Example of drill core storage in PVC tubes (HB05-02 0 - 3 m)

2.4.3 Location, description and construction of the wells

Exploration drills of the year 1999 are notated with "B0X-99". Based on the findings achieved in 1999, ten new drillings were performed in 2002 with the notation "HBX-02". In 2003, the measurement network was supplemented by an additional well (HB11-03). The location of all wells is shown in Fig. 15. Altogether, the three following areas were covered:

- Three of the ten wells (HB01-02, HB02-02 and HB08-02) reach the Keuper sandstone and characterise the upstream area of groundwater inflow.

- Six wells (HB03-02 to HB07-02 and HB11-03) were drilled in the North field of the Tertiary basin in the actual uranium enrichment area and will be referred to as Tertiary rim wells in the following.

- Two wells of the Tertiary basin are located outside the uranium-enriched area. This is, on the one hand, well HB10-02 at Lake Knappensee. It characterises the the groundwater downstream area and will also be referred to as downstream well. On the other hand, this is well HB09-02, drilled in the area of the former East field.

Directly after extraction of the sediment cores, the wells were lined as 2" measuring points, except for HB11-03. Nearly all of the wells were equipped with filters in sections with identified gamma enrichments. As a consequence, this procedure partly led to the installation of filter elements covering different lithologic units (see Fig. 16 as an example). For HB11-03, filters were only installed in the lignite layer to enable the injection of a tracer exclusively into this sediment layer. An overview of locations, final depths and filter sections is given in Table 3 and Table 4.

Wells located on private ground (HB01-02, HB03-02 to HB06-02, HB08-02, HB11-03 and B01-99) are underfloor constructions. All other measuring points are secured with galvanised protection tubes and locked with standard SEBA top pieces.

Table 3:   Location, final depth and filter sections of the wells at the Heselbach site

Drilling	Easting	Northing	Height [m a.s.l.]	Final depth [m b.g.l.]	Filter section from to [m b.g.l.]		Area
HB01-02	4514027	5461927	392.38	9.40	2.3	8.3	upstream
HB02-02	4513911	5462061	393.48	11.00	4.3	10.3	
HB08-02	4513823	5461933	388.13	5.00	1.3	4.3	
HB03-02	4513829	5461976	387.44	6.00	2.2	5.2	uranium-bearing Tertiary rim
HB04-02	4513814	5461983	386.48	8.00	1.7	6.7	
HB05-02	4513796	5461992	385.72	11.40	3.3	8.3	
HB06-02	4513809	5461974	386.94	6.90	0.9	5.9	
HB11-03	4513811	5461974	386.95	2.65	0.9	1.9	
HB07-02	4513772	5461973	386.16	7.00	1.8	5.8	
B01-99	4513789	5461976	386.38	6.00	2	5.0	
B02-99	4513771	5461981	386.17	7.95	4	6.0	
B03-99	4513758	5461986	385.89	10.30	6	9.0	
HB09-02	4513679	5461823	385.37	8.50	1.5	6.5	East field
HB10-02	4513265	5461990	376.63	13.00	4	11.0	downstream

Table 4:   Filter layer and corresponding sediments of the wells at the Heselbach site

Well	Filter section [m b.g.l.]	Corresponding sediments
HB01-02	2.3 – 8.3	Keuper (Burgsandstein = sandstone)
HB02-02	4.3 – 10.3	
HB08-02	1.3 – 4.3	
HB03-02	2.2 – 5.2	Cover, lignite, Keuper sandstone
HB04-02	1.7 – 6.7	Lignite
HB05-02	3.3 – 8.3	Lignite
HB06-02	0.9 – 5.9	Lignite, Keuper sandstone
HB11-03	0.9 – 1.9	Lignite
HB07-02	1.8 – 5.8	Lignite, Keuper sandstone
B1-99	2.0 – 5.0	Lignite, Keuper sandstone
B2-99	4.0 – 6.0	Lignite
B3-99	6.0 – 9.0	Lignite
HB09-02	1.5 – 6.5	Lignite, sandy interlayer
HB10-02	4.0 – 11.0	Backfill, lignite
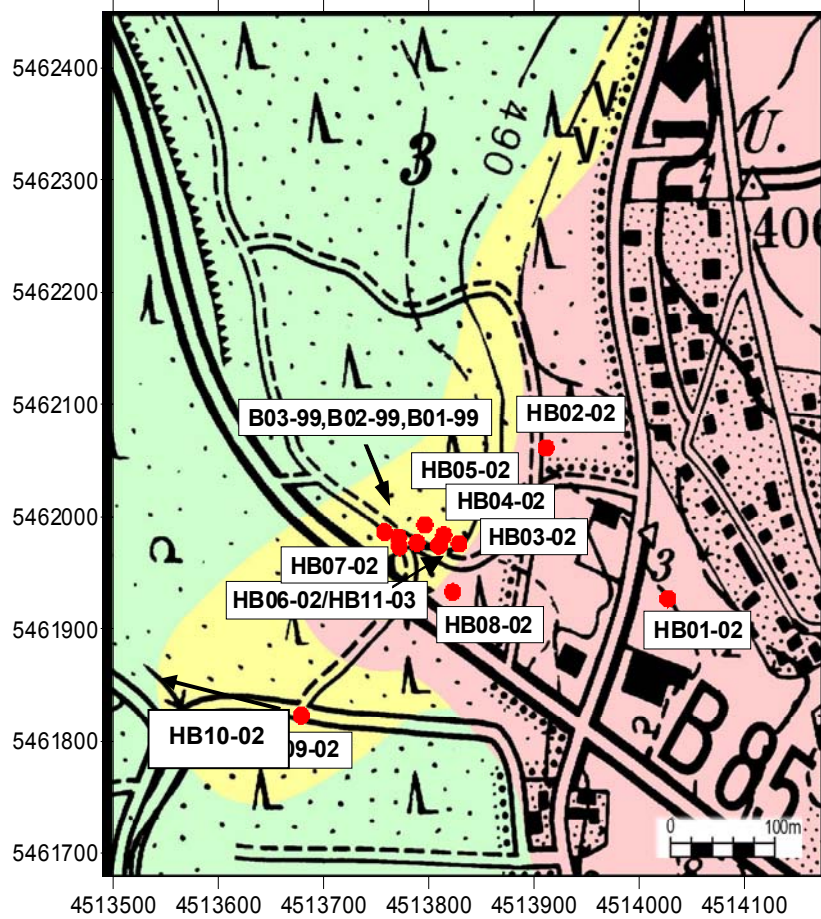
Fig. 15: Location of investigation wells at Heselbach (base: geological map 1:10'000; green = backfill; yellow = Tertiary sediments; red = Keuper)

HB10-02

m u. GOK (376,63 m NN)

Depth	Label
-0,80	Abschlußkappe Aluminium
0,00	Schutzrohr verz. Stahl
	Compaktonit
3,00	Vollrohr Kunststoff 50mm
4,00	
	Bohrlochdurchmesser 100mm
	Filterkies 1,0 - 2,0mm
	Filterrohr quer geschlitzt Kunststoff 50mm
11,00	Sumpfrohr Kunststoff 50mm
12,00	
13,00	

Projekt:	**Heselbach**		
Bohrung:	**HB10-02**		
Auftraggeber:	GRS mbH	Rechtswert:	4513266
Bohrfirma:	E & M GmbH	Hochwert:	5461990
Bearbeiter:	Dagmar Schönwiese	Ansatzhöhe:	376,63m
Datum:	08.03.2002	Endtiefe:	13,00m

IUG
INSTITUT FÜR UMWELTGEOLOGIE
TECHNISCHE UNIVERSITÄT BRAUNSCHWEIG

Fig. 16: Exemplarily sketch of drillhole lining (HB10-02)

3   Sediment characterisation

Different sedimentological on-site and laboratory investigations as well as chemical and mineralogical rock analyses were performed for the characterisation of the sediments. The sedimentological investigations primarily describe the soil physical properties and are of special importance regarding the determination of rock permeabilities and effective pore volumes. A chemical analysis of the rock provides, in addition to the main element composition, detailed information on the uranium and thorium distribution within the sediments and forms the basis for further analyses. From the mineralogical investigations, statements can be derived on the prevailing geochemical environment and the swelling capacity of the clay layers.

3.1   Sedimentological investigations

For the characterisation of the soil/rock-physical properties of the sediments, eight samples were taken from the Keuper and lignite horizon. The following parameters were investigated at the engineering geological laboratory of the Institute of Environmental Geology (IUG):

- Determination of the natural water content (DIN 18121, T.1)
- Determination of the grain size distribution (DIN 18123, T.1)

3.1.1   Water content

The natural water content w of the samples was determined by application of the drying oven method. The major part of the Keuper samples has a small water content of 9.4 to 12.6 weight %. Clayey horizons within the Keuper sandstone reach a maximum water content of 17.9 % (Fig. 17).

Clayey samples from the lignite Tertiary of Heselbach have natural water contents > 40 %. Samples HB10-02/7,42 til HB10-02/8,84 (Fig. 18) have been taken exemplary which all originate from a clayey interbedded sediment. Clays with a high content of lignite components have water contents of about 30 %. All samples with noticeable sand or silt content are characterised by lower water contents (< 20 %).
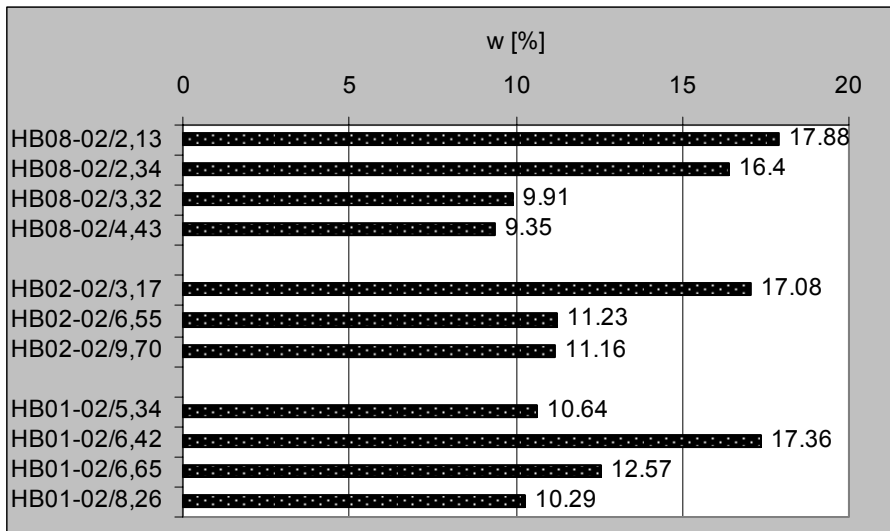
Fig. 17: Natural water content of samples from Keuper sandstone
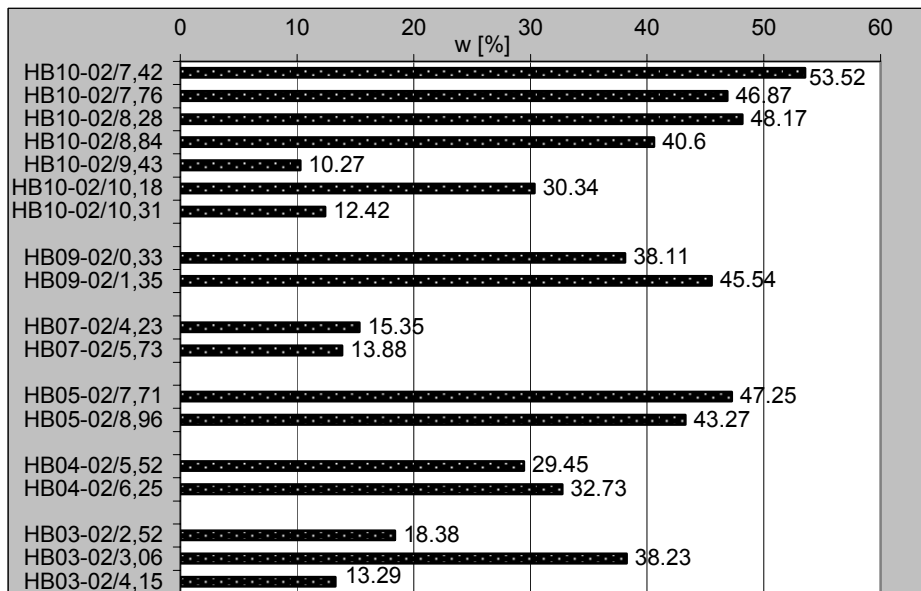
Fig. 18: Natural water content of samples from Tertiary

3.1.2   Grain size distribution

The grain size distribution of the Keuper sands was determined by means of a combined sieve and hydrometer analysis. The grain sizes of the individual fractions of the coarse-grained fraction (>0.125 mm) were determined by sieving, the fine-grained fractions (<0.125 mm) by a hydrometer analyses. Fig. 19 clearly shows (two samples of well HB08-02) that the major part of the grain fraction (82 and 77 %) presents sandy material. 8 resp. 5 % are to be assigned   to the silt fraction and 10 % to the clay

fraction. This results in inhomogeneous grain size curves (Fig. 20), showing poor sorting of the sediments.
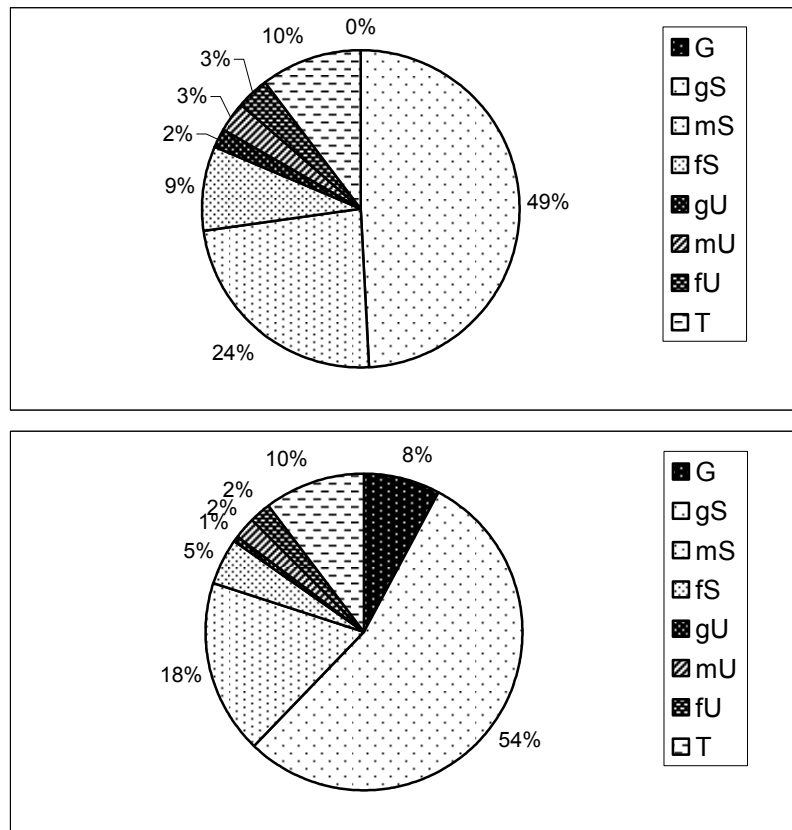
Fig. 19: Grain size distribution of samples HB08-02/2,10-2,20 (top) and HB08-02/4,40-4,45 (bottom) from Keuper sandstone

3.1.3 Hydraulic conductivity (k_f values) and effective pore volume

Important rock parameters to be considered for flow and transport processes are the hydraulic rock conductivity, given as coefficient of hydraulic conductivity (k_f-value) and the effective pore volume (n_e) of the sediments. The k_f-value was determined on-site and in the lab by means of different methods:

Determination of k_f-values on-site

- Short-term pumping test
- Slug and bail tests

Determination of k_f-values in the laboratory

- Determination of the grain size distribution (DIN 18123, T.1)
- Determination of the specific permeability (DIN 4022)

27

Korngrößenanalyse
nach DIN 18 123

Projekt: Heselbach
Datum: 19.08.2002
Bearbeiter: D.Schönwiese

Gew.-%	Ton	Schluff			Sand			Kies			Steine
		Fein-	Mittel-	Grob-	Fein-	Mittel-	Grob-	Fein-	Mittel-	Grob-	

Korndurchmesser in mm

Bezeichnung		HB01-02 ●	HB01-02 ■	HB01-02 ▲	
Kf-Wert		-	-	-	
	Ungleichf.-Zahl U		147.03	381.48	
Stratigraphie		Keuper	Keuper	Keuper	
Bohrung		HB01-02	HB01-02	HB01-02	
Entnahmetiefe		4,85-4,95m	6,59-6,72m	8,20-8,33m	

Fig. 20: Grain size distribution of samples from Keuper sandstone: drill core HB01-02

k_f-value determination by short-term pumping test

During the groundwater sampling campaign in October 2002, a short-term pumping test was performed. Water was extracted with a pump rate of $5.5 \cdot 10^{-5}$ m³/s from well HB06-02. At a pump duration of 65 minutes and a postulated aquifer thickness of 5.6 m, the evaluation yields a coefficient of hydraulic conductivity of $3.2 \cdot 10^{-6}$ m/s, applying the Theis recovery curve. Due to the fact that with this drilling not only Tertiary lignite layers were explored but also underlying sandy parts, the determined k_f-value is to be regarded as reference value for aquifers.

k_f-value determination by slug & bail tests

In wells where filter piping was completely below the groundwater level, slug & bail tests were performed. A standardised slug body with a length of 1 m was inserted into the borehole and the change of the piezometric level over time was monitored. The evolution according to the Bouwer & Rice method yielded a k_f-value of $1.54 \cdot 10^{-5}$ m/s for the Keuper sandstone. Coefficients of hydraulic conductivity in the clayey lignite horizon vary between $1.1 \cdot 10^{-6}$ and $6.8 \cdot 10^{7}$ m/s.

28

k_f-value determination by grain size analyses

Due to the high degree of asymmetry of the grain size curves of the Heselbach Keuper samples, a simple calculation of the k_f-value with Hazen's formula is not possible. For the calculation, the modified formula, developed by Beyer in 1964, was applied which considers the different inhomogeneity degrees by varying proportionality factors C. For U > 20 holds:

$$k_f = 0{,}006 \ (d_{10} \ [mm])^2 \ [m/s] \tag{1}$$

The calculated hydraulic conductivity coefficients for the Heselbach Keuper samples are given in Table 5.

Table 5: k_f-values for Keuper sandstone calculated from grain size distributions

Well	Depth [m bgl]	k_f-value (Beyer) [m/s]
HB01-02	4.85-4.95	$7.56 \cdot 10^{-07}$
HB01-02	6.59-6.72	$2.02 \cdot 10^{-06}$
HB01-02	8.20-8.33	$6.10 \cdot 10^{-08}$
HB02-02	6.50-6.60	$7.77 \cdot 10^{-07}$
HB02-02	9.65-9.75	$1.82 \cdot 10^{-06}$
HB08-02	2.10-2.20	$4.70 \cdot 10^{-07}$
HB08-02	4.40-4.45	$1.18 \cdot 10^{-07}$

For the Keuper sand of the investigation area, k_f-values between $1.8 \cdot 10^{-6}$ and $6 \cdot 10^{-8}$ m/s were calculated. The low hydraulic conductivities are assigned to the argillaceous magenta/red interbeds and the kaolinised sandstone areas (Fig. 21). The hydraulic conductivity of the weathered loose material is larger by two orders of magnitude which fulfils the function of an aquifer, as can be seen by the structure and the oxidation-induced orange/yellow discolouration.

Fig. 21: Drill core HB01-02/8,20-8,50 (left) and drill core HB02-02/9,55-9,80 (right)

k_f-value determination by specific permeability

The specific permeability was determined at the GRS geomechanical laboratory by taking drill core material from the lignite horizon.

Fig. 22: Samples used for permeability measurement. Drill core HB11-03/1,00 – 1,035

From the intact drill cores, an upright sample with a length of 39 mm and a diameter of 50 mm was extracted. Before insertion of the sediment sample into the measurement apparatus, the sample was stabilised by means of an adjusted placeholder and a jacket. After installation of a flow-through cell (Fig. 23), the sample was exposed to an external jacket pressure. The flow rate was recorded [cm^3/min] which was determined at regular intervals by weight determinations.
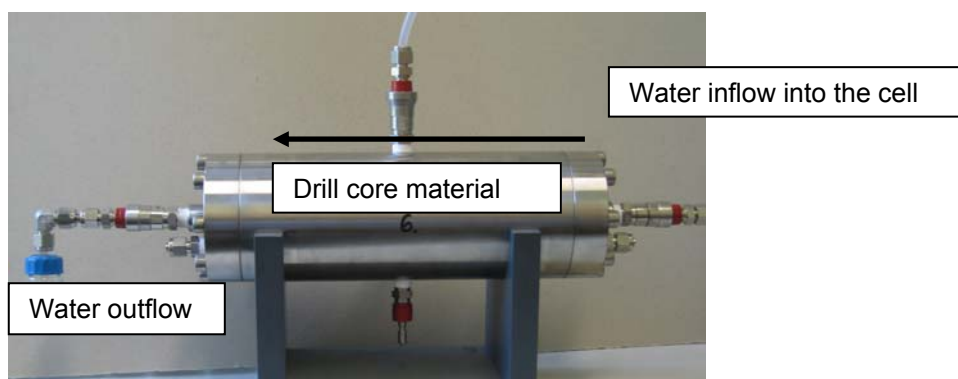
Fig. 23: Apparatus for determination of specific permeability of sediment samples

The permeability is a rock-specific constant which describes the pore properties of a rock independent of the fluid /HOE 96/. It is referred to as k and is expressed in units of Darcy [D]. Under consideration of the fluid properties (density ρ, viscosity μ, temperature) and the pore volume of the conductive layer, the actual rock permeability

can be calculated. According to /LAN 80/, the recalculation of the permeability into k_f-values [m/s] can be performed by multiplication with the factor 10^{-5}. Relevant groundwater parameters of the groundwater used (from B03-99), the permeability as well as the calculated vertical coefficients of hydraulic conductivity for the Heselbach lignite sample are summarised in Table 6.

Table 6: Groundwater parameters, permeabilities and k_f-values of the lignite sample from drilling HB11-03

Time	GW parameter	Permeability k	k_f-value
[h]	T [°C]; μ [Pa s]; ρ [g/cm^3]	[D]	[m/s]
0		$7.26 \cdot 10^{-02}$	$7.26 \cdot 10^{-07}$
30	20; $9.69 \cdot 10^{-04}$; 0.9984	$6.12 \cdot 10^{-04}$	$6.12 \cdot 10^{-09}$
75		$2.89 \cdot 10^{-04}$	$2.89 \cdot 10^{-09}$

At the beginning of the test, the sample was not water-saturated. Only after 75 h, the sediment reached complete saturation and a constant value of the vertical hydraulic conductivity of $2.89 \cdot 10^{-9}$ m/s.

The space between rock components usable for water movement is referred to as effective or usable pore volume (n_e) (Table 7). It depends on the respective grain consistence, grain shape and compactness of the sediment and decreases with increasing fine grain size due to the increasing adhesion of the water molecules /MAT 03/.

Table 7: Overview of effective pore volumes [%] in sediments /HOE 96/

Sediment	Effective pore volume n_e [%]
clay	< 5
fine sand	10-20
medium sand	12-25
coarse sand	15-30
gravelly sand	16-28
fine gravel	15-25
medium gravel	14-24

For the Keuper aquifer, a hydraulic conductivity (k_f-value) of $1.54 \cdot 10^{-5}$ m/s was determined on the basis of in-situ tests. With the hydraulic conductivity of $> 2,9 \cdot 10^{-9}$ m/s, the clay layer of the interbedded sediment serves as a barrier so that the direct uranium input from the underlying Keuper into the Tertiary basin is rather improbable.

The overlying Tertiary sediments with coefficients of hydraulic conductivity of 10^{-5} to 10^{-6} m/s, however, enable a groundwater flow. All k_f-values determined for the Heselbach sediments and the effective pore volumes estimated on the bases of these are summarised in Table 8.

Table 8: k_f-values and effective pore volumes (n_e) of Heselbach sediments [U: silt, S: sand, T: clay, Bk: lignite; f: fine, g: coarse]

Stratigraphy		Lithology	Procedure for determination of k_f value	k_f value [m/s]	n_e [%]
Tertiary	overlying Tertiary	U,fS-gS	literature (DIN 130, Part 1)	$1 \cdot 10^{-05}$- $1 \cdot 10^{-06}$	10-25
	lignite	Bk,T	on-site: slug & bail	$3.15 \cdot 10^{-06}$	5-20
	interbedded clay	T	laboratory: spec. permeability	$2.89 \cdot 10^{-09}$	<5
Keuper	sandstone	fS-gS,U	on-site: slug & bail	$1.54 \cdot 10^{-05}$	10-30

3.2 Chemical rock analyses

The selection of samples for the chemical analyses was based on the uranium distribution determined by gamma scanning. In addition to samples from horizons with positive gamma anomalies, reference samples from horizons without gamma activity were also selected for detailed chemical rock analyses. In addition, Keuper- and backfill material was also analysed. Sediment slices with a thickness of 2 to 4 cm were cut into four samples of the same size and sent to different institutes for the analyses to be performed.

3.2.1 Uranium distribution in the sediments

Gamma measurements on fresh drill core material show uranium enrichment with two clearly distinguishable peaks. The upper peak is within the lignite horizon, the lower one can be identified in the interbedded clay sediment.
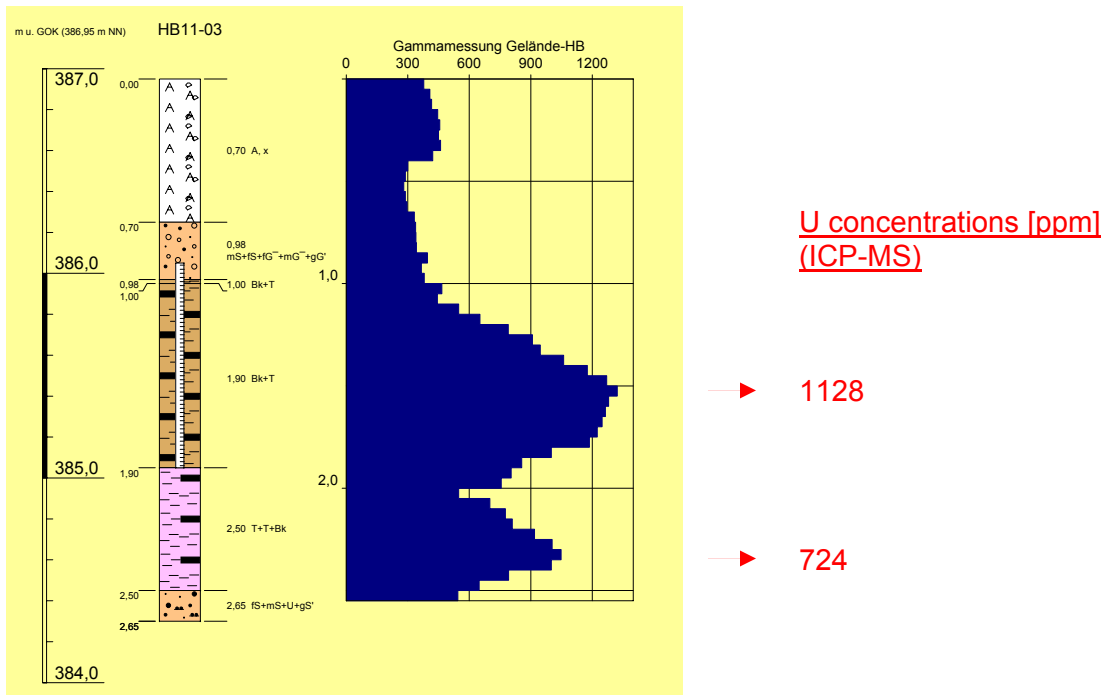
Fig. 24: Drilling HB11-03 with gamma counts (left) and measured uranium concentrations (right)

Fig. 24 documents the uranium distribution in drill core HB11-03, based on gamma scan and lab-analyses. Up to 1128 ppm in the lignite horizon and 724 ppm in the underlying clay were identified by means of ICP-MS. HB07-02 (Fig. 25), localised 30 m further towards the centre of the basin, shows a similar distribution despite the generally significantly lower uranium contents.

A possible explanation for the existing uranium distribution may be given by means of a multi-level process. Here, it is postulated that the uranium reached the lignitic layers of the Tertiary basin through advective transport from the Keuper. Subsequent diffusion processes may be responsible for a remobilisation of the uranium from the lignite horizon and movement to the underlying clay layers. For the verification of this postulation, uranium/thorium activity ratios in the underlying clay are currently determined in co-operation with the University of Helsinki.

Another possibility to explain the uranium distribution is a lithologic change of the sediment composition. This, however is not visually noticeable. An increased water movement at the bottom of the lignite layer due to the underlying clayey sediments is also imaginable. Even a low base flow within the lignite horizon may have the effect that in this area less uranium reacts with the sediment inducing locally a minor uranium

33

enrichment (and this is less enriched). In this connection, later wash-out / leaching of already deposited uranium due to increased influx would also be possible.
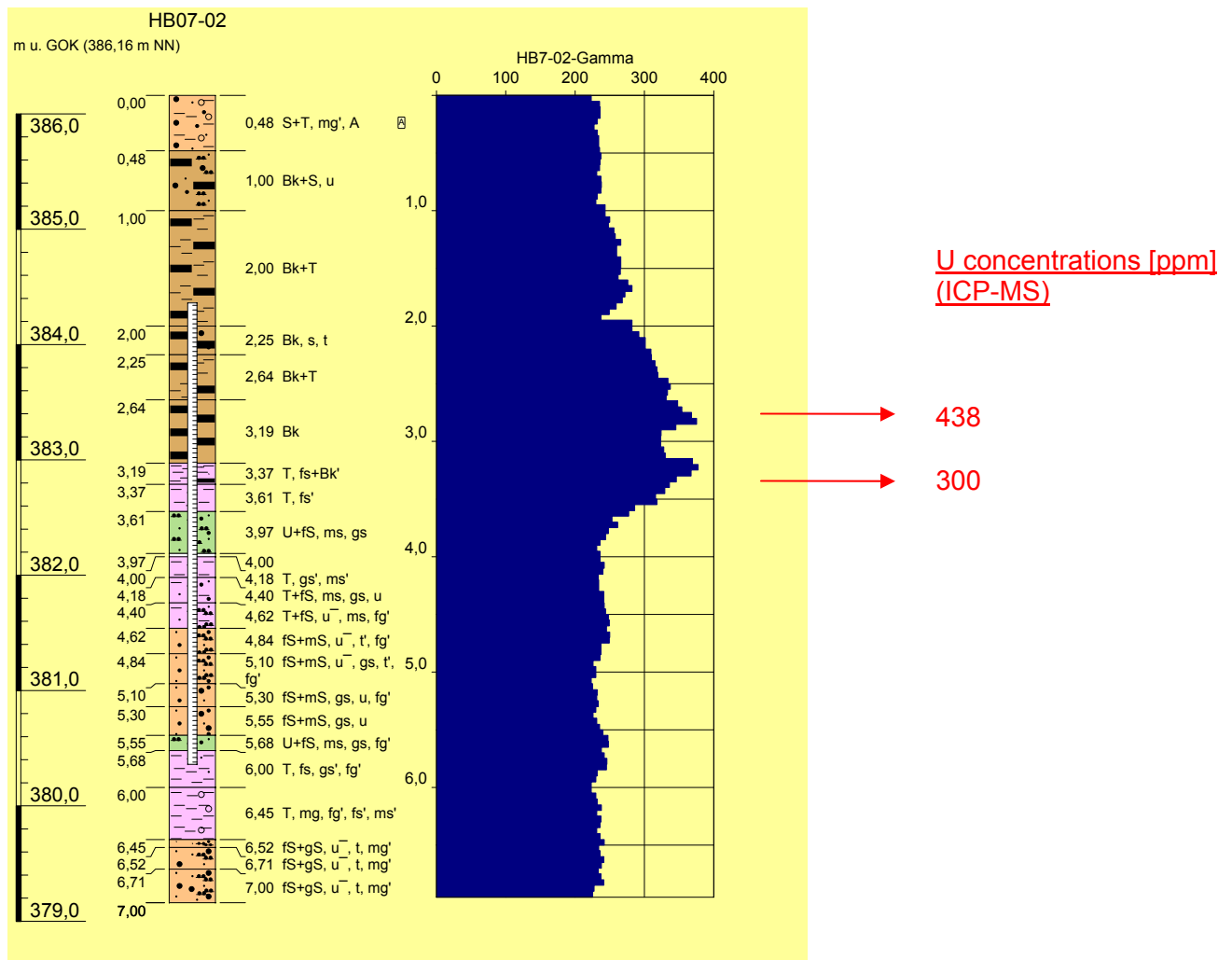
Fig. 25: Drilling HB07-02 with gamma counts (left) and uranium concentrations (right)

3.2.2 XRF analyses

The rocks were analysed by means of XRF analyses on 40 samples, enabling the comparison of the main components of different sediment layers in Heselbach.

Samples with uranium content < 20 ppm are characterised by particularly high SiO_2-contents (46 - 90 %) which originate from the Keuper sandstone and the backfill area. The Al_2O_3-content varies between 4.9 and 32.5 % and is the second abundant sediment component. An exception are two samples from the lignite horizon. In these samples, the water and gas contents dominate with 63 % and 85 % (loss).

The samples of drilling HB03-02 selected for XRF analyses show uranium contents between 200 and 400 ppm (Fig. 26). With a maximum of 8.1 % of the total content, their Fe_2O_3 contents are significantly higher than in all other samples. X-ray analyses of these samples identified the existence of pyrite and marcasite.
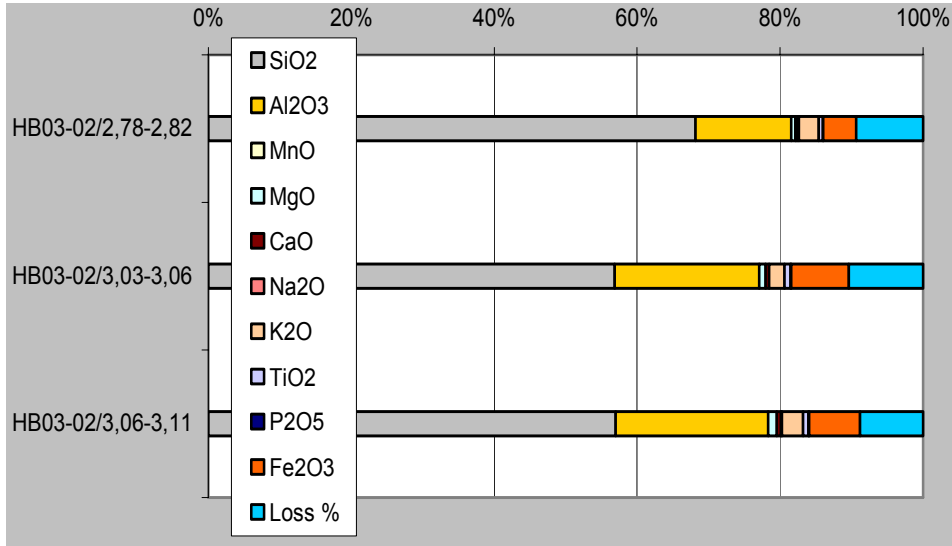
Fig. 26: XRF analyses of sediment samples from Heselbach with uranium contents between 200 and 400 ppm
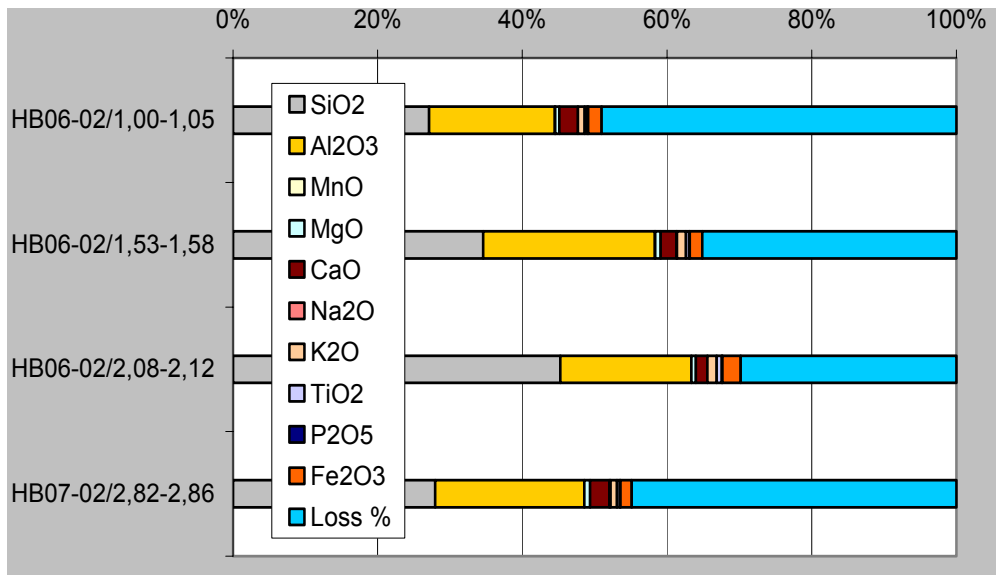
Fig. 27: XRF analyses of sediment samples from Heselbach with uranium contents > 400 ppm

The sediments with the highest uranium enrichment (> 400 ppm, Fig. 27) show high concentrations (30 - 50 %) of volatile matter. Accordingly low (< 45 %) is the SiO_2

content. The Fe_2O_3 content is also distinctively low which accounts for a maximum of 2.5 % of the total rock composition. This is a striking difference from the samples of drilling HB03-02 presented in Fig. 26.

3.2.3   ICP analyses

In addition to the determination of the main elements, the ICP analyses comprise the quantitative determination of trace elements. Correlations of selected elements are presented in the following chapter. The contents of the trace elements uranium and thorium are presented in Table 9. For the Heselbach sediment samples, the results of the bulk rock analyses (ICP-MS) show a maximum uranium concentration of 1128 ppm. Here, the strong variations of more than 500 ppm within a sample (HB11-03/2,34-2,37) document the extreme heterogeneity of the sediments.

The contents of uranium and thorium presented in Table 9 in italics are suitable for the determination of the geogenic background concentration because they have been taken from the directly adjacent 'Burgsandstein'. The averaged background value is 2.64 ppm for uranium and 13.84 ppm for thorium. On this basis, a thorium/uranium ratio of 5.2 is calculated for the Keuper sandstone (mean value for sandstone /MEY 93/). Accordingly, the mobile uranium is slightly enriched compared to thorium. This confirms the theory that uranium from the crystalline was secondarily / intermediatly fixed in the Keuper sandstone before it was leached again and transported into the tertiary basin structure. Most conspicuous are the increased thorium contents of the samples HB05-02/0,00-0,06 and HB08-02/0,65-0,68. These are coarse-medium sand backfill material that has been shuffled and relocated during paving work in 2002, thus not representing autochthonous material. This assumption is supported by identification of allochthonous material via X-ray mineralogy. Related to the geogenic background concentration, the maximum enrichment factor calculated for uranium is 427.5 in drilling HB11-03 (see Table 10). High enrichments (290.5; 279.5) were also identified in drillings HB06-02 and HB03-02. The uranium content varies in the cm range (example: 3.02 to 3.11 m, Fig. 28) and therefore has to be attributed to small-scale Eh/pH changes within the rock layers or to local presence of fixing material. Since the uranium was not only enriched at the margins but also inside this clay layer, small-scale microstructure must admit the water and/or gas transport through this clay package. In addition to the groundwater flow-through, diffusion processes may also be possible and lead to uranium enrichment.

Table 9: Uranium and thorium content in bulk rock samples from Heselbach. All depths in [m bgl]

Drilling	HB01-02			HB02-02		HB03-03
Depth [m]	2.46-2.52	5.38-5.43	8.72-8.78	3.38-3.44	8.97-9.00	2.77-2.78
U [ppm]	*3.4*	*3.0*	*2.2*	*4.2*	*1.4*	375.0
Th [ppm]	*20.3*	*20.2*	*15.9*	*17.0*	*6.4*	12.9
Drilling	HB03-02					
Depth [m]	2.78-2.82	2.96-2.99	3.02-3.03	3.03-3.06	3.06-3.11	5.36-5.41
U [ppm]	367.6	166.3	738.0	324.2	345.1	17.9
Th [ppm]	10.4	13.2	9.4	16.8	10.0	6.5
Drilling	HB04-02				HB05-02	
Depth [m]	0.27-0.31	2.38-2.44	7.48-7.52	7.61-7.66	0.00-0.06	6.42-6.46
U [ppm]	2.4	8.4	23.1	20.7	4.1	58.8
Th [ppm]	23.4	4.5	11.4	6.2	88.0	15.0
Drilling	HB05-02		HB06-02			
Depth [m]	8.40-8.45	10.47-10.51	1.00-1.05	1.05-1.055	1.53-1.58	2.07-2.08
U [ppm]	6.0	8.8	722.0	767.0	458.3	429.0
Th [ppm]	13.2	8.8	7.7	4.5	7.2	12.3
Drilling	HB06-02				HB07-02	
Depth [m]	2.08-2.12	2.80-2.81	2.81-2.85	6.46-6.50	1.68-1.72	2.77-2.78
U [ppm]	446.3	45.2	54.0	5.1	72.6	375.0
Th [ppm]	23.9	9.9	12.3	14.0	10.2	10.6
Drilling	HB07-02					
Depth [m]	2.82-2.86	3.00-3.02	3.22-3.24	3.24-3.28	3.24-3.28	5.06-5.10
U [ppm]	437.7	394.0	300.0	95.1	16.9	4.3
Th [ppm]	7.5	11.9	24.9	17.5	11.1	6.0
Drilling	HB07-02		HB08-02			HB09-02
Depth [m]	5.94-5.98	6.81-6.85	0.65-0.68	2.36-2.40	3.53-3.57	1.10-1.14
U [ppm]	4.7	3.3	3.1	2.5	1.6	3.9
Th [ppm]	8.7	4.6	102.8	11.0	6.1	10.1
Drilling	HB09-02	HB10-02				
Depth [m]	2.46-2.51	3.34-3.38	6.02-6.06	8.01-8.06	11.89-11.93	12.24-12.28
U [ppm]	3.0	4.1	3.2	4.7	3.2	1.7
Th [ppm]	12.6	10.3	2.4	11.2	18.1	9.8
Drilling	HB11-03					
Depth [m]	1.51-1.54	2.34-2.37 (bright)	2.34-2.37 (brown)	2.34-2.37 (black)		
U [ppm]	1127.8	559.7	501.3	1111.4		
Th [ppm]	9.6	14.9	21.7	37.6		

The determination of correlation coefficients reveals the common geochemical properties of different elements. For a correlation analysis, Heselbach samples were differentiated according to their lithology and their location. The samples were divided intro groups of sandy samples, pure clay samples and lignite-containing samples. In

addition, selected samples from the Tertiary rim are analysed separately. The correlation coefficients listed in Table 11 show for sandy samples a clear correlation of uranium with phosphor (0.83). This confirms the assumption that apatite-bounded uranium could exist in the hinterland which, however, is contradicted by the negative correlation coefficient for calcium (-0.06). In the clay and lignite samples, uranium correlates best with the elements magnesium, aluminium and calcium, and in the pure clay samples also with manganese.

Table 10: Maximum enrichment factors for uranium and thorium in sediment samples from Heselbach related to regional background values

Drilling	Stratigraphy	Enrichment factor U	Enrichment factor Th
HB01-02	Keuper	1.3	1.5
HB02-02		1.6	1.2
HB08-02		1.2	7.4
HB03-02	Tertiary	279.5	1.3
HB04-02		8.7	1.7
HB05-02		22.3	6.3
HB06-02		290.5	1.7
HB07-02		165.8	1.3
HB09-02		1.6	0.9
HB10-02		1.8	1.3
HB11-03		427.5	0.7

Fig. 28: HB03-02/3.00-3.20 core section with measured uranium contents [ppm]

The trace element analyses showed for nearly all of the trace elements a positive correlation with uranium (Fig. 29). Uranium and chromium correlate in the lignite

samples (0.74) and clay samples (0.44). In sandstone, however, no correlation (0.02) was identified. With a peak value of 183.7 ppm in sample HB06-02/2.06, an increased enrichment was identified for chromium in the lignite-containing sediment.

Table 11: Correlation coefficients of major elements with TOC and uranium

	Sandy samples		Clay samples		Lignite samples	
	TOC	U	TOC	U	TOC	U
Al	-0.33	-0.30	0.04	0.24	-0.60	0.56
Ca	0.12	-0.06	-0.05	0.38	0.39	0.46
Na	0.07	0.41	-0.01	0.004	-0.34	0.19
K	-0.47	-0.36	-0.17	-0.05	-0.96	0.04
Mg	-0.17	-0.20	-0.20	0.68	-0.39	0.62
Ti	-0.09	-0.13	0.02	0.32	-0.78	0.30
Fe$_{total}$	-0.13	0.59	-0.23	0.36	-0.45	-0.05
Fe(II)	-	-	0.88	0.65	0.13	0.44
Mn	-0.17	0.05	-0.25	0.65	-0.47	0.01
P	-0.09	0.83	-0.22	0.10	0.01	0.37

Further to the bulk rock analyses, the fractions of divalent iron (Fe(II)) and sulphide were determined on 12 samples. For the determination of Fe(II), the sediment was subjected to hydrofluoric digestion in a nitrogen environment with the addition of H_2SO_4 and then absorbed in saturated boric acid. Fe(II) was converted into the bipyridine complex and measured photometrically. The total iron fraction was determined by means of XFR analyses. According to the different analysis methods applied, there are minor deviations so that the calculations for some samples yield Fe(II) fractions > 100 %. All results are presented in Table 12.
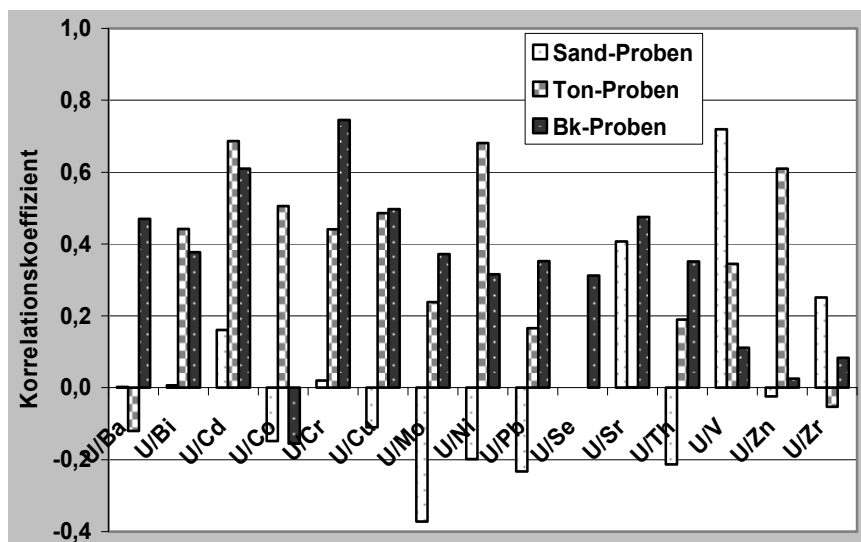
Fig. 29: Correlation coefficients of uranium with trace elements, differentiated for sand-, clay- and lignite- (Bk) samples

Table 12: Iron and uranium content of selected sediment samples

Drilling	Depth [m b.g.l.]	Total Fe [wt. %]	Fe (II) [wt. %]	Fe (II) fraction [%] of total Fe	U [ppm]
HB02-02	3.38-3.44	1.50	0.14	9.3	4.2
HB03-02	2.78-2.82	3.22	2.23	69.4	368.0
	3.03-3.06	5.63	1.15	20.3	324.0
	3.06-3.11	4.97	1.23	24.8	345.0
HB04-02	7.48-7.52	4.24	0.23	5.5	23.1
HB05-02	6.42-6.46	5.68	1.25	22.0	58.8
	8.40-8.45	2.55	0.65	25.5	6.0
HB06-02	2.08-2.12	1.76	1.79	101.8	446.0
	2.81-2.85	4.59	0.20	4.4	54.0
HB07-02	2.82-2.86	1.08	1.09	101.0	438.0
	3.24-3.26	1.33	0.91	68.4	95.1
	3.26-3.28	0.99	0.23	22.9	16.9
HB10-02	6.02-6.06	1.19	1.27	106. 6	3.2
	8.01-8.06	1.89	1.62	86.0	4.7

Table 12 shows the correlation between iron phases in reduced form with uranium. Drillings located within the Tertiary rim, where iron is reduced to 100 % in some segments (HB06-02 und HB07-02), have very high uranium concentrations. However, the reducing environment is not the only criterion for uranium accumulation. Uranium is also enriched in sediments with Fe(II) fractions of only 20 to 70 % (HB03-02). Altogether, the Tertiary rim samples have a relatively high U/Fe(II) correlation factor, i. e. 0.74 as a mean (Table 13).

Possible processes to explain this correlation are, on the one hand, a reduction of U(VI) to U(IV) and subsequent co-precipitation on FeS_2 minerals (pyrite, marcasite) and, on the other hand, sorption processes on mineral grains. However, the correlation analysis of uranium with sulphur shows no positive trend, independent of the oxidation state of the sulphur (Table 13). A co-precipitation of uranium with FeS_2 minerals can therefore be excluded. Uranium and Fe(II) are both present, but do not form a joint phase. This result is confirmed by sequential extraction and spectroscopic investigations.

Table 13 also shows the negative correlation of uranium with Fe(III). As a consequence, a joint uranium/Fe(III) phase seems not to be the cause for a uranium enrichment process at Heselbach. A detailed evaluation of the redox sensitive elements iron and sulphur reveals the different distribution of the oxidation states of these two elements. While in the downstream area iron is reduced to nearly 100 %,

only 5 to 25 % of the reduced form remained immediately at the rim, apart from one exception. At the rim, oxidation from Fe(II) to Fe(III) took place in the sediments. The sulphide content, however, showed no change compared to the reference samples from the downstream area and is between 60 and 98 % in the entire investigation area.

Table 13: Correlation coefficients of redox sensitive elements Fe and S with U in samples from the Tertiary rim

	Fe$_{tot}$	Fe(II)	Fe(III)	S$_{tot}$	S^{2-}	SO$_4^{2-}$	U
Fe$_{total}$	-	-0.01	0.89	0.81	0.85	0.16	0.22
Fe(II)	-0.01	-	-0.47	0.42	0.31	0.72	0.74
Fe(III)	0.89	-0.47	-	0.52	0.61	-0.20	-0.15
S$_{total.}$	0.81	0.42	0.52	-	0.99	0.67	-0.22
S^{2-}	0.85	0.31	0.61	0.99	-	0.55	-0.19
SO$_4^{2-}$	0.16	0.72	-0.2	0.67	0.55	-	-0.28
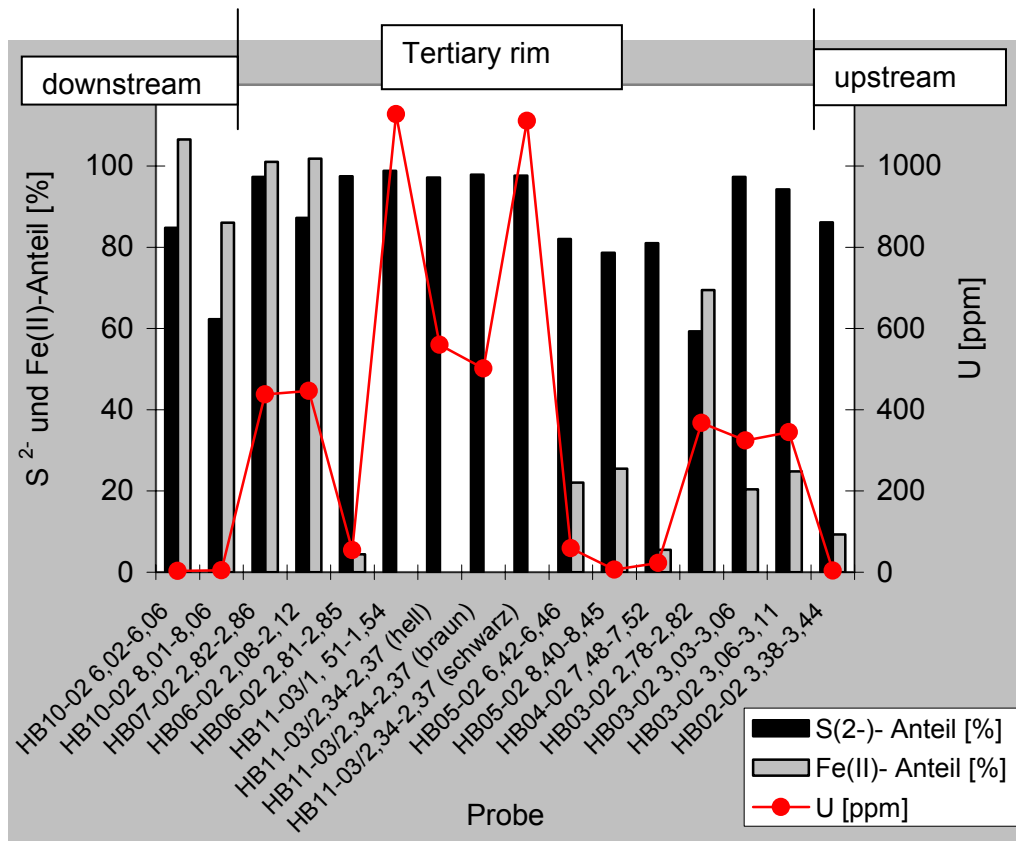
Fig. 30: Sulphide and Fe(II) fraction [%] and U content [ppm] in selected samples

41

3.2.4 Cation exchange capacity

Ion exchange is one of the most important processes in soil and sediments, thus being a decisive factor regarding the formation of the geochemical environment. One method for the quantitative determination of ion absorption in the sediment is to determine the cation exchange capacity (CEC). In this respect, distinction is made between CEC (sum of all exchangeable cations) and exchange capacity EC (fraction of single cations).

Generally, the first step to determine the CEC is to occupy all exchangeable cation sites in the sediment by an ion not existing in the sediment (Sr or Ba). Subsequently, surplus ions, e. g. those bound to colloids, are removed by adding distilled water. To determine the CEC, the ions inserted are re-exchanged by the addition of Mg ions (Table 14).

The exchangeable ions Ca, Mg, K and Na and the potential cation exchange capacity were determined by means of ten selected samples. For the determination of EC and CEC, the calculated amount of wet samples (weight related to dry substance = 1 g) was filled up with quartz sand to 5 g. The sample/quartz mixture was again mixed with 30 ml solvent in an agate mortar and then transferred into a 50 ml centrifuge tube. Further treatment was performed according to DIN ISO 13536. The results are presented in Table 14 and Fig. 31.

Table 14: Solvents used for determination of EC and CEC in Heselbach samples

	Run A / EC of Mg, Ca, Na, K	**Run B / CEC**
Solvent	$BaCl_2$ solution (buffered at pH 8,1)	$MgSO_4$ solution
Reaction	Adsorption of Ba-ions and desorption of cations	Re-exchange of sorbed Ba ions by Mg ions

As expected, the highest EC values were found in the coaly samples HB06-02/2,08-2,12 and HB07-02/2,82-2,86. With 89 and 87 cmol•z/kg, however, the CEC values are below those cited in literature for organic matter (100 - 500 cmol•z/kg; cited in /VOI 90/). This can be explained by the fact that the sediment samples from the Heselbach coal seam are strongly argillised material. Kaolinite is an important component of the Wackersdorf interbedded clays /TIL 54/ and has a low CEC of 3 - 50 cmol*z/kg (cited in /VOI 90/). The comparably high CEC of a purely organic substance is thus considerably reduced in presence of these clay minerals. That the existing clays

mainly account for the clay mineral kaolinite is also confirmed by the exchange capacities of the pure clay samples HB03-02/3,03-3,11. The CEC values are < 25 cmol•z/kg and exclude the presence of swellable clay minerals, such as montmorillonite and vermiculite. The presence of illite or allophane (CEC 10 - 50 cmol•z/kg; cited in /VOI 90/), however, might be possible. For this reason, X-ray images were taken from clayey material to identify the individual clay components.

Table 15: EC and CEC for sediment samples from Heselbach

Bore hole	Depth [mbgl]	Lithology *)	EC [cmol·z/kg]				Sum [cmol·z/kg]		pH sed
			Mg	Ca	Na	K	Run A	Run B	
HB02-02	3.38-3.44	tS, light grey	2.55	8.05	0.05	0.63	11.28	13.8	-
HB03-02	2.78-2.82	T, black	2.04	3.20	0.06	0.18	8.90	9.8	-
	3.03-3.06	T, grey, dense. schlieric	3.67	15.30	0.06	1.13	20.16	24.7	3.6
	3.06-3.11	T, grey, dense, schlieric	3.17	13.70	0.23	1.04	18.14	22.4	3.5
HB05-02	6.42-6.46	Lignite, cohesive fractions	1.51	12.51	0.1	1.01	15.13	50.0	2.6
HB06-02	2.08-2.12	T, with lignite, black	3.58	50.98	0.1	0.37	55.03	88.7	4.8
	2.81-2.85	T, with S-lots, light brown	2.64	11.66	0.13	0.95	15.4	28.6	4.57
HB07-02	2.82-2.86	lignite seam	6.11	60.54	1.61	0.70	68.98	82.4	4.20
	3.24-3.28	coal, black, sT layer, brown	2.72	18.94	0.29	0.98	22.93	30.1	4.88
	3.24-3.28	S, brown	0.65	3.99	0.03	0.25	4.92	9.0	-

*) abbreviations acc. to German nomenclature: S = sand; s = sandy; T = clay; t = clayey
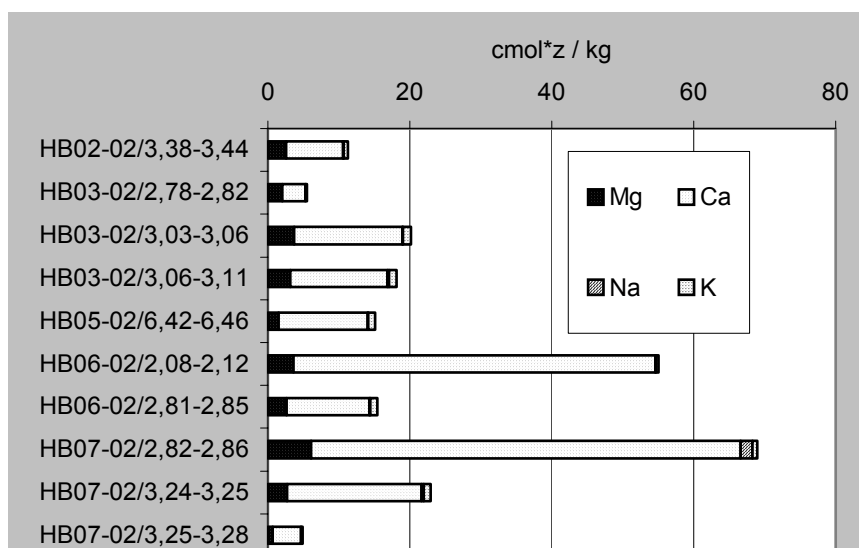
Fig. 31: EC of Mg, Ca, Na and K ions in different sediment samples

The fact that all sediment samples have a high content of adsorbed calcium (max. 73 %) and 3 to 20 % magnesium is an indication that organic matter is the most important adsorbent. Potassium, which is mainly bound selectively to three-layer minerals (illite) is only represented to a minor degree with a maximum of 4.6 % of the adsorbed ions. Sodium can be neglected completely.

Table 16: CEC and fraction of single cations of total CEC

Drilling	Depth [m bgl]	CEC [cmol·z/kg]	Fraction of Mg [%]	Fraction of Ca [%]	Fraction of Na [%]	Fraction of K [%]
HB02-02	3.38-3.44	13.81	18.46	58.29	0.36	4.56
HB03-02	2.78-2.82	9.80	20.82	32.65	0.61	1.84
	3.03-3.06	24.72	14.85	61.89	0.24	4.57
	3.06-3.11	22.38	14.16	61.22	1.03	4.65
HB05-02	6.42-6.46	50	3.02	25.02	0.20	2.02
HB06-02	2.08-2.12	88.74	4.03	57.45	0.11	0.42
	2.81-2.85	28.60	9.23	40.77	0.45	3.32
HB07-02	2.82-2.86	82.38	7.42	73.49	1.95	0.85
	3.24-3.26	30.14	9.02	62.84	0.96	3.25
	3.26-3.28	9.04	7.19	44.14	0.33	2.77

3.2.5 Carbon content

The carbon contents of the sediment samples were determined with a Leco CS 144 analyser according to DIN 10694. The samples were combusted in an induction furnace under oxygen. Untreated material yields the total carbon content; samples

treated with HCl yield the organic fraction of the carbon. The inorganic carbon content is calculated from the difference between the measured values.

The carbon analyses performed show the dominance of the organic carbon content. Inorganic carbon accounts for less than 1.3 weight % of the sediments. The TOC (total organic carbon) contents, however, reach 44.6 weight % in samples from the lignite seam (drilling HB10-02 in the former opencast mining area). While the Keuper sands just contain little organic matter (0.02 weight %), the drillings from the Tertiary rim locally reach contents of up to 33.9 weight %. Here, a direct correlation can be drawn between high uranium contents and the organic content (Fig. 32).
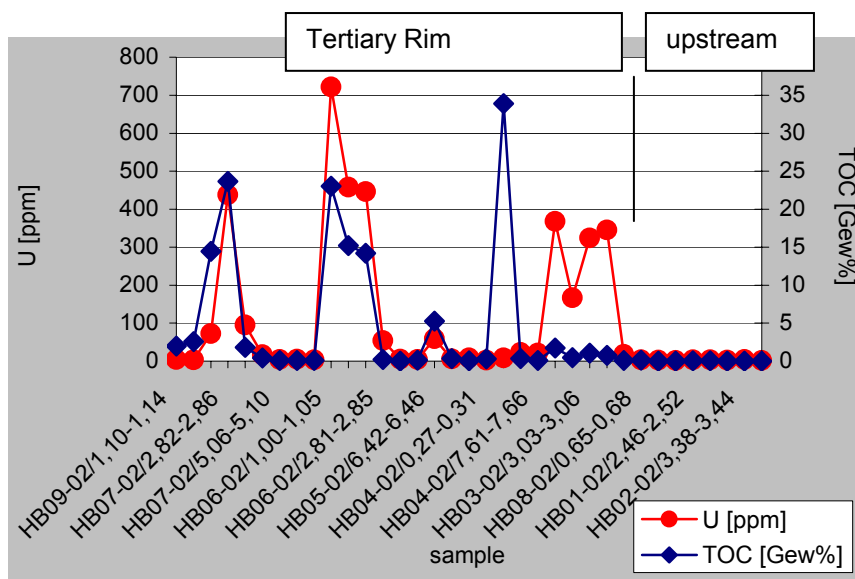
Fig. 32: Correlation of U and TOC content in samples from Tertiary rim

Looking at the U/TOC diagram, the low TOC concentration in drilling HB03-02 is due to the fact that this borehole was drilled directly at the border of the Tertiary rim and coal relics only exist in traces.

3.3 Mineralogical investigations

Roentgenographic investigations represent an easy method to obtain a general outline of the mineral contents of a rock sample. As analyser, a counter tube goniometer of Philips (X`Pert-MPD) with computer-based analysis methods was available. The mineral reflections were determined by CuKα1 radiation (λ = 0.15418 nm) of a copper anode. The analysis is limited to minerals whose weight amounts to a minimum of 3 to 5 % of the bulk rock composition. From the dried, pulverised and homogenised

material, powder samples were produced and diffractograms recorded whose interpretation is listed in Table 17, also presenting the uranium contents determined by ICP-MS.

The samples selected for clay mineral analyses were treated separately. After separation of the sediment grains >2 µm, the clay fraction was measured in the range of 4 - 35Φ untreated, glycolised and glowed.

The X-ray analyses of the Keuper samples demonstrate their uniform composition. The analyses from drillings HB01-02, HB02-02 and HB08-02 (Burgsandstein) indicate quartz, orthoclase and muscovite as main components, in argillised sections also kaolinite.

Sample material from the Tertiary rim area displays, depending on organic components and local site conditions, different mineral formations. E. g., samples with a high content of organic matter often show gypsum efflorescences. Iron is mineralised in form of pyrite, marcasite or jarosite crystals. Here, the prevailing Eh/pH environment is of particular importance. While pyrite (FeS_2) is a mineral with a large stability field, marcasite (FeS_2) preferably crystallises from acidic solutions /MAT 94/ as they exist in the carboniferous sediments from Heselbach. Jarosite is a typical mineral of the oxidation zone of Fe-sulphide horizons. Samples containing jarosite only have a small distance to the surface (2.78 and 2.81 m). The conversion of pyrite and marcasite to jarosite in these samples was probably due to the entry of oxygen. Divalent iron was oxidised to trivalent iron before jarosite was formed by the following reaction /MER 97/:

$$2Fe^{3+} + 4SO_4^{2-} + 6H_2O + 8H^+ \rightarrow 2HFe_3(SO_4)_2(OH)_6 + 6H^+$$
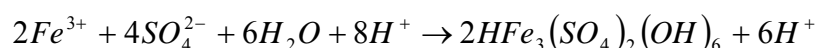
The samples of surface-near boreholes HB05-02 and HB08-02 are the only ones showing albite and clinochlore in the diffractograms. These minerals are not autochthonous and were formed in another area. The material presumably originates from the metamorphites of the Upper Palatinate or Bavarian Forest and was used as backfill material.

Six selected sediment samples were analysed for their clay mineral content. All samples originate from the drill cores of the Tertiary rim; four samples were taken from the interbedded clay, and two from the clayey parts of the lignite horizon.

Table 18 gives an overview of the identified clay minerals and demonstrates the homogeneity of the clay mineral composition of these sediment layers. The original diffractograms of these analyses are presented on the enclosed CD-ROM.

Table 17: Main minerals identified by XRD analysis and U content

Sample	Main mineral content						U [ppm]
HB01-02/2.46-2.52	quartz	orthoclase	muscovite				3.41
HB01-02/5.38-5.43	quartz	orthoclase	muscovite	kaolinite			3.04
HB01-02/8.72-8.78	quartz	orthoclase	muscovite	kaolinite			2.25
HB02-02/3.38-3.44	quartz	orthoclase	kaolinite				4.15
HB02-02/8.97-9.00	quartz	orthoclase	kaolinite	muscovite			1.45
HB03-02/2.78-2.82	quartz	orthoclase	kaolinite	muscovite	gypsum	jarosite	367.62
HB03-02/2.96-2.99	quartz	orthoclase	kaolinite	pyrite	gypsum		166.34
HB03-02/3.03-3.06	quartz	pyrite	kaolinite	marcasite	orthoclase		324.17
HB03-02/3.06-3.11	quartz	pyrite	kaolinite	orthoclase			345.10
HB03-02/5.36-5.41	quartz	orthoclase	kaolinite				17.90
HB04-02/0.27-0.31	quartz	orthoclase	anorthite	kaolinite			2.37
HB04-02/2.38-2.44	quartz	gypsum					8.45
HB04-02/7.48-7.52	quartz	kaolinite					23.05
HB04-02/7.61-7.66	quartz	orthoclase	kaolinite				20.68
HB05-02/0.00-0.06	quartz	orthoclase	albite	muscovite	clinochlore		4.05
HB05-02/6.42-6.46	quartz	pyrite	gypsum	kaolinite	rutile		58.79
HB05-02/8.40-8.45	quartz	kaolinite	rutile?				6.00
HB05-02/10.47-10.51	quartz	orthoclase	kaolinite				8.84
HB06-02/1.00-1.05	quartz	kaolinite					722.02
HB06-02/1.53-1.58	quartz	kaolinite	kaolinite				458.25
HB06-02/2.08-2.12	quartz	orthoclase	kaolinite				446.29
HB06-02/2.81-2.85	quartz	orthoclase	jarosite	muscovite			54.01
HB06-02/6.46-6.50	quartz	orthoclase	muscovite	kaolinite			5.09
HB07-02/1.68-1.72	quartz	orthoclase	anorthite	muscovite	kaolinite		72.56
HB07-02/2.82-2.86	quartz	kaolinite					437.67
HB07-02/3.24-3.28	quartz	orthoclase	kaolinite	muscovite			95.15
HB07-02/3.24-3.28	quartz	orthoclase	kaolinite	muscovite			16.89
HB07-02/5.06-5.10	quartz	orthoclase	kaolinite				4.31
HB07-02/5.94-5.98	quartz	orthoclase	kaolinite				4.71
HB07-02/6.81-6.85	quartz	orthoclase	kaolinite	muscovite			3.30
HB08-02/0.65-0.68	quartz	orthoclase	albite	clinochlore			3.06
HB08-02/2.36-2.40	quartz	orthoclase	microcline	muscovite	kaolinite		2.54
HB08-02/3.53-3.57	quartz	orthoclase	muscovite	kaolinite			1.64
HB09-02/1.10-1.14	quartz	orthoclase	kaolinite	muscovite			3.92
HB09-02/2.46-2.51	quartz	orthoclase	microcline	kaolinite	muscovite	gypsum	3.00
HB10-02/3.34-3.38	quartz	orthoclase	kaolinite	muscovite	microcline		4.15
HB10-02/6.02-6.06	quartz	kaolinite	gypsum				3.21
HB10-02/8.01-8.06	quartz	orthoclase	kaolinite	muscovite	rutile?		4.70
HB10-02/11.89-11.93	quartz	orthoclase	kaolinite				3.15
HB10-02/12.24-12.28	quartz	orthoclase	microcline	kaolinite			1.69

All clays primarily consist of kaolinite and to a minor degree of illite and halloysite. While kaolinite is formed under tropical/subtropical climatic conditions and slightly acidic to neutral pH conditions from feldspars, thus having favourable conditions for its formation at the time of the Tertiary, illite is formed by K^+ release from muscovite. This process often takes place in soils and sediments in moderate latitudes /HEI 90/. Swellable clay minerals have not been identified. This result is confirmed by the low cation exchange capacity of the clay samples of < 25 cmol*z/kg.

Table 18: Clay minerals in lignite and interbedded clay samples

Drilling / depth [m b.g.l.]	Lithology	pH ($CaCl_2$)	Identified peaks [2Φ-angle]	Identified clay minerals
HB03-02/2.77-2.78	BkT	4.64	8.9/12.35/17.8/20.8/24.7/26.5	kaolinite / illite
HB03-02/3.02-3.03	T	2.95	8.9/12.35/17.8/20.8/24.7/26.5	kaolinite / illite
HB04-02/7.48-7.52	T	5.78	8.6-8.9/ 12.35/17.8/20.8/4.7/26.5	kaolinite / illite
HB06-02/2.07-2.08	BkT	5.54	8.9/12.35/17.8/20.8/24.7/26.5	kaolinite / illite
HB06-02/2.81-2.82	T	5.61	8.9/12.35/17.8/20.8/24.7/26.5	kaolinite / illite
HB07-02/3.22-3.24	T	5.67	8.9/12.35/17.8/20.8/24.7/26.5	kaolinite / illite

BkT = coaly clay from lignite horizon; T = interbedded clay

Original-mineral   **Weathering product**

Quartz: SiO_2 →   Quartz: (SiO_2)

K-Feldspar: $K\,[AlSi_3O_8]$ →   Kaolinite: $Al_4[(OH)_8/Si_4O_{10}]$

Loss of potassium

Muskovite: $KAl_2\,[(OH,F)_2/AlSi_3O_{10}]$ →   Illite: (lower K / higher Si/Al ratio)

Pyrite / Markasite: (FeS_2) →   Jarosite: $KFe_3[(OH)_6/(SO_4)_2]$

Weathering / Oxidation
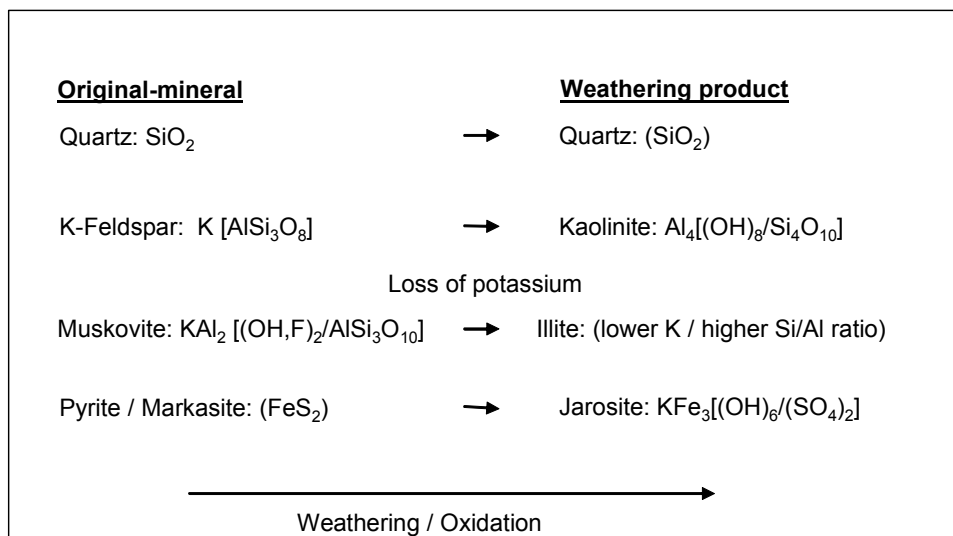
Fig. 33:   Minerals and weathering products observed at Heselbach site

3.4 Characterisation of the uranium phases

An important prerequisite for transport calculations for all natural uranium deposits is the description and identification of the existing immobile and mobile uranium phases. For this reason, different methods will be explained in the following chapters which may contribute to the clarification of this issue and that were applied to Heselbach samples. In the first part, the immobile uranium phase is investigated by means of spectroscopic methods, in the second part, the mobile phases are identified by sequential extraction.

Autoradiographic measurements have been performed at Institut für nukleare Entsorgung (INE), Karlsruhe /GEC 02/. The filter image of a core segment from drilling HB03-02 is shown in Fig. 34, left side. Green colour indicates areas with higher radioactive radiation, the edges of the sample are blue. On the right side the α-activity in the top sediment layer along the profile line (as indicated on the left) is shown.
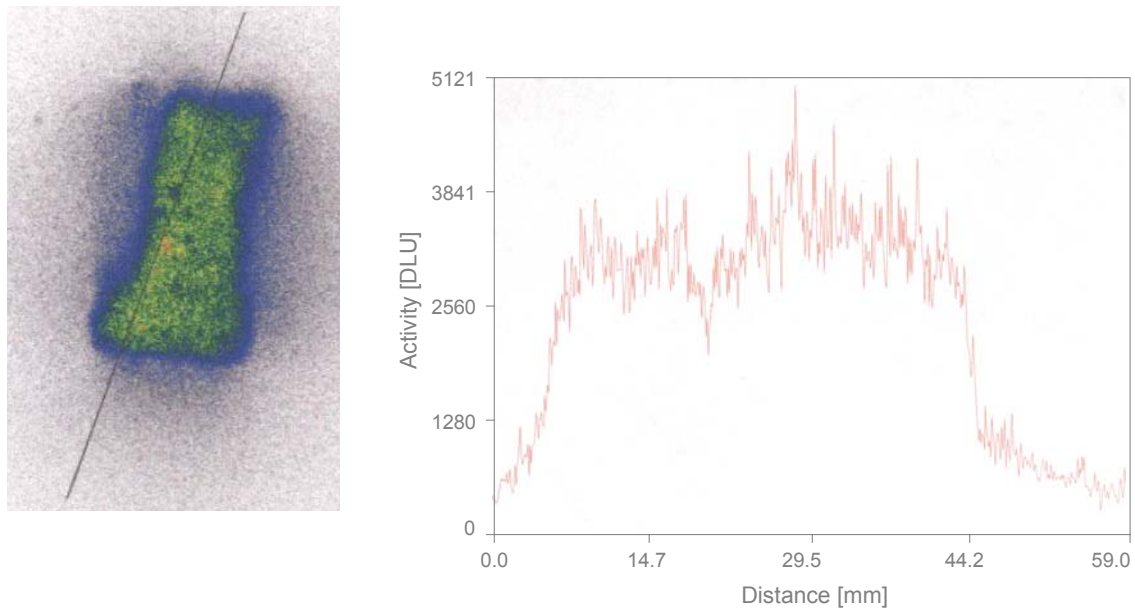
Fig. 34: Autoradiography of core section HB03-02/2,78-2,82 /GEC 05/.

The autoradiographic image shows, that uranium is distributed rather similar over the whole sample cross section. There are areas with slightly increased radioactivity but single spots as expected for locally occurring uranium mineral phases are not identified.

3.4.1 Electron microscopy

Selected samples were analysed by the SEM-EDX (scanning electron microscopy / energy dispersive X-ray) method. This is a high-resolution method which, under ideal conditions allows a differentiation up to the 10 - 100 nm range. In natural samples, however, particles < 1 µm are not identified adequately so that a minimum size of the crystalline phase is required. Further, an integrated EDX analyser enables element mapping and selective element analyses /REE 96/, /AMT 01/.

For the Heselbach sediments, focus is laid on the determination of the uranium phases and BSE images were taken from the samples. Fig. 35 shows two typical examples.

The investigations were performed at the Institute for Building Materials, Concrete Construction and Fire Protection (iBMB) of the Technical University of Braunschweig. As analyser, a JSM-6700F field emission scanning electron microscope of the company Jeol was used. Detection was performed by means of the $U_{M\alpha}$ line.
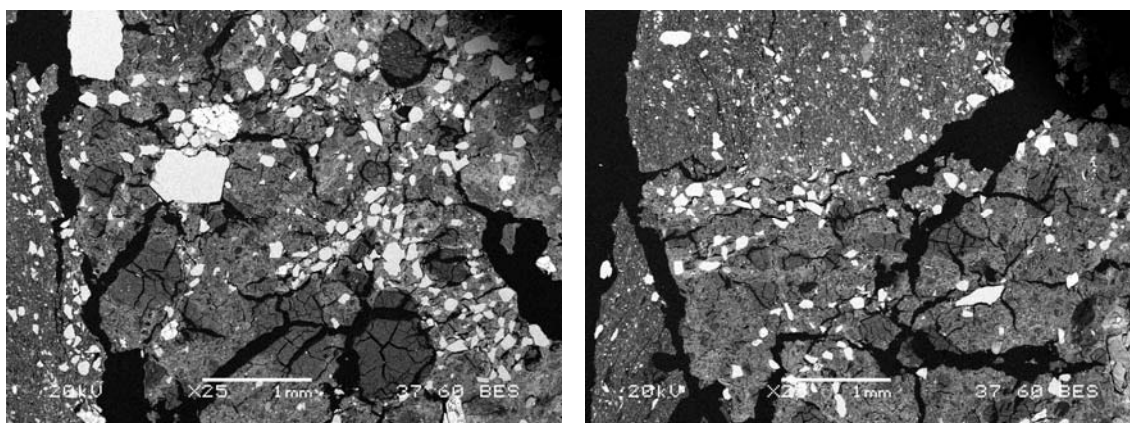
Fig. 35: BSE images of HB11-03/1,51-1,54 (left) and HB11-03/2,34-2,37 (right)

The mineral grains, clearly to be seen in white in the BSE images, are minerals with a high average atomic number (Z). In this case, it is pyrite and marcasite (Z = 20.7). Their size varies from a few µm up to several millimetres. In some cases, gypsum crystals (Z = 12.4) were identified. The light grey matrix is formed by orthoclases (Z = 11.9) and clay minerals (Z kaolinite = 10.4); the dark parts are coal particles (see Fig. 35). In the samples from the lower horizon (interbedded clay), the clayey matrix clearly dominates. Nevertheless, this sample cannot be characterised as homogeneous clay. Lignite and pyrite minerals are abundant in this sample.

All BSE images of the sediment sample do not show crystalline uranium phases. Regarding the identification of uranium, selective element analyses around defined mineral grains (pyrite, coal) were as unsuccessful as a long-term mapping of several subareas performed over night. From this fact, the following conclusions can be drawn:

1) Uranium does not exist in crystalline form - or else

2) Uranium forms crystalline minerals; these, however, are too small and, moreover, finely dispersed so that the local concentration is not sufficient for detection.

3.4.2   XANES and EXAFS measurements

XANES (X-ray absorption near edge structure) and EXAFS (X-ray absorption fine structure) measurements represent a spectroscopic method where absorption of the radiation is measured in dependence of wave length and energy. Here, the radiation with sufficient energy to cause electron transitions from the L to the K shell is absorbed. The increase of the adsorption coefficients becomes manifest in the spectrum as so-called adsorption edge. The structures in the range of about 10 eV below up to about 50 eV above the adsorption edge energy are analysed with the XANES method. Above this energy up to about 1 keV, the EXAFS spectra are measured /AMT 01/.

The interaction between the radiation and the neighbouring atoms leads to an increase or decrease of absorption which can be seen in the spectrum by the so-called fine structure. So, in contrast to X-ray diffractometry, statements can be made on the chemical bond lengths and the environment of a specific atom.

Eight uranium-containing sediment samples from the Heselbach lignite and clay horizon were analysed at the Institute for Nuclear Waste Disposal (INE) of the Forschungszentrum Karlsruhe to clarify the actual bond form of the uranium. Fig. 36 and Fig. 37 show the U L_{III} lines detected with XANES and EXAFS measurements.

The XANES spectrum of the Heselbach sample (Fig. 36) covers a wide energy range (about 14 eV). This structure is an indication to hexavalent uranium in the sediment sample. In comparison to it, the spectra of two sediment samples from Ruprechtov (Czech Republic) show the presence of tetravalent uranium.
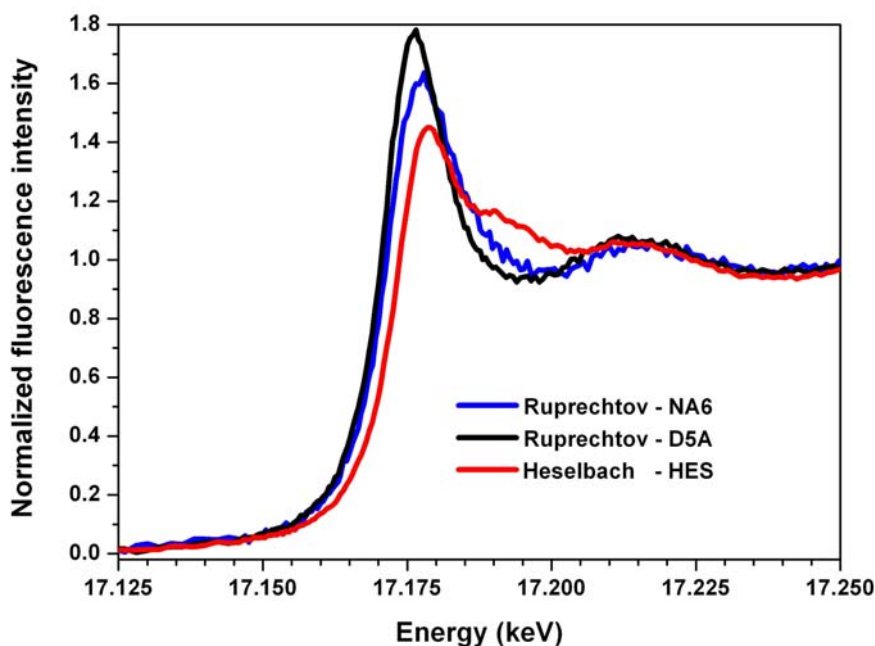
Fig. 36: Standardised U L$_{III}$ XANES spectra of three different sediments; red curve = sample from Heselbach /DAR 04/ (black and blue curves represent samples from Czech Ruprechtov site)

The EXAFS spectra (Fig. 37) of the Heselbach samples show typical bond lengths for oxygen atoms (1.78 and 2.42°A) as they exist in an uranyl ion (UO$_2^{2+}$). In addition to the oxygen bonds, another bond length of 3.08°A was identified. This is too short for an inorganic bond. Possibly, this bond is an uranyl adsorption to functional groups of organic matter.

3.4.3   Chemical separation of U(IV) and U(VI)

On two representative samples from drill core HB11-03 the Department of Chemistry of the University of Helsinki determined the uranium valence states.

The sediments were treated with conc. HCl and HF under reducing conditions. For the determination of the oxidation state, the two valence states were separated using an ion exchanger column. U(VI) is sorbed on the column while U(IV) is washed out as first fraction. The subsequent addition of 0.1 M HCl remobilises the fixed U(VI) from the column.
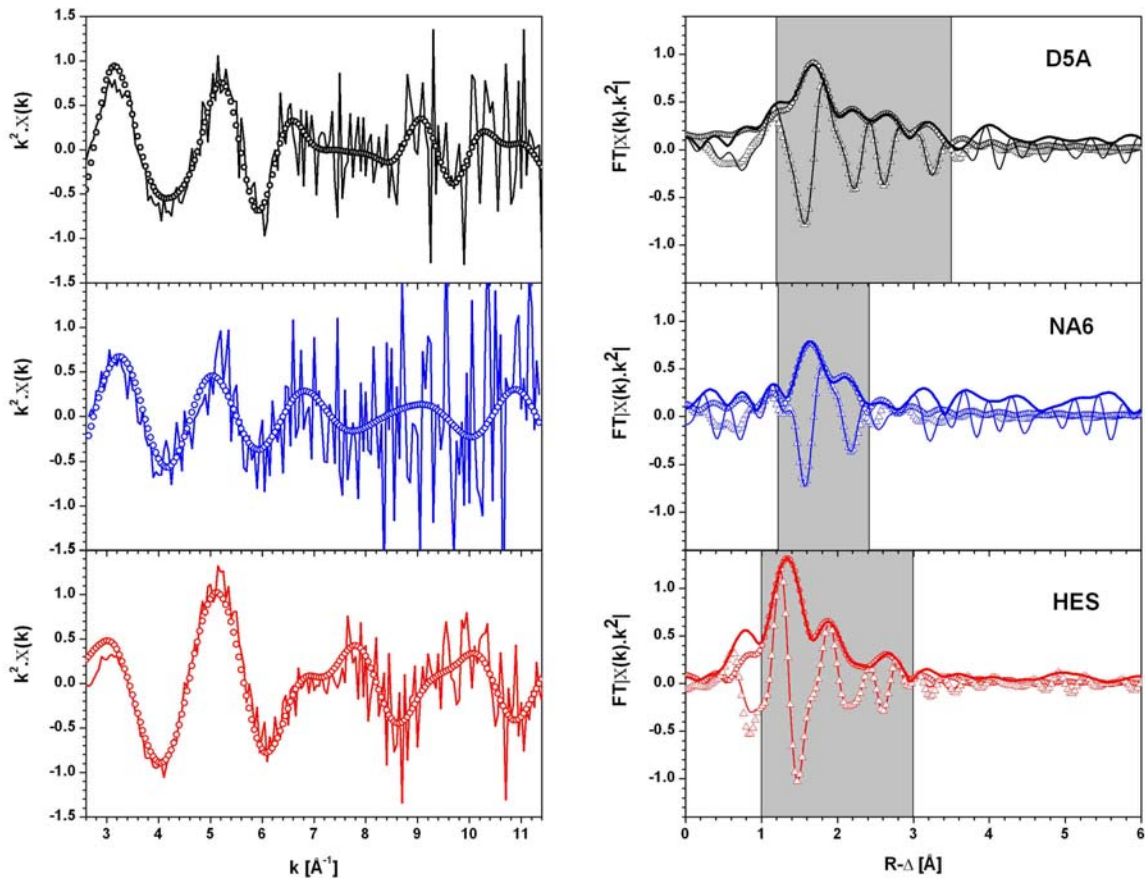
Fig. 37: U L$_{III}$ EXAFS spectra of three different sediments; red curve = sample from Heselbach /DAR 04/ (black and blue curves represent samples from Czech Ruprechtov site)

Measurement of the uranium in the respective fraction by ICP-MS gave the clear result of uranium occuring for more than 99 % in hexavalent form (Table 19).

Table 19: Results of chemical separation of U(IV) and U(VI) in sample HB11-03

Sample	U(IV) fraction [%]	U(VI) fraction [%]
HB11-03/1.53-1.57	< 1%	> 99%
HB11-03/2.34-2.37	< 1%	> 99%

Together with the EXAFS investigation, a uniform picture is given for the Heselbach sediments. Both investigation methods show that no uranium(IV) minerals exist. There is no uraninite as secondary uranium phase. In addition to the results described, the high Eh values of the groundwaters and the fact that uranyl ions in lignite preferably react with the carboxylate groups of the humic acids also indicate that uranium was transported into tertiary sediments and immobilised there as uranyl ion [UO_2^{2+}] in hexavalent form.

3.4.4 Sequential extraction

The chemical form of elements within the sediments is relevant for the assessment of their mobility. It is therefore not sufficient to know their total concentration. Therefore, eight different samples were extracted according to the method of /PER 90/ to give a prediction on the bonding states of the uranium in the sediments. On the basis of the results achieved with it, a method, especially adjusted to the Heselbach sediments, was applied to two additional samples. The different methods are presented in the following two chapters.

3.4.4.1 The Percival method

For the radionuclide determination on Heselbach sediments, a method was chosen first, which is particularly developed and applied to uranium-containing samples. Percival /PER 90/ developed a five-level method for samples from the Cigar Lake uranium deposit in Canada which extracts uranium effectively and proved to be insensitive towards small changes of concentration, extraction time and temperature. One and the same sample is mixed with increasingly aggressive solutions. In each phase, different bonds are attacked. Depending on the accumulation, uranium can be assigned to one or several phases. Which phase corresponds to which bond form is presented in Table 20. All five phases of the sequentially extracted samples were analysed with regard to the following elements

1) Fe, Mn, P, S, Cu, Cr   by ICP-OES (ARL 3520 and Fisions Maxim)
2) U and Th   by ICP-MS (Micromass Platform)

Table 20: Overview of the phases and reactants used for sequential extraction according to /PER 90/

Phase	Description	Reactant	Chemical form
1	exchangeable and carbonate phase	1 M Na-acetate, pH 5	adsorbed. easy soluble or carbonate except siderite
2	organic-sulphidic phase	H_2O_2 30%; Na_2CO_3 2.5%	bound to organic matter or in sulphide
3	easily reducible phase	0.25M NH_2OHHCl in 0.25M HCl	bound to Fe oxy-hydroxides (amorphous)
4	difficult reducible phase	0.68M tri-Na-citrate-dihydrate with 16 g/l Na-dithionite	bound to Fe oxides (crystalline)
5	residual phase	full digestion with H_2O_2 (30%); HNO_3 (65%); $HClO_4$; H_2F_2	in silicates and accessory minerals

On the basis of the gamma spectrometric measurements, eight sediment samples were selected for this sequential selection. The samples originate from four drillings of the Tertiary rim area. Table 21 summarises the samples selected for sequential extraction and some of the most important results of the bulk rock analyses.

Table 21: Selected results from bulk rock analyses of samples used for sequential extraction

Drilling	Depth [m b.g.l.]	Lithology[*)]	$Fe_{tot.}$ [%]	Fe(II) [%]	Fe(II)-fraction of Fe_{tot} [%]	U [ppm]	TOC [%]	Water content [%]	pH [$CaCl_2$] Sed.
HB03-02	2.78-2.82	T,black	3.22	2.23	69.25	368	1.747	10.67	2.60
	3.03-3.06	T,dense,grey	5.63	1.15	20.42	324	1.047	21.17	3.63
	3.06-3.11	T,dense,grey	4.97	1.23	24.75	345	0.73	25.83	3.50
HB05-02	6.24-6.46	Coal,cohesive fractions	5.68	1.25	22.01	58.8	5.25	18.72	2.59
HB06-02	2.08-2.12	T with coal, black	1.76	1.79	101.70	446	14.21	36.77	4.81
	2.81-2.85	T with S-sections, light brown	4.59	0.20	4.36	54.0	0.21	20.58	4.80
HB07-02	2.82-2.86	coal seam	1.08	1.09	100.92	438	23.67	44.78	4.57
	3.24-3.28	transition coal / sT location. brown	1.33/ 0.99	0.91/ 0.23	68.42/ 23.23	95.1/ 16.9	1.83/ 0.41	18.20	4.20

*) abbreviations acc. to German nomenclature: S = sand; s = sandy; T = clay; t = clayey

To obtain a sufficiently high concentration of the isotopes in the individual extraction steps for the following radiometric measurements, 7.24 g of dry sediment was weighed in for the first phase. The first work step of the sequential extraction was performed, including filtration, under argon atmosphere. Since hydrogen peroxide was added as oxidising agent already in the second step, it was possible to perform all following working steps outside the glove box.

An overview of all concentrations determined for the eight elements is given in Table 22. A conversion to percentages illustrates the distribution on the individual phases and is discussed by means of the following figures.

Table 22: Element contents [ppm] in the five extraction phases (acc. to /PER 90/) of eight sediment samples

Element	Phase	HB03-02			HB05-02	HB06-02		HB07-02	
		2,78-2,82	3,03-3,06	3,06-3,11	6,42-6,46	2,08-2,12	2,81-2,85	2,82-2,86	3,24-3,28
P	1	10.6	2.8	5.7	8.5	0	2.8	4.3	2.8
	2	123.6	211.8	158.7	76.7	168.7	297.3	208	254
	3	22.3	66.9	121.3	77.2	44.7	0	33.7	22.2
	4	10.4	7.5	22.3	10.9	15.9	165.6	0	0
	5	36.2	182.1	143.5	74.5	282.9	268.8	80.0	333.7
S	1	17931	1051	1104	25338	39	71	1216	45
	2	17212	21049	23224	40803	3579	3460	21198	408
	3	540	1510	619	1041	111	386	377	10
	4	n.n.	n.n.	n.n.	n.n.	n.n.	n.n.	n.n.	n.n.
	5	2000	15873	9685	3201	1440	2964	1028	1274
Mn	1	28.0	11.2	8.9	99.4	22.3	17.1	9.6	3.6
	2	0.2	0.2	0.0	0.2	1.7	0.0	10.9	0.0
	3	10.3	50.8	19.0	64.5	23.9	5.4	2.7	2.7
	4	1.0	3.5	1.5	3.5	1.5	3.5	0.5	1.0
	5	13.9	67.9	56.7	25.8	16.5	66.3	4.7	9.7
Fe	1	11696	486	370	12237	16	6	43	1
	2	8	7	8	28	287	5	4134	4
	3	9465	10778	12559	17561	1138	6078	404	399
	4	366	679	457	467	440	21448	120	254
	5	3463	14800	10414	5572	1769	9150	4695	3722
Th	1	1.90	0.55	0.12	2.05	0.02	0.05	0.02	0.06
	2	0.06	0.11	0.14	0.14	6.4	0.36	7.0	0.72
	3	0.36	1.3	0.91	0.76	0.32	0.59	0.35	0.33
	4	0.5	4.9	4.3	4.0	8.3	4.7	0.59	6.8
	5	3.0	5.2	6.1	0.55	5.6	2.7	0.78	1.4
U	1	237.5	139.4	204.0	23.1	73.9	8.8	99.82	24.15
	2	29.93	251.37	431.41	8.84	303.3	26.6	306.43	60.85
	3	2.19	16.21	17.67	0.19	4.60	3.92	5.21	0.36
	4	1.17	3.18	2.07	0.20	1.99	7.82	0.46	0.15
	5	2.20	0.85	1.19	0.28	2.15	1.20	0.20	1.24
Cu	1	0.39	0.78	0.85	0.80	0.85	1.65	0.44	0.31
	2	2.69	2.21	2.44	1.57	15.93	0.32	30.18	7.04
	3	16.3	18.6	22.3	18.0	37.0	13.5	6.6	26.9
	4	4.3	1.5	3.2	2.6	11.0	17.2	2.6	10.9
	5	25.4	51.0	30.4	24.9	70.3	74.5	14.3	63.7
Cr	1	4.5	0.41	0.4	3.8	0.86	0.0	0.24	0.42
	2	5.5	5.2	6.7	3.10	96.8	6.5	71.0	45.3
	3	3.3	5.2	7.1	16.2	8.9	2.1	3.0	2.5
	4	0.75	2.5	2.2	1.3	3.6	7.8	0.63	1.4
	5	14.2	43.5	36.2	17.7	24.8	47.4	29.7	22.4

As shown in Fig. 38, almost 95 % of the uranium concentrations are distributed on phases 1 and 2, independent of the total uranium concentration. Only the sandy, oxidised sample HB06-02/2,81-2,86 m (only 4.4 % of the iron exists in the reduced form) shows an uranium distribution of 24.3 % on phases 3 and 4. For the majority of the samples, phase 2 accounts for the largest share of uranium distribution. This clearly demonstrates uranium bound to organic matter and/or sulphides. According to this statement, the samples with the highest coal content (HB06-02/2,08-2,12 and HB07-02/2,82-2,86) show, with 78.6 and 74.4 %, the largest percentage of all samples in Phase 2.
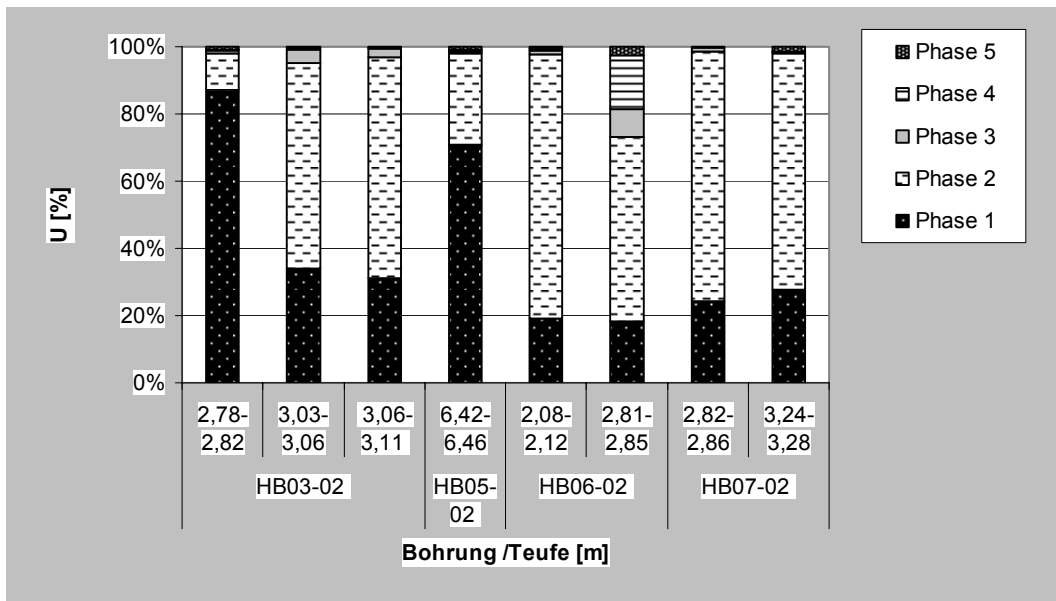
Fig. 38:   Uranium distribution [%] on phases 1 to 5 (acc. to /PER 90/) for Heselbach sediment samples

Further, samples HB03-02/2,78-2,82 and HB05-02/6,42-6,46 were particularly distinctive. In these two samples, uranium accumulated to a considerable amount in the first phase (87 and 70.9 %). Since in the Heselbach sediments no carbonates were identified, an association of uranium with carbonates can be excluded. Accordingly, adsorption or coupling of the uranium with a readily soluble is the main bond in the Heselbach sediments, in addition to uranium bound to organic matter.

Compared to uranium, the thorium distribution (Fig. 39) on the different phases is more variable. In the two samples that contain coal (TOC > 14 %), the shares of thorium in the second phase amount to 30 and 80 %. In the other samples, however, phases 3 to

5 are dominating (66.4 to 97.8 %). Special emphasis is placed, as is the case with the uranium distribution, on the samples HB03-02/2,78-2,82 and HB05-02/6,42-6,46. In these samples, thorium is fixed in Phase 1 to a maximum of 32,6 % and thus can also be remobilised very easily.
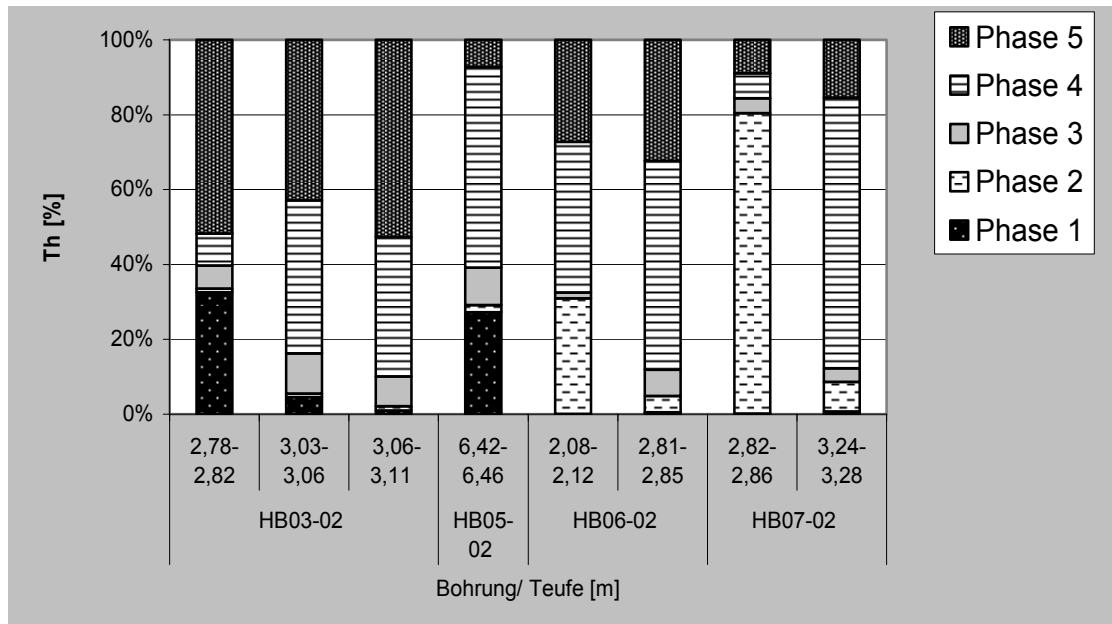
Fig. 39: Thorium distribution [%] on phases 1 to 5 for Heselbach samples, SE 2003

As an interrelation between uranium and Fe(II) concentrations was already observed in the previous ICP measurements, iron and manganese were particularly taken into consideration as potential main elements involved in uranium immobilisation. In the presentation of the iron distribution on the different phases of sequential extraction (Fig. 40), a readily mobilisable fraction in phase 1 can only be verified for two samples. These are the samples with the already mentioned increased uranium content in phase 1. The coaly samples contain a considerable percentage of iron in phase 2 (7.9 and 44 %). Due to the reducing properties of the lignite, the iron of these two samples is reduced to 100 % (Table 21). In all other samples (except for the sandy, oxidised sample HB06-02/2,81-2,85), the phases 3 and 5 are particularly dominating. In the sandy, oxidised sample, iron exists, as expected, in form of haematite or goethite in phase 4 (58.5 %). The pyrite and marcasite minerals identified by X-ray diffractometry from horizon HB03-02/3,03-3,11 were not found in the sequential extraction in the expected phase 2. Apparently, FeS_2 was not dissolved by oxidation with hydrogen peroxide and shaking out with Na_2CO_3. The iron content of these minerals is only released by complete digestion in phase 5.

The difference between the manganese distribution (Fig. 41) and the iron distribution within the sediments is that all samples contain manganese in the adsorbed phase. Analogous to iron, it only exits in coaly samples in phase 2. In the other samples, the amorphous Mn-oxide phase with 30 % at an average and the residual phase with a maximum of 72 % are the prevailing bound form.
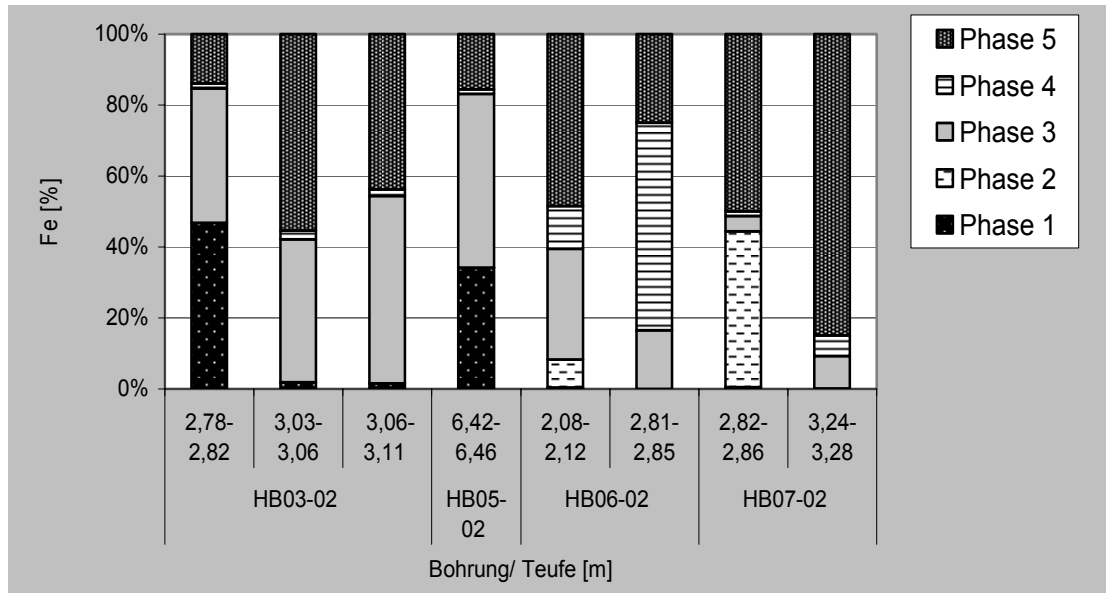
Fig. 40: Fe distribution [%] on phases 1 to 5 (acc. to /PER 90/) for Heselbach samples
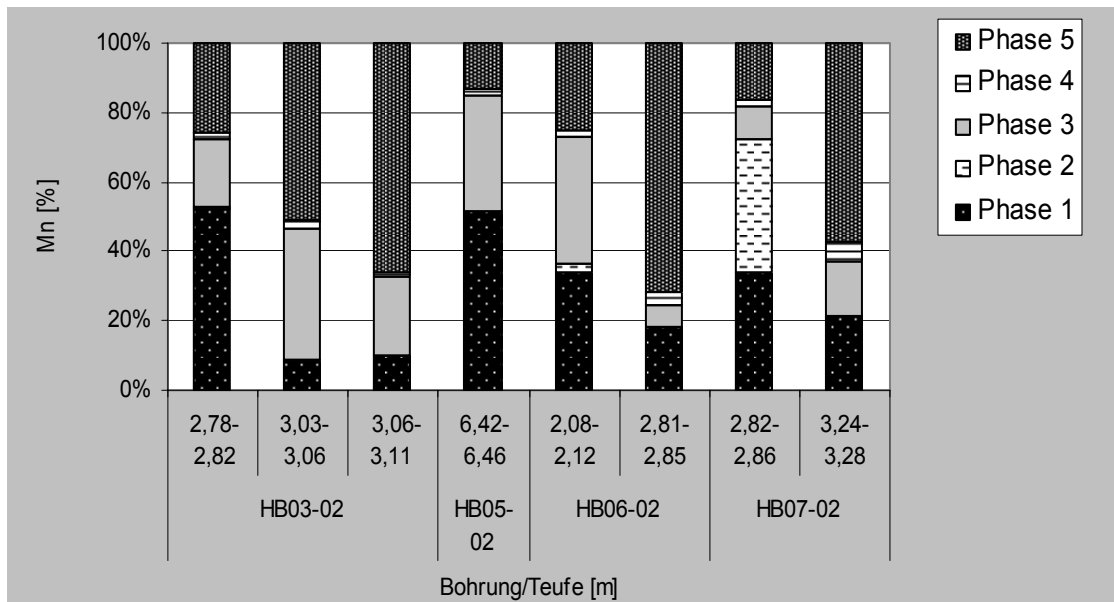
Fig. 41: Mn distribution [%] on phases 1 to 5 (acc. to /PER 90/) for Heselbach samples

Phosphorous (Fig. 42) shows, not dependent on lithology, a considerable percentage in phase 2 of the sequential extraction. On the other hand, phases 3 and 5 contain a large part of the phosphorous (30.5 to 66 %) and hardly make it accessible.
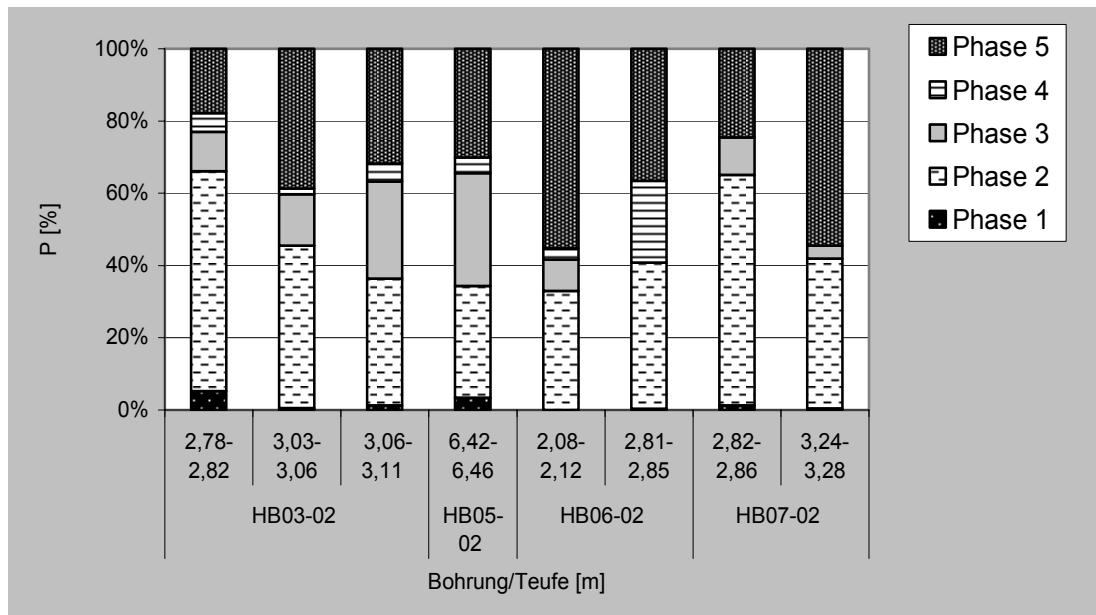
Fig. 42: P distribution [%] on phases 1 to 5 (acc. to /PER 90/) for Heselbach samples
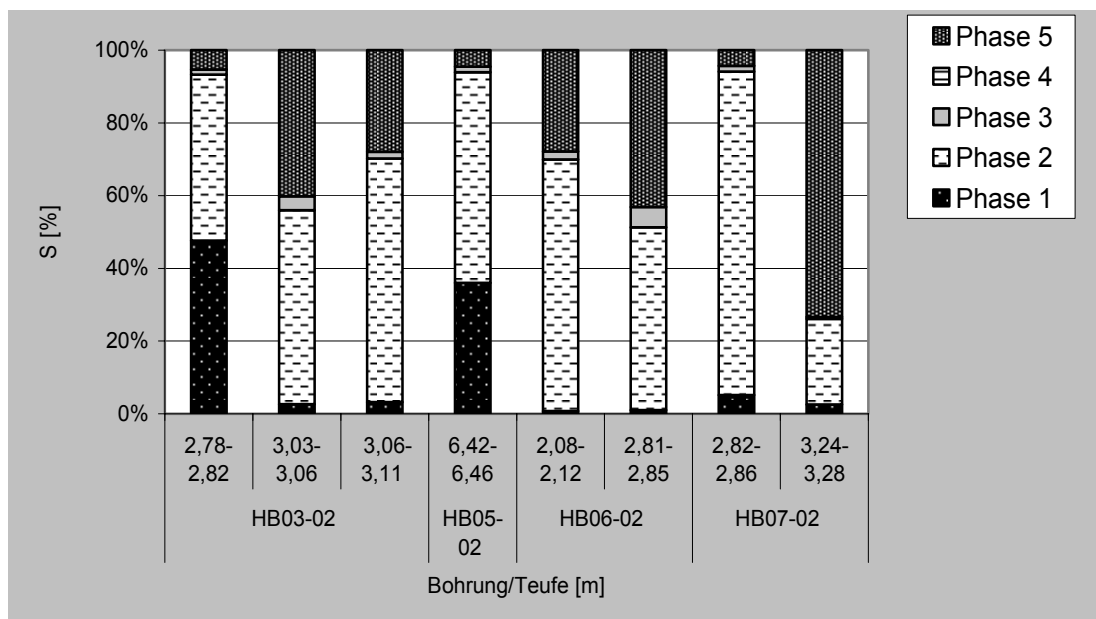
Fig. 43: S distribution [%] on phases 1 to 5 (acc. to /PER 90/) for Heselbach samples

Fig. 43 shows that sulphur exists in phases 1 and 2 up to 94 %. The samples HB03-02/2,78-2,82 and HB05-02/6,42-6,46 contain up to 47.6 % of the sulphur in phase 1 which is due to dissolution of the gypsum minerals detected by X-ray diffraction (XRD). The sulphur content of the residual phase is mainly immobilised in existing pyrite and marcasite crystals (see iron description).

3.4.4.2   Optimised method for Heselbach sediment samples

The results of the sequential extraction according to *Percival* show that uranium in the sediments mainly exists in the easily available adsorbed or in the organic and sulphidic phases. The amorphous Fe-Mn compounds play a minor role. For clarification of the actual bond, a modified extraction method was chosen which considers these three phases and also considers the sulphidic phase separately from the organic-rich phase. The method applied in the second run is presented in Table 23 where 1 M NH_4NO_3 solution was used for phase 1. This solution adjusted to a pH value of 7 is particularly mild and, in contrast to sodium acetate, does not dissolve any Fe oxides as this could be the case with the Percival method. Accordingly, uranium in this phase definitely exists in an adsorbed form. The amorphous Fe-Mn compounds are already considered in phase 2. As shown before, crystalline Mn-Fe oxyhydroxides are not relevant for the Heselbach sediments and therefore were not further considered. In phase 3, a 0.025M NH4-EDTA solution was used for the extraction of the organically bound elements. As a strong, polydentate ligand, EDTA forms extremely stable complexes with divalent cations and can thus remove uranium, which is bound to organic components, from these. The sulphides are not attacked; they are dissolved in the residual phase.

Table 23: Sequential extraction procedure applied to samples from core HB11-03, SE 2004 (modified according to /ZEI 89/)

Phase	Description	Reactant	Chemical form
1	exchangeable phase	1 M NH_4NO_3 (pH7)	adsorbed
2	easily reducible phase	0.25M NH_2OHHCl in 0.25M HCl (pH6)	bound to Fe oxyhydroxides (amorphous)
3	organic phase	0.025M NH4-EDTA (pH 4.6)	bound to organic matter
4	residual phase	total digestion with H_2O_2 (30%); HNO_3 (65%); $HClO_4$; H_2F_2	in silicates and accessory minerals

To avoid early oxidation of the sediments, extractions of phases 1 to 3 were performed in a glove box. Phase 4 was performed under atmospheric conditions.

Phase1: Adsorbed phase

After weighing of the representative, wet samples (calculation after water content determination), the two original samples selected were mixed with 100 ml 1 M NH_4NO_3 solution (pH 7) and shaken for 24 hours. After that, the solutions were centrifuged at

4500 r.p.m. for 15 minutes and filtrated < 0.45 µm. To avoid precipitations, the filtrate was stabilised with 1 ml HNO_3 (65 %).

Phase 2: Easily reducible phase

The filtrate from phase 1 was mixed with 160 ml 0.25 M NH_2OHHCl in 0.25 M HCl (pH6) and stirred in the water bath at 50°C for 30 minutes. After centrifugation and filtration (see above), the filtrate was available for the next phase.

Phase 3: Organic phase

160 ml of a 0.025 M NH_4-EDTA solution, whose pH value was adjusted to 4.6 with NH_4OH and HOAc, was stirred with the filtrate from phase 2 at 20°C for 90 minutes and then, analogous to the two preceding phases, centrifuged and filtrated.

Phase 4: Residual phase

An adequate fraction (~0,25 g) of the dried and pounded residual sample from phase 3 was subjected to complete digestion with 3 ml H_2O_2 (30 %), 3 ml HF (48 %), 1.5 ml $HClO_4$ (70 %) and 7 ml HNO_3 (65 %). After subsequent concentration and displacement of the acids, the remaining solution was transferred quantitatively in a 100 ml volumetric flask and filled with distilled water to the calibration mark.

Sample description

The sequentially extracted samples from drilling HB11-03 have high uranium contents and both have a considerable content of organic matter (Table 24). With 4.5, the pH value of these sediments is in the normal range of the Heselbach sediments, i. e. despite the nearness of the samples to the surface no oxidation took place, which would have led to a decrease of the pH value.

Table 24: Results from bulk rock analysis of samples from core HB11-03

Depth [m b.g.l.]	Lithology	U [ppm]	Th [ppm]	TOC [%]	S as SO_4 [ppm]	S^{2-} [ppm]	P_{tot} [ppm]	pH sed. [$CaCl_2$]
1.51-1.54	lignite,clay black	1127.8	9.6	28.1	152	12508	682	4.54
2.34-2.37	clay,dense grey-black	1111.4	37.6	16.1	67	2763	413	4.66

Results

The results of the modified sequential extraction are presented in Table 25 and Fig. 44. The evaluation of this method shows that the used, mild extracting agent NH_4NO_3 leaches less than 0.1 % of the total uranium, i. e. only small amounts of the uranium are in the adsorbed phase. This finding is inconsistent with the results obtained by the method acc. to /PER 90/. The assumption that in phase 1 of the first series other readily soluble minerals were dissolved in addition to the adsorbed fraction is confirmed by this result. In phase 2 of the new, modified method, i. e. the amorphous iron-manganese phase, only very small uranium contents were identified (max. 0.34 %). The major part of the uranium is in the residual phase with 92.6 and 96.1 % which is an indication either to secondary uranium minerals or to incomplete dissolution in one of the three preceding phases. Spectroscopic investigations demonstrate the existence of hexavalent uranium phases. Therefore, a formation of secondary, hexavalent uranium minerals would be possible, but thermodynamic calculations with the PHREEQC code show that for the existing geochemical conditions no saturation of U(VI) mineral phases is to be expected. It is therefore more probable that the uranium was not completely extracted from the organic phase by the NH_4-EDTA reactant. Difficulties in the extraction of uranium with EDTA are also described by /SCH 02/. Iron and manganese show different distributions on the phases. While only about 9 % of the iron exists as amorphous form (phase 3), for manganese this phase accounts for 63 %. 35 % of the iron is extractable by EDTA solution, but the major fraction exists in form of iron sulphides which are only dissolved in the residual phase.

3.4.4.3 Conclusions

As already stated, in sequential extrations acc. to /PER 90/, uranium is remarkably easily available in samples HB03-02/2,78-2,82 and HB05-02/6,42-6,46 with more than 65 %. Further, these samples show increased Fe, Mn, Cr, Th and sulphur contents in phase 1. Since analyses with the modified method only show low adsorption of uranium, it can be assumed that in phase 1 of the first series already other phases went into solution when using a 1 M sodium acetate solution (pH 5).

The proven positive correlation of the uranium with divalent iron (see ICP analyses) first indicated a uranium compound with pyrite or marcasite minerals. As in phase 1, however, mineralised pyrite or marcasite minerals cannot be present and,

nevertheless, a correlation with iron is obvious, it is to be assumed that the uranium extracted in phase 1 from these samples exists in combination with an already oxidised, readily soluble iron phase.

Table 25: Element concentrations in [ppm] and [%] in the four extraction phases of samples from HB11-03 (modified extraction method)

Element	Phase	HB11-03/		HB11-03/	
		1,51-1,54	2,34-2,37	1,51-1,54	2,34-2,37
		ppm		%	
U	1	0.30	0.73	0.0	0.09
	2	2.81	2.74	0.2	0.34
	3	52.71	56.56	3.7	7.01
	4	1358.12	746.42	96.1	92.56
Th	1	< 0.009	< 0.009	< 0.02	< 0.02
	2	< 0.009	< 0.009	< 0.02	< 0.02
	3	47.62	10.73	99.9	99.94
	4	< 0.009	< 0.009	< 0.02	< 0.02
Fe	1	13.93	11.72	0.2	n.a.
	2	602.22	n.a.	9.2	n.a.
	3	2337.76	253.11	35.8	n.a.
	4	3585.21	8894.47	54.8	n.a.
Mn	1	2.22	2.96	3.2	n.a.
	2	44.14	n.a.	63.3	n.a.
	3	15.54	3.74	22.3	n.a.
	4	7.87	20.65	11.3	n.a.
S	1	491.23	547.22	2.3	n.a.
	2	272.74	n.a.	1.3	n.a.
	3	1132.92	55.56	5.4	n.a.
	4	19176.05	5504.45	91.0	n.a.

n.a. = not analysed

These two samples are also outstanding due to their low pH value (2.6) and thus differ considerably from the other samples (Fig. 45). The oxidation of the pyrite minerals led to the formation of sulphuric acid and a lowering of the pH value. It is difficult to determine whether these samples have been stored without adequate protection against oxygen or whether oxidation of the sediments already took place in situ.

With simultaneous formation of trivalent iron, the conditions for the formation of jarosite are given (formula 2) which explains the increased iron and sulphur concentrations in phase 1:

$$2Fe^{3+} + 4SO_4^{2-} + 6H_2O + 8H^+ \rightarrow 2HFe_3(SO_4)_2(OH)_6 + 6H^+ \qquad (2)$$
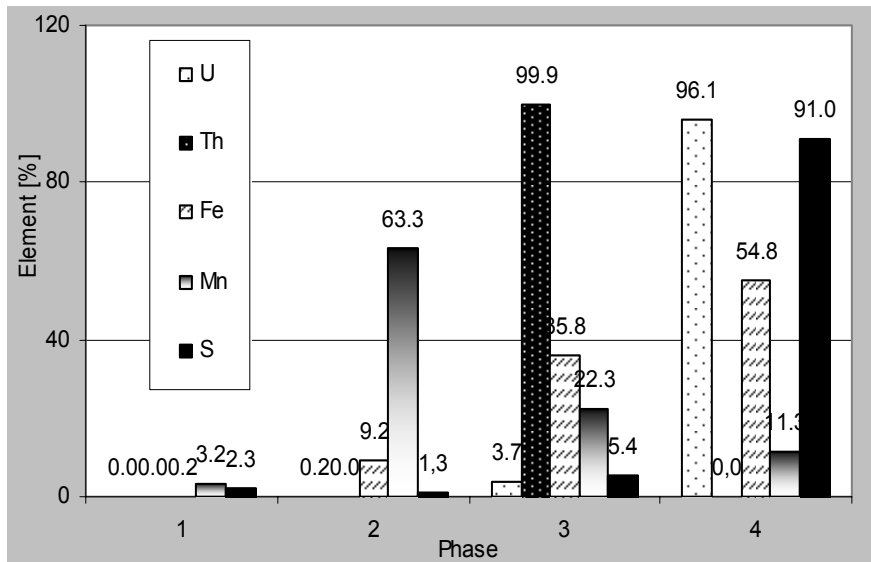
Fig. 44: Element concentrations in [%] in the four extraction phases in sample HB11-03/1,51-1,54 (modified extraction method)

Actually, the existence of jarosite was demonstrated in one of the two samples by X-ray diffraction. For all samples, a strong dependence of uranium accessibility from pH value of the sediments becomes apparent. The more acid the environment, the larger the uranium content in phase 1 and the more easy the remobilisation of the uranium (Fig. 45).
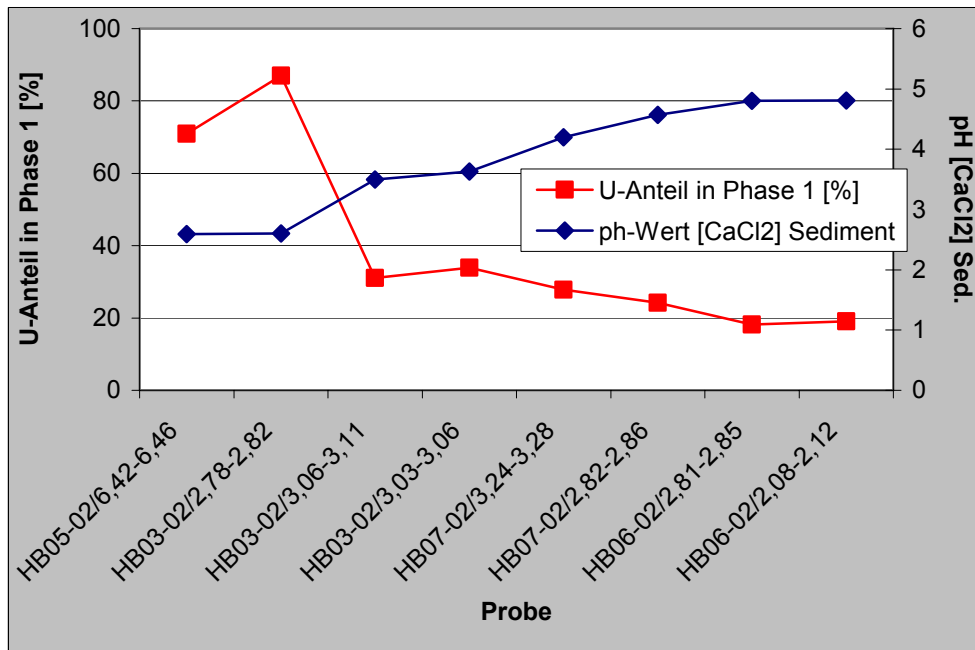
Fig. 45: Uranium distribution in phase 1 of sequential extraction (acc. to /PER 90/) correlated to pH value of the sediments

An indication of uranium adsorption on Mn phases is given, on the one hand, by the also increased Mn content in phase 1 of the first series and, on the other hand, by a good correlation factor (0.65) between U/Mn in clay samples. However, the results obtained by the new modified method showed no correlation with uranium despite a large fraction of amorphous Mn oxyhydroxide phases (63 %). Accordingly, the amorphous Mn and Fe phases are irrelevant as primary uranium enrichment process, only in oxidised samples, a correlation with uranium can be observed.

Coprecipitation processes of uranium with FeS or FeS_2 minerals can also be excluded due to the different uranium and iron distribution as well as negative correlations with sulphur.

As a major chemical form for uranium, the investigations of the first series identified the organic phase. Following investigations with the new modified method did not confirm this result which is probably due to insufficient dissolution of the uranium in the reactant used (0.025 M EDTA solution). A combined evaluation of the results of the first series with spectroscopic investigations suggests the conclusion that the major part of the uranium are uranyl ions which, bound to humic acids, exist finely distributed over the sediment.

4 Hydrological and hydrogeological investigations

In the exogenic cycle, uranium is transported in oxidising waters over large distances as hexavalent species. To be able to understand and judge the flow paths of the groundwater and thus of the uranium transported into Heselbach sediments, knowledge of the local hydrological and hydrogeological conditions is needed. In this chapter, first the meteorological parameters, required for determining the groundwater recharge rate, are evaluated. After that, a description of the groundwater dynamics and groundwater chemistry is given. In addition, the determination of the groundwater age with natural isotopes allows the assessment of the processes over time. All analyses together give a picture of the current hydrological situation which is summarised in form of a hydrogeological model.

4.1 Water balance

The hydrologic cycle of a region can be shown by means of the water balance equation which considers, in addition to climatic factors, also soil conditions, vegetation and height of the water table as input parameters. Basis for the water balance is the groundwater recharge rate. The groundwater recharge describes the access of infiltrated water to the near-surface groundwater body through percolation and depends on the respective water availability. In the humid regions of Europe, precipitation plays a decisive role. Bank filtrates or anthropogenic influences, however, such as irrigation, can be assumed to be negligibly low for the investigation area. Evaporation processes and direct surface discharge minimise the availability of water and are considered in the calculation as loss.

For the quantitative description of the areal groundwater recharge, the most important meteorological data (precipitation, relative humidity and global radiation) were recorded by an own weather station (manufacturer: Thies company) every ten minutes and registered as mean value every half hour in the period from March 2002 to June 2004.

In the following, the different parameters will be explained and calculated for two annual cycles. After that, a quantitative prediction on groundwater recharge for the investigation area is given.

4.1.1 Precipitation

Evaluations of the precipitation and snow measurements show a wet year 2002 with unusually high precipitation in the summer and autumn months June to November (Fig. 46). For the period from March 2002 to March 2003, an average precipitation of 855 mm was measured. By this, the mean annual areal precipitation of the Wackersdorf region of 757 mm/y /MEY 93/ is exceeded. In the second year, with 470 mm/y, the total precipitation was clearly below the annual average. According to DIN 4049, the second year can be categorised as dry year.
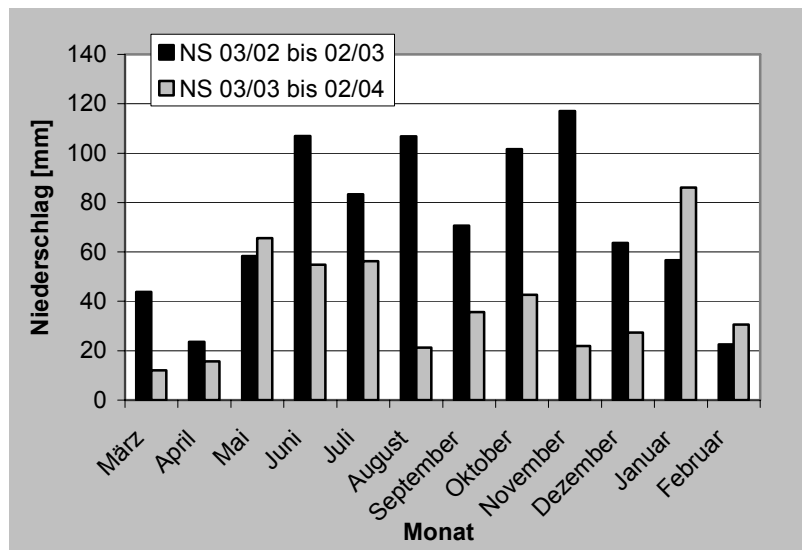
Fig. 46: Monthly precipitation [mm] in the period 03/02-02/03 (black) and 03/03-02/04 (grey) at Heselbach weather station

4.1.2 Evapotranspiration

For a first assessment of the prevailing potential evapotranspiration *ETp* in the Heselbach region, the simplified, empirical calculation method for homogeneous surfaces, low grass cover with good water availability according to Haude /DVW 96b/ was applied. For this method, it is only required to know the relative air humidity and the saturation deficit derived from it as well as the associated air temperature at the time of the highest day temperature (per definition: 14:30 h) (DIN 19685). The calculation method is suitable for a survey of the average monthly sum and trends over many years. Calculation methods that consider the energy balances are better suited for drawing conclusions about the evaporation of individual days or the assessment of areas with vegetation. For this reason, the ETp calculation was subsequently

supplemented by more complex calculation methods of Makking /DVW 96b/ which consider the energy balance in form of the global radiation.

The method according to *Haude* /DVW 96b/ is applied for the calculation of monthly sums of *ETp*. The daily sums of the *ETp* are calculated by means of the saturation deficits of the individual days and the respective factors and summed up over the month. This calculation may yield day values of ETp > 7 mm/d which is improbable in reality for energetic reasons. Such values were reduced to 7 mm/d. The Makking equation /DVW 96b/ is a simplified Penman equation which considers complex physical interactions.

For the summer months, the Haude equation yields slightly increased *ETp* values (Fig. 47). This is due to the low data density. With only one measurement at midday, this time of the day is considered disproportionately high with the Haude approach. With the Makking approach, however, data averaged over 24 hours are considered in the calculations.
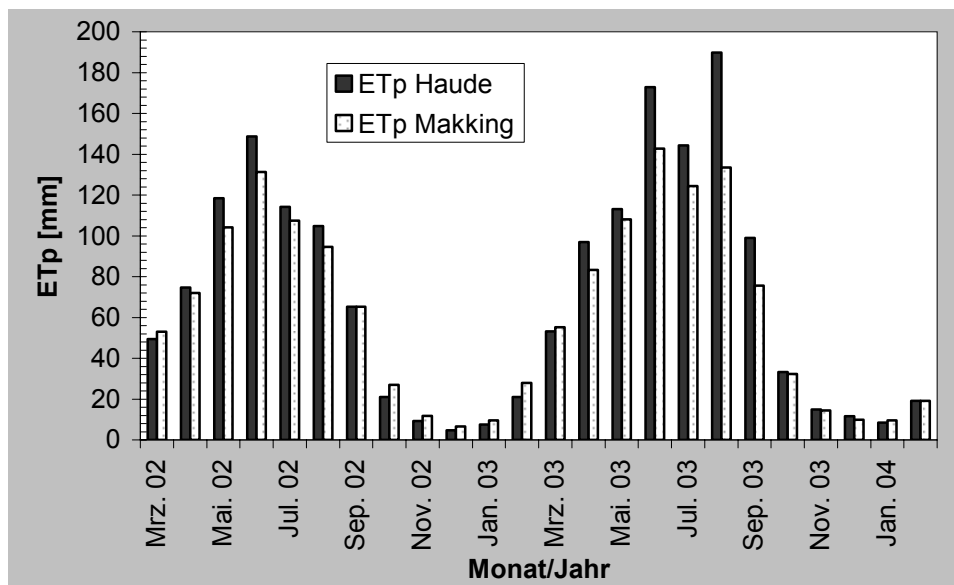
Fig. 47: Potential evapotranspiration (ETp) per month in the project area for the period from March 2002 to February 2004: comparison of Haude und Makking method

The actual evapotranspiration *ETa* varies site-specifically. The investigation area is therefore divided into approximately homogeneous areas and the *ETa* determined separately for different areas. About 75 % of the investigation area consists of coniferous forest, 25 % are sealed areas (Fig. 48).

69
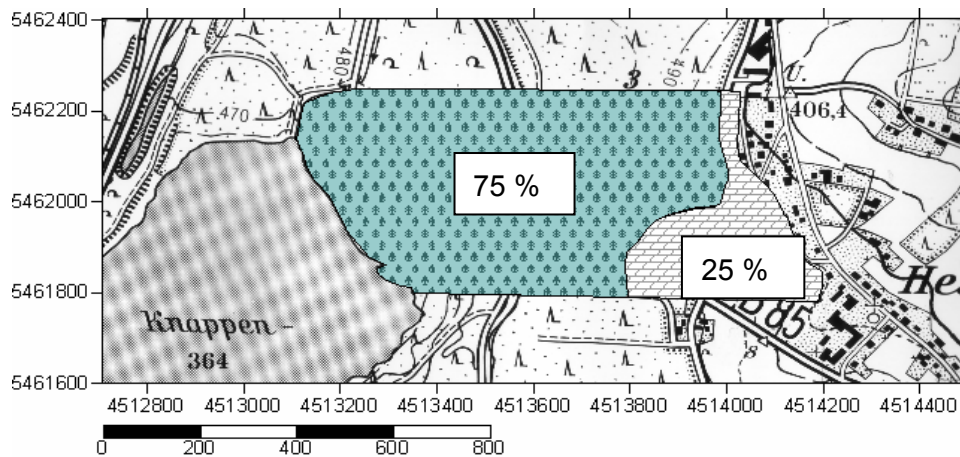
Fig. 48: Partitioning of the investigation area into areas with similar site factor; green = forest area, grey = sealed area

In spring, high groundwater levels and local wetland zones show a soil filled with water up to field capacity. The approach of Renger and Wessolek /REN 90/, which requires such conditions, may therefore be a suitable method to determine the annual evapotranspiration sum of a loose rock area. The main data for evapotranspiration calculated by the described methods and precipitation values at Heselbach are summarized in Table 26.

Table 26: Main climatic data at Heselbach site for the period March 2002 to February 2004

	03/02 - 02/03	03/03 - 02/04
ETp acc. to Haude [mm/y]	739	957
ETp acc. to Makking [mm/y]	710	808
ETa acc. to Renger & Wessolek [mm/y]	709	630
NS (precipitation) [mm/y]	855	470
NS_{So} (summer precipitation) [mm/y]	450	249
NS_{Wi} (winter precipitation) [mm/y]	405	221
T [Ø-°C/y]	9.0	9.9

4.1.3 Discharge

The discharge, divided into surface runoff, interflow and groundwater runoff (DIN 4049 T3), describes the movement of precipitation water after reaching the earth's surface. Since discharge measurements within the project area are not available, the total

annual discharge (mm/y) is estimated by means of the regression equation empirically developed by Liebscher & Keller in 1979 and advanced by /WEN 91/, also considering the soil type and the effectively available water (nFK_{We}).

$$A = 0{,}86 * N_J - 111{,}6 * NS_{So} / NS_{Wi} - 120 * \log(nFK_{We})$$ (2)

with:
N_J = annual precipitation [mm/y];
NS_{SO} = summer precipitation [mm/y];
NS_{Wi} = winter precipitation;
nFK_{We} = available water

Decisive for the groundwater recharge rate of a region is the surface runoff. This water is discharged directly and does not reach the groundwater body. The portion of surface runoff from the total discharge is calculated as follows:

$$A_D = A * 2 * 10^{-6} * (N_J - 500)^{1{,}65}$$ (3)

Table 27: Discharge parameters for the period from March 2002 to February 2003 at Heselbach site

Soil type	A [mm/y]	A_D [mm/y]	Fraction A_D from A [%]
Coniferous forest	407	13.2	3.24
Sealed area	453	14.6	3.22

Table 27 shows that the surface runoff in Heselbach only accounts for 3 % of the total discharge and can be categorised as very low with 14.6 mm/y.

4.1.4   Groundwater recharge

During the vegetation period, the loss of soil water by evapotranspiration is larger than the available precipitation. Thus, in this period, water can only contribute to groundwater recharge in case of extremely strong rainfalls. In winter, however, precipitation dominates so that this period is the actual period of groundwater recharge /DYC 95/.

On the basis of the climate data determined, the water actually available for groundwater recharge can be estimated. Fig. 49 shows a positive water balance for the months August to January during the first investigation year.
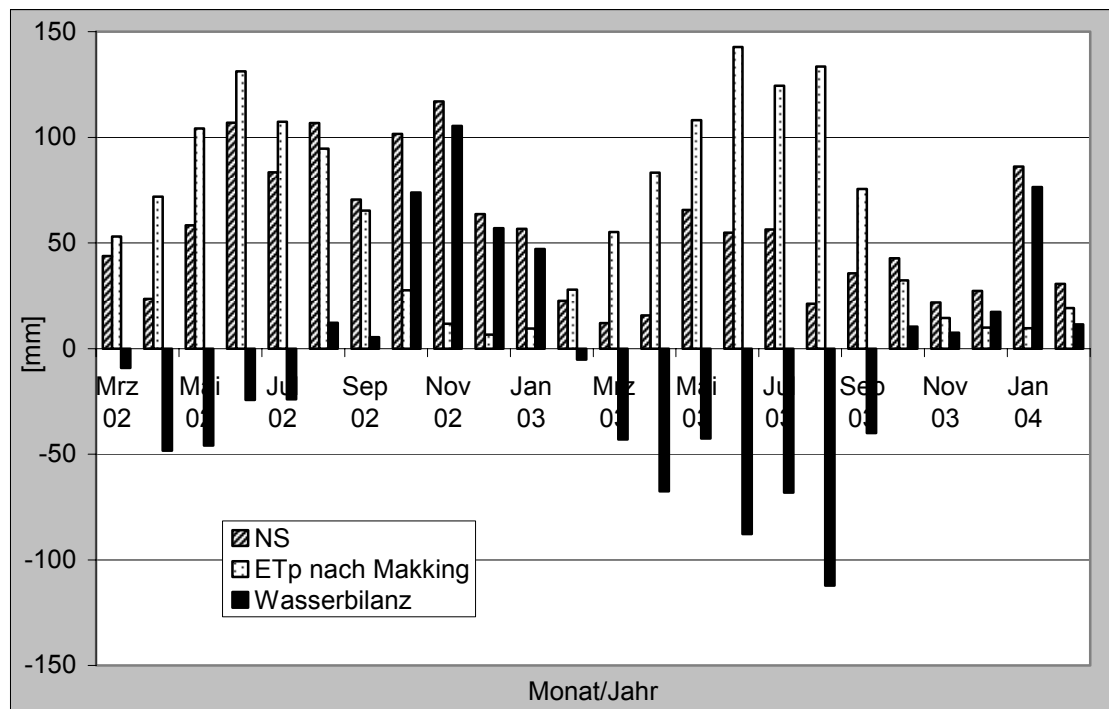
Fig. 49: Monthly precipitation (striped), ETp according to Makking (dots) and resulting climatic water balance (black)

In this respect, it has to be considered that the months August and September have unusually high precipitation due to the extreme precipitation event ("1000-year flood" in several European regions). As shown in the second investigation year, excess precipitation normally only happens in autumn and winter months and results in an increased infiltration.

The groundwater recharge (G) of the total area is calculated according to the water balance equation based on annual precipitation, actual evapotranspiration and the discharge above ground.

$$G = N_J - ETa - A_D \qquad (4)$$

with:
N_J = annual precipitation [mm/y];
ETa = calculated actual areal evaporation [mm/y];
A_D = direct discharge

Since the actual evaporation exceeds the defacto precipitation in the second investigation year, no groundwater recharge rate can be calculated for this period. For the first investigation year, a precipitation excess of 132 mm/y was calculated which corresponds with a groundwater recharge rate of 4.18 l/(s km^2).

72

4.2 Groundwater dynamics

For the description of the flow regime and thus of the uranium transport of a region, the distribution of the relevant aquifers and water-retaining layers have to be known in addition to the hydraulic rock parameters. This chapter describes the hydrodynamic situation of the investigation area as it was determined in situ by means of groundwater level measurements, long-term monitoring of selected groundwater gauges and a tracer test, and the initial concept of groundwater flow movement is verified.

4.2.1 Groundwater levels

Table 28 lists the measured groundwater levels of the individual drillings. The groundwater level variations within a year are most apparent in the up- and downstream area. Well HB01-02 reaches a maximum level difference of 3.07 m, HB10-02 of 2.07 m. On the other hand, drillings from the Tertiary basin, especially the Tertiary rim zone vary only in the range of the maximum air pressure variation of 0.5 m (HB06-02).

Table 28: Ground water levels [m a.s.l.] in the Heselbach area

Drilling		Spring		Summer		Autumn		Winter	
		04/02	04/04	07/02	07/04	10/02	09/03	01/03	01/04
HB10-02	Down-stream	370.22	368.48	369.59	-	368.90	369.10	370.30	368.23
HB09-02	Tertiary basin	-	383.70	383.84	-	383.88	-	-	-
B03-99		384.96	383.33	384.70	382.90	384.59	382.95	385.15	383.43
B02-99		-	-	385.76	-	-	-	386.10	-
HB07-02		385.89	385.54	385.89	-	385.74	-	386.07	-
B01-99		386.26	385.66	385.73	385.48	385.82	385.55	386.23	385.73
HB06-02		386.06	385.73	385.93	385.54	385.78	385.56	386.08	385.68
HB05-02		384.55	384.31	384.40	-	-	-	384.68	-
HB04-02		386.22	385.83	386.05	-	385.97	-	385.17	-
HB03-02		385.69	386.11	385.73	385.78	385.79	385.72	385.87	386.24
HB08-02	Up-stream	387.59	-	386.30	-	-	-	-	-
HB02-02		389.15	388.38	388.94	388.21	388.89	388.42	389.50	387.43
HB01-02		390.49	389.56	390.03	389.35	-	392.38	390.71	389.31
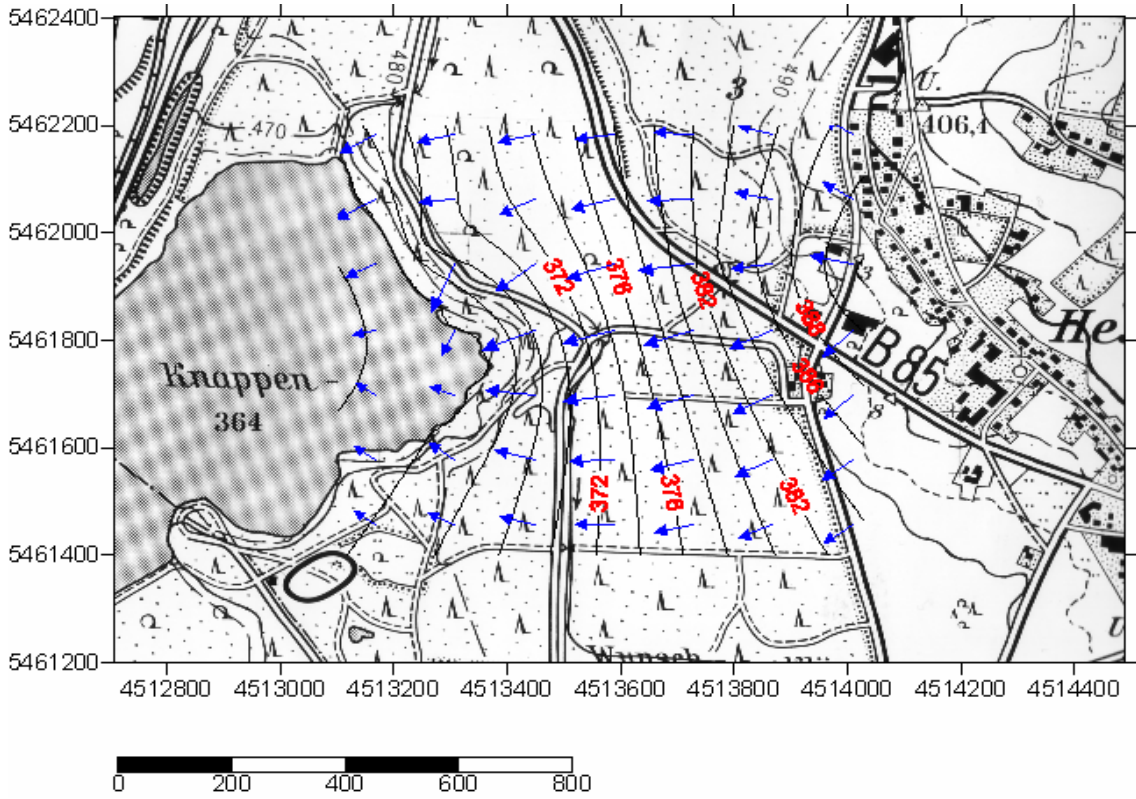
Fig. 50: Groundwater level contour map of Heselbach site at 17.09.2003
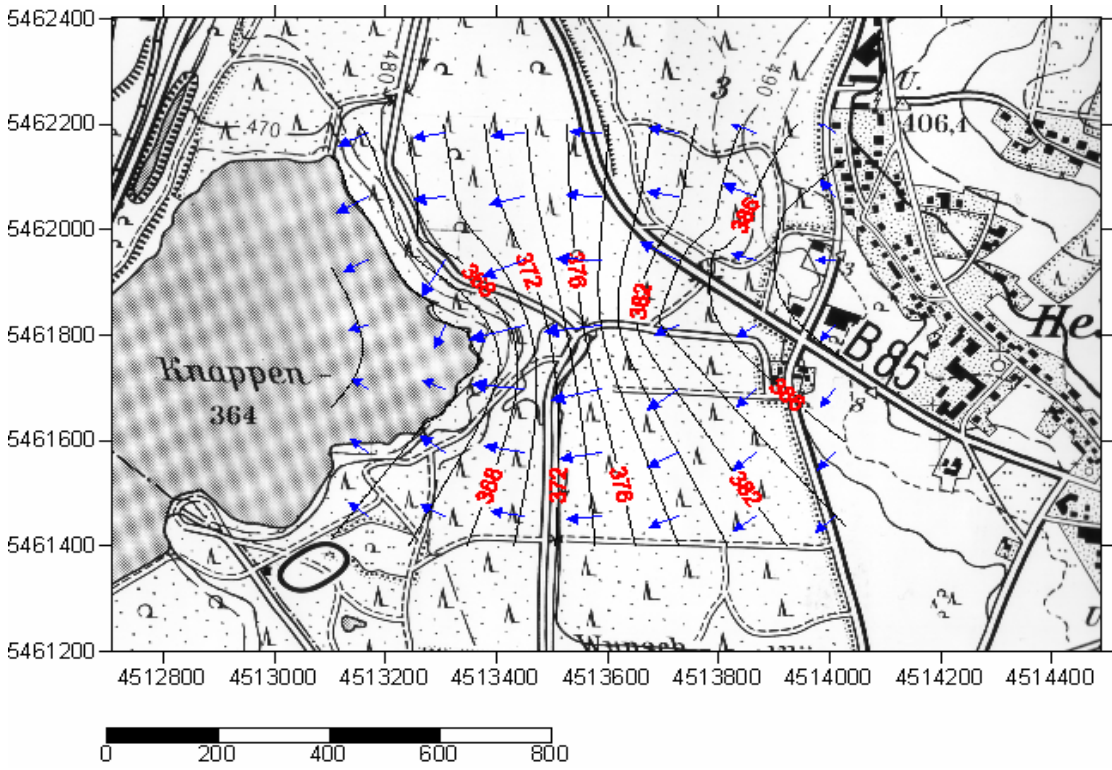
Fig. 51: Groundwater level contour map of Heselbach site at 27.04.2004

74

The groundwater levels measured in different seasons served as a basis for the development of GW-contour maps of the area. In addition to the gauge measurements, fixed data, such as the surface level of lake Knappensee, were considered in the interpolation. A selection is shown in Fig. 50 and Fig. 51.

As indicated by groundwater level measurements and the contour maps, only the area of the Keuper aquifer shows a slight increase in groundwater level after the groundwater recharge phase in winter. In the Tertiary basin, no significant changes of the groundwater levels were observed between autumn and spring.

4.2.2 Pore velocity

The pore velocity can be calculated according to Darcy's law under consideration of the effective pore volume by the following formula:

$$v_a = \frac{v_f}{n_e} = \frac{k_f}{n_e} * J \qquad (5)$$

with:
v_f = Darcy velocity (infiltration velocity);
k_f = hydraulic permeability coefficient;
n_e = effective porosity;
J   = hydraulic gradient

The hydraulic gradient J is calculated from the difference between groundwater levels and their longitudinal distance. A value of 0.024 is taken for the investigation area. The k_f values are based on in-situ slug & bail measurements and for drilling HB11-03 on the determination of the specific permeability in laboratory. All data for effective pore volume are taken from literature /HOE 96/. These yield groundwater pore velocities for the different lithological units in Heselbach, as shown in Table 29.

Table 29: Hydraulic parameters of different lithologic units and flow velocities at the Heselbach site (Bk = lignite, T = clay)

Drilling	Stratigraphy	Lithology	J	n_e [%]	k_f [m/s]	v_f [m/s]	v_a = [m/y]
HB01-02	Keuper	sandstone	0.024	25	1.54E-05	3.7E-07	46.62
B03-99	Tertiary basin	Bk, T	0.024	10	5.12E-06	1.2E-07	38.75
HB04-02	Tertiary basin	Bk, T	0.024	10	3.15E-06	7.6E-08	23.84
HB11-03	Tertiary rim	T, Bk	0.024	5	2.9E-08 - 2.9E-09[*]	6.6E-10 - 6.9E-11	0.44 - 0.04

Within the Keuper aquifer, the groundwater velocity is 46.6 m/y. Strongly argillised sediments at the rim zone (HB1-03), however, show a low velocity of a few cm to 0.4 m/y. For less argillised sediments within the lignite horizon, 23 to 38 m/y has been determined as pore velocity. It has to be taken into account that this value strongly varies according to the seam formation and thickness. Further, this estimation is based on in-situ slug & bail measurements and not on more accurate measurements of the clay in laboratory. Therefore, these k_f values are to be understood as upper reference values under consideration of potential disturbances of the annular space.

4.2.3   Tracer test

For further clarification of the hydraulic properties of the uranium-containing Tertiary rim, a tracer test was performed in well HB11-03. The filter length of this well is 1 m and is exclusively restricted to the lignite horizon. Surface water inflow and groundwater discharge was prevented by clay barriers. NaCl p.a. was used as tracer. The time of arrival of the tracer in detection well HB06-02 at a distance of 1.1 m was continuously recorded by CTD data logger.
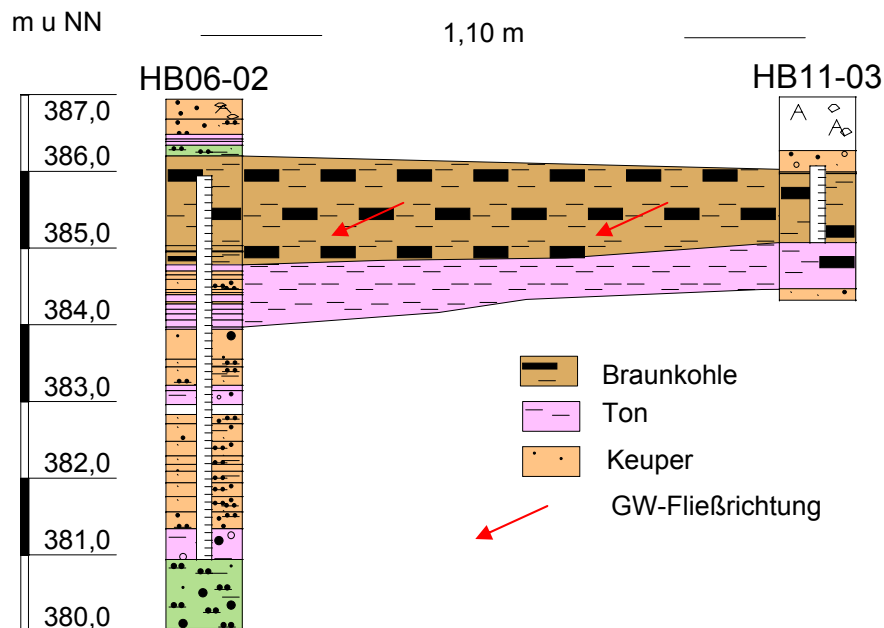
Fig. 52:   Tracer test: lithology and filter horizon of injection well (HB11-03) [input of 8 l saturated NaCl solution] and detection well (HB06-02); GW-flow direction is indicated by red arrows

Before injection of the tracer, the natural groundwater level was measured and water extracted by subsequent pumping was kept for chemical analyses. Then, the tracer was injected into the groundwater-saturated zone by means of a PVC tube. 8 litres of saturated NaCl solution, corresponding to 2.635 kg salt, were injected into the well. The initial piezometric head was not exceeded to avoid that the tracer intrudes into the unsaturated zone and remains there. Injection and start of the tracer test took place on 14.01.2004. Until 13.07.2004, the specific electrical conductivity was recorded hourly.

Within the test period (app. half a year), the injected tracer did not reach detection well HB06-02 at a distance of 1.10 m. The recorded conductivity data strongly vary between 200 µS/cm and 1000 µS/cm (mean value 450 µS/cm) but did not show a peak.
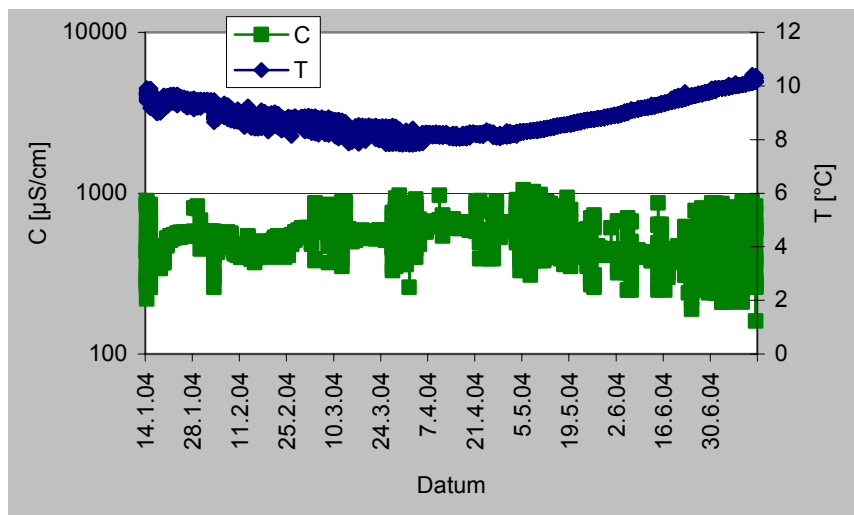
Fig. 53: Specific electrical conductivity [C] (green) and temperature [T] (blue) in detection well HB06-02 in the period 14.01.04 - 14.07.04

Conclusion

The pore velocity of the groundwater within the lignite layer is considerably lower than expected. 2D transport calculations in advance of the test, using k_f values of the slug & bail tests as data basis, initially calculated the arrival of the tracer within the first three weeks. Since after six months, no clear peak was detected, it is to be assumed that the k_f values used were definitely too high. The measurement of the specific permeability of the clay sample HB11-03, performed in parallel to the tracer test, confirms the result of the tracer test. Under the assumption of groundwater moving with only 0.44 m/y, the tracer would only reach the detection well after 2.5 years, i. e. in July 2006. The groundwater conditions at the Tertiary rim therefore can't be regarded as an aquifer. An almost stagnant groundwater is more likely. This assumption is confirmed by tritium analyses and by small groundwater level variations.

4.3   Groundwater chemistry

Uranium transport in groundwater is dependent on its physical/chemical properties. Of special importance is the prevailing redox environment, but also ions like CO_3^{2-} may promote a complexation of uranium and keep it in solution. The chapter "Groundwater chemistry" contains the results of on-site measurements as well as lab-analyses and characterises the recent chemical groundwater environment regarding a potential uranium transport at the site.

4.3.1   On-site measurements

All groundwater samples were taken by pumping with a standard submersible pump (Comet, 12 Volt). Pumping was continued until stability of the electrical conductivity. Subsequently, the environmental parameters of the water were determined in a flow cell. In addition, organoleptic analyses and photometric determinations of iron and sulphur were performed. Temporarily, a 1" oxygen probe was available for in-situ measurements. In July 2004, it was also possible to insert a 4" multiparameter probe into three additional wells in the vicinity, owned and operated by E.ON company. For the assessment of the chemical environment parameters, the following on-site measurements were performed which will be addressed separately.

1) organoleptic analyses

2) pH, T [°C], C [µS/cm], redox [mV]

3) O_2 [mg/l]

4) Fe_{tot}, Fe^{2+}, SO_4^{2-}, S^{2-} [mg/l] (photometric measurements)

5) in-situ measurements with a multiparameter probe

Altogether, eight measurement campaigns were performed. Samples were taken from the drillings according to interests. The main groundwater parameters are summarised in Table 30.

Regarding the organoleptic analyses, clear distinction is to be drawn between the Keuper drillings and the Tertiary drillings. The Keuper groundwater is characterised by its mainly clear and sometimes milky, only slightly yellowish colouring and its neutral smell.

Table 30: Main groundwater parameters (on-site measurements)

Drilling	Stratigraphy	Date	pH	T [°C]	C [µS/cm]	Redox [mV] *	O$_2$ [mg/l]	Fe$_{tot}$ [mg/l]	Fe^{2+} [mg/l]	SO$_4^{2-}$ [mg/l]	S^{2-} [mg/l]
HB01-02		18.04.02	5.52	10.5	420			0.09	0.03	71	0.014
		11.07.02	5.58	11.0	284	395.4	1.12	1.43	0.20	20	
		15.09.03	6.12	-	308	248.6	-	0.08	0.07	-	0.013
		13.01.04	5.08	7.3	280	>399.9	-	-	-	-	-
		15.07.04	5.08	12.8	-	300.0	-	-	-	-	-
HB02-02	Keuper upstream	18.04.02	5.60	12.1	146			0.29	0.07	140	0.066
		08.07.02	5.47	9.0	140	380.1	2.34	1.12	0.12	38	
		14.10.02	5.21	11.1	269	287.6	2.96	NWG	65	0.026	
		22.01.03	5.31	8.0	152	334.8	0.70	-	-	63	0.020
		07.04.03	5.89	7.8	145	-	0.23	0.06	0.06	41	0.055
		17.09.03	6.16	-	252	76.8	-	0.08	0.04	59	0.012
		15.07.04	5.49	11.1	-	135.2	-	-	-	-	-
B01-99	Tertiary basin	16.04.02	5.25	8.9	665						
		11.07.02	5.12	9.3	456	334.8	1.40	3.30	0.18		
		15.10.02	5.12	10.7	448	365.8	1.83	0.13	0.14	80	0.453
		21.01.03	5.61	4.9	443	>399.9	2.40	0.44	0.36	48	0.114
		08.04.03	5.42	8.8	433	-	1.97	0.28	0.28	145	0.084
		17.09.03	5.55	9.2	438	338.7	-	0.10	0.02	80	0.013
		14.07.04	5.39	15.7	-	-	-	--	-	-	--
B02-99	Tertiary basin	10.07.02	5.28	9.3	421	323.5	3.72	1.08	0.14	100	-
		21.01.03	5.27	5.2	431	335.8	4.66	0.12	0.08	90.0	0.032
B03-99	Tertiary basin	16.04.02	6.35	9.8	392						
		10.07.02	5.41	11.4	390	354.7	5.26	0.50	0.0	60	
		21.01.03	5.43	4.2	398	>399.9	3.65	0.02	0.01	90	0.019
		18.09.03	6.91	-	442	24.9	-	0.10	0.08	133	0.020
		14.01.04	5.18	6.8	405	371.5-	-	-	-	-	-
		15.07.04	5.40	13.7	-	316.2	-	-	-	-	-
HB03-02	Tertiary rim	16.04.02	5.49	10.2	283						
		09.07.02	6.24	10.2	359	182.3	0.44	0.13	0.13	32	
		15.10.02	5.96	13.7	267	272.8	4.34	0.04	0.0	66	0.061
		20.01.03	5.59	9.1	296	278.0	0.30	0.22	0.04	37	0.058
		08.04.03	6.61	7.3	376	-	0.12	0.12	0.10	43	0.015
		17.09.03	7.27	-	552	263.0	-	0.07	0.01	65	0.015
		14.01.03	7.07	6.2	545	206.7	-	-	-	-	-
HB04-02	Tertiary rim	16.04.02	5.40	11.1	600						
		09.07.02	4.96	9.3	438	282.4	0.68	0.41	0.01	> 75.0	
		08.04.03	5.42	8.6	443	-	1.33	0.14	0.11	130	0.206
HB05-02	Tertiary rim	17.04.02	5.89	8.9	497						
		11.07.02	5.22	9.2	453	382.6	3.06	1.68	0.64		
HB06-02	Tertiary rim	09.07.02	5.14	9.8	547	301.2	1.34	3.30	0.29	66	
		15.10.02	4.99	12.9	432	294.8	1.17	0.12	0.02	63	0.067
		08.04.03	5.47	7.2	449	-	1.47	0.23	0.18	145	-
		17.09.03	5.34	-	474	300.3	-	0.01	0.0	105	0.015
		13.01.04	5.20	9.5	383	243.2	-	-	-	-	-
		15.07.04	5.54	14.9	-	319.0	-	-	-	-	-
HB07-02	Tertiary basin	17.04.02	6.05	9.8	606						
		10.07.02	5.20	9.1	439	> 399	2.18				
		16.10.02	5.12	11.0	445	278.3	2.53				
		09.04.03	5.47	-	439	-	2.34	0.43	0.40	130	0.118
HB09-02	Tertiary basin	16.04.02	6.21	6.8	465						
		10.07.02	5.90	9.1	570	37.6	0.06				
HB11-03	Tert. rim	14.01.04	6.90	-	-	250.0	-	-	-	-	-
HB10-02	Down-stream	15.04.02	5.57	11.5	930			33.22	9.36	536	0.078
		10.07.02	5.60	9.9	1040	-10.2	0.05	40.38	16.45	600	
		16.10.02	5.60	11.1	1011	27.7	0.12	27.60	11.05	420	0.510
		22.01.03	5.67	8.8	878	-34.0	0.11	55.75	44.0	630	0.270
		18.09.03	6.84	-	1254	94.7	-	47.50	26.4	660	0.240

*) values of on-site measurements related to Pt-Ag/AgCl electrode; for standardisation on standard hydrogen electrode app. 210 mV have to be added

The water from lignite-containing Tertiary drillings is brown to dark brown, strongly milky with small suspended coal particles. The H_2S smelling identified in the downstream drilling HB10-02 at lake Knappensee results from degradation of organic matter (lignite seam) and confirms reducing conditions in this drilling. The on-site parameter sets were determined with a WinLAB electrode measurement set directly beside the borehole(s). With 140 to 308 µS/cm, the specific electrical conductivity in the Keuper drillings is in the range of low-mineralised fresh groundwater /HUE 94/. The drillings at the Tertiary rim show a mean conductivity of 260 to 600 µS/cm, and the downstream drilling HB10-02 clearly higher ion concentrations (878 to 1254 µS/cm) which is, on the one hand, due to an increased sulphide concentration by degradation processes within the lignite seam and, on the other hand, due to the backfill material (Al-Ca rich slags, lignite fly ash).

Alltogether, the redox measurements indicate oxidising conditions even at the Tertiary rim (lignite seam). Well HB10-02 with the deepest filter position represents the lowest Eh values. The pH values of the Keuper groundwaters vary between 5.1 and 6.2. The values determined correlate with the pH value of mixed water analyses of the Middle Burgsandstein cited in literature (pH 6.26) /MEY 98/. The pH value of the Tertiary drillings is generally below 6. In this respect, a variation between 4.87 up to 5.96 was observed. Since performance of the pavement work (spring 2003) an increased pH value (up to 7.27) was reached in rim well HB03-02. It is to be assumed that this increased pH value can be attributed to the influence of the backfill material used (lime gravel). In general, surface waters have pH values > 6. The border area of the lake Knappensee itself is slightly acid with pH value of 6.12; in a creek located in the upstream zone, the environment is almost neutral (6.82).

While in the Keuper drillings carbonic acid is the dominating acid, a large fraction of organic acids is to be expected in the Tertiary drillings due to the decomposition of organic matter (in the existing acid environment mainly with humic and fulvic acids). The oxygen content was determined by means of a 1" in-situ data logger (van Essen company). The O_2 contents of the drillings vary between 0.05 and 5.26 mg/l. S of the interstate road B85, reducing conditions (O_2 content between 0.05 and 0.12) in drillings HB09-02 and HB10-02 are dominating. These drillings are characterised by a relatively thick covering with backfill material, which also protects the groundwater. N of B85, in the uranium-containing rim area, the oxygen contents vary between 0.12 and 5.26 mg/l. Due to the nearness to the surface, oxygen enters the groundwater system in this area at least temporarily.

For photometric mesurements, a portable spectrophotometer (Hach company) was used: until July 2002 unfiltrated and from October 2002 filtrated samples (< 0.45 µm). This separation of sediment particles led to a considerable reduction of the overall concentrations. So, e. g., the iron content in the upstream drilling was temporarily below the detection limit. The total iron concentrations are between 0.02 and 3.3 mg/l, the Fe^{2+} content varies between 0.02 and 0.64 mg/l. The downstream drilling HB10-02 represents an exception. Here, the maximum total iron content is 55.8 mg/l due to a mixture of fly ash from lignite and backfill material, resulting in more reducing conditions. Accordingly high is the Fe^{2+} content with 44 mg/l. The iron contents of the samples taken in September 2003 (presented in Fig. 54) clearly show an oxidising environment at the Tertiary rim wells. With increasing distance from the rim towards the centre of the basin, the filter depth increases continuously and the Fe^{2+} content increases from 14.2 to 75 % of total Fe (Fig. 54).
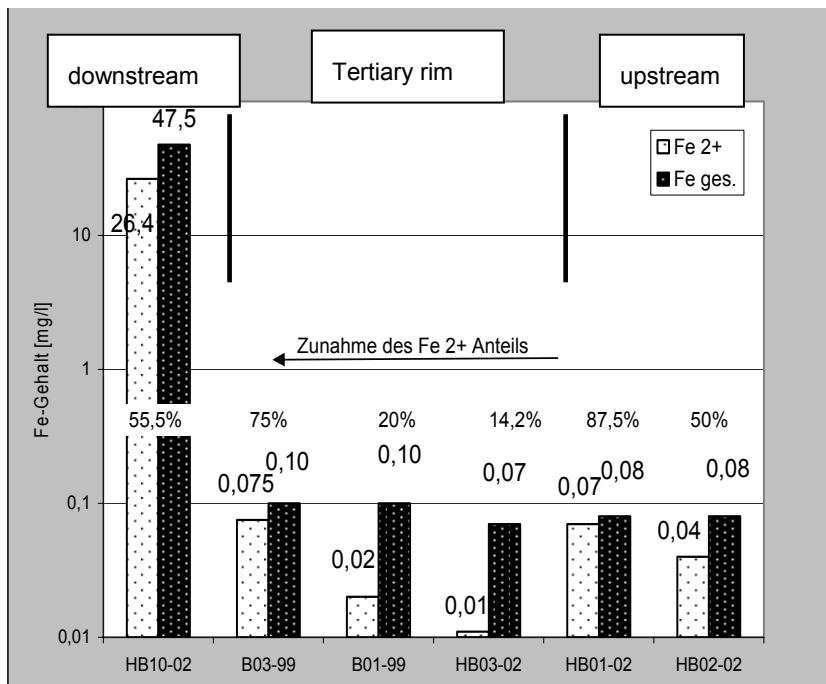
Fig. 54: On-site Fe content of groundwater in Heselbach wells in Sep. 2003 detected by a portable spectrophotometer; black bars = Fe_{tot}, white bars = Fe^{2+}; red numbers = Fe^{2+} fraction [%] of total Fe

Fig. 55 displays the oxidised sulphur (SO_4^{2-}) in comparison with the reduced sulphur (S^{2-}). It becomes evident that nearly the whole fraction of sulphur exists in the oxidised form.
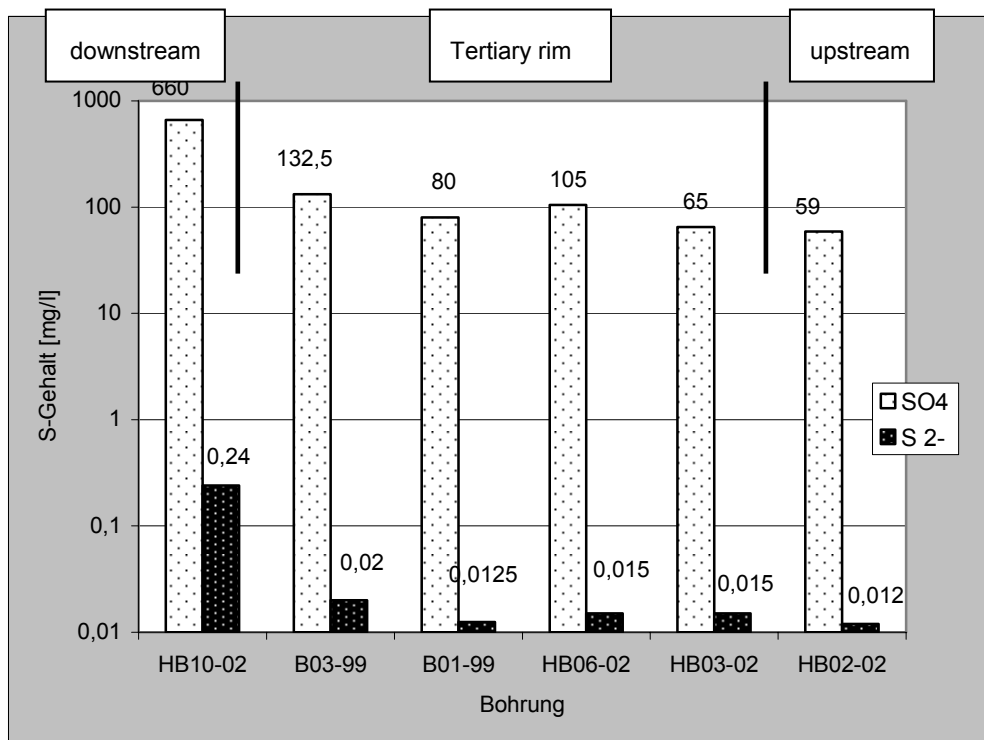
Fig. 55: On-site detected S content of groundwater in Heselbach wells in Sep. 2003 (white bars = SO_4^{2-}; black bars = S^{2-})

The high sulphate content of 65 - 133 mg/l in the Tertiary rim wells can be explained by oxidation processes of pyrite. Further, high sulphate concentrations are reached by degradation of organic matter. Under reducing conditions, this may also result in the formation of HS^- and H_2S, as is the case in the downstream well HB10-02. The very high sulphate content of 660 mg/l in this well is also to be explained by addition of gypsum-containing ashes during backfilling.

In four wells, in-situ measurements were performed with a multiparameter probe (UIT Dresden) (Table 31). One of these wells (HB11-03) is located within the investigation area itself, three other wells provide data from the surrounding area.

Table 31: Groundwater parameters (measured in-situ with a multiparameter probe) from Heselbach site and surrounding area

Drilling	Date	Lithology	Conditions	T [°C]	pH	Eh [mV][*)
SL8	15.07.04	sand	undisturbed / upstream	9.22	6.08	484.3
ST16	16.07.04	clay lignite	disturbed / Tertiary basin	10.26	5.61	317.1
HB11-03	14.07.04	clay lignite	disturbed / Tertiary rim	14.79	5.92	321.9
Bk6a	16.07.04	clay lignite	low disturbed / Tertiary basin	10.01	8.59	-17.5

[*)Eh values are related to standard hydrogen electrode

From the data obtained by in-situ measurements it can be concluded that only wells in lignite, drilled down in a low disturbed area, show slightly negative Eh values (-17.5 mV) and thus clearly a reducing environment. Drillings in disturbed areas and drillings at the rim indicate oxidising conditions (above 300 mV).

4.3.2   Laboratory analyses

The main and trace element analyses were performed at the GRS laboratory, using ICP-MS or ICP-OES according to the respective element. Carbonate was determined by titration, and the concentrations of phosphate, nitrate and ammonia by photometry. The analysis of the TC, TIC, DOC contents was performed with a C-mat 5500 analyser (Ströhlein GmbH & Co). The elements uranium and thorium were analysed at the geochemical laboratory of Prof. Zachmann (TU Braunschweig) with ICP-MS.

The chemism of selected groundwaters is presented exemplary in Table 32 for the sampling campaign January 2003.

Uranium and thorium contents

The uranium and thorium contents of filtrated groundwaters (< 0.45 µm) are listed in Table 33. In the upstream zone (HB01-02, HB02-02 and SL8), the uranium and thorium contents vary between 0.01 and 1.7 ppb. In general, the uranium content of well HB02-02 is a little higher than in HB01-02. Very variable, however, well HB03-02 at the Tertiary rim reacts. This well located directly in the transition area to the Keuper, the uranium content varies by two orders of magnitude. The thorium concentrations, however, remain constant. Already at a distance of 25 m, in drilling HB06-02, both the uranium and the thorium contents are again in the order of magnitude of the upstream concentration. Further towards the former open pit mining, the concentration decreases rapidly. In downstream well HB10-02, the uranium concentration is further reduced.

Table 32: Results from groundwater and surface water analyses (Jan. 2003) [mg/l]

Drilling/element	B01-99	B02-99	B03-99	HB02-02	HB03-02	HB10-02	HB-creek	Knappen-see
Si< 0,02µm	8.78	8.79	8.56	8.04	8.46	9.69	n.b.	n.b.
Cl	62.11	51.68	74.08	0.748	44.04	10.35	33.27	23.21
TC	21.9	21.8	21.9	20.5	15.2	42.8	n.a.	n.a.
TIC	13.2	15.3	4.5	14.6	10.4	33.3	n.a.	n.a.
TOC	8.8	6.5	21.5	5.9	4.8	9.5	n.a.	n.a.
DOC	9.05	7.88	9.85	6.05	38.2	11 .4	23.7	n.a.
CO_2	119.3	104.3	65.8	90.0	60.2	263.5	n.a.	n.a.
$HCO3^-$	15.31	12.21	10.68	15.08	14.95	58.03	n.a.	n.a.
$SO4^{2-}$ (calc.)	92.44	88.16	78.71	54.02	32.1	496.6	398.7	40.29
Ca	50.46	45.5	45.7	18.26	28.98	150.4	141.4	37.84
K	8.93	9.22	10.77	2.62	3.46	8.85	11.02	8.07
Mg	9.97	8.95	9.16	3.66	4.84	21.22	14.24	6.38
Na	14.93	15.93	13.80	1.57	5.76	3.62	17.54	10.98
$NH4^+$	0.877	1.012	0.970	0.852	0.628	0.196	0.246	0.042
$NO3^-$	30.13	34.71	44.95	4.409	17.02	n.b.	5.188	29.32
$PO4^{3-}$	n.b.	n.b.	n.b.	n.b.	n.b.	n.b.	n.b.	n.b.
Al	0.37	0.267	0.2	0.12	0.15	0.4733	0.7167	0.21
Ba	n.b.	n.b.	n.b.	0.02	0.299	n.b.	n.b.	n.b.
B	n.b.	n.b.	n.b.	n.b.	n.b.	n.b.	0.19	n.b.
Fe	n.b.	n.b.	n.b.	n.b.	n.b.	73.42	0.823	0.123
Mn	0.27	n.b.	0.303	n.b.	0.235	4.25	0.907	0.079
Ni	n.b.	n.b.	n.b.	n.b.	n.b.	n.b.	n.b.	n.b.
Zn	0.233	0.237	0.19	n.b.	n.b.	n.b.	n.b.	n.b.
Ti	0.11	0.112	0.149	0.073	0.058	0.559	0.561	0.083
V	n.b.	n.b.	n.b.	n.b.	n.b.	n.b.	n.b.	n.b.
Cr	n.b.	n.b.	n.b.	n.b.	n.b.	n.b.	n.b.	n.b.
Co	n.b.	n.b.	n.b.	n.b.	n.b.	n.b.	n.b.	n.b.
Cu	0.391	n.b.	n.b.	n.b.	n.b.	n.b.	0.143	n.b.
Sr	0.117	0.114	0.116	0.044	0.085	0.448	0.514	0.082
Cd	n.b.	n.b.	n.b.	n.b.	n.b.	n.b.	n.b.	n.b.
Sb	n.b.	n.b.	n.b.	n.b.	n.b.	n.b.	n.b.	n.b.
La	n.b.	n.b.	n.b.	n.b.	n.b.	n.b.	n.b.	n.b.
As	n.b.	n.b.	n.b.	n.b.	n.b.	n.b.	n.b.	n.b.
Pb	n.b.	0.701	n.b.	n.b.	0.011	n.b.	0.046	n.b.
Th	0.00027	0.00023	0.0002	0.00018	0.00019	0.00036	n.a	n.a.
U	0.00105	0.00046	0.00013	0.00069	0.00109	0.0001	n.a.	n.a.
iodide	2.15	2.2	1.86	2.60	0.73	14.49	n.a.	n.a.

n.b. = below detection limit, n.a. = not analysed

Uranium and hydrogen carbonate contents

To clarify the question in which form uranium is transported in the Heselbach groundwater, carbonate analyses were performed additionally, starting in October 2003 (Table 34). The Keuper groundwaters contain 4 - 35 mg/l HCO_3^- which corresponds

with the background value of the Burgsandstein. Groundwater samples of the Tertiary basin are in the range of 7 - 58 mg/l. With a maximum of 348 mg/l, drilling HB03-02 at the rim border clearly deviates from it. In this drilling, already fixed uranium can be remobilised and go into solution preferentially as $UO_2CO_3^0$ (Fig. 56). Under the existing geochemical conditions (max. 348 mg/l HCO_3^- and O_2 contents up to 4.3 mg/l), the uranium concentration increases up to 134 ppb in drilling HB03-02.

	HB06-02	B03-99	B01-99	HB03-02	HB01-02	HB02-02
■ HCO3 Sep.03	14,53	9,945	11,35	330,5	3,97	35,02
□ CO2 Sep.03	109,7	77,64	105,8	20,2	79,31	50,88
▨ U [ppb]	1,09	0,1	1,02	51,89	0,13	1,46
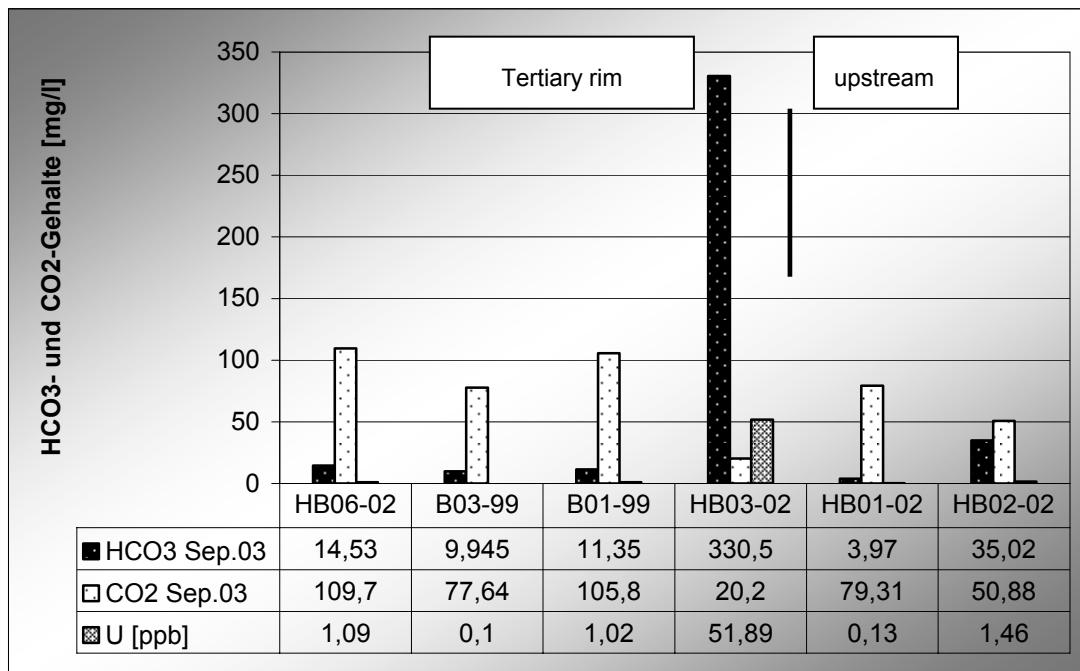
Fig. 56: Bicarbonate, CO_2 [mg/l] and uranium [ppb] concentrations in groundwaters from Heselbach wells, September 2003
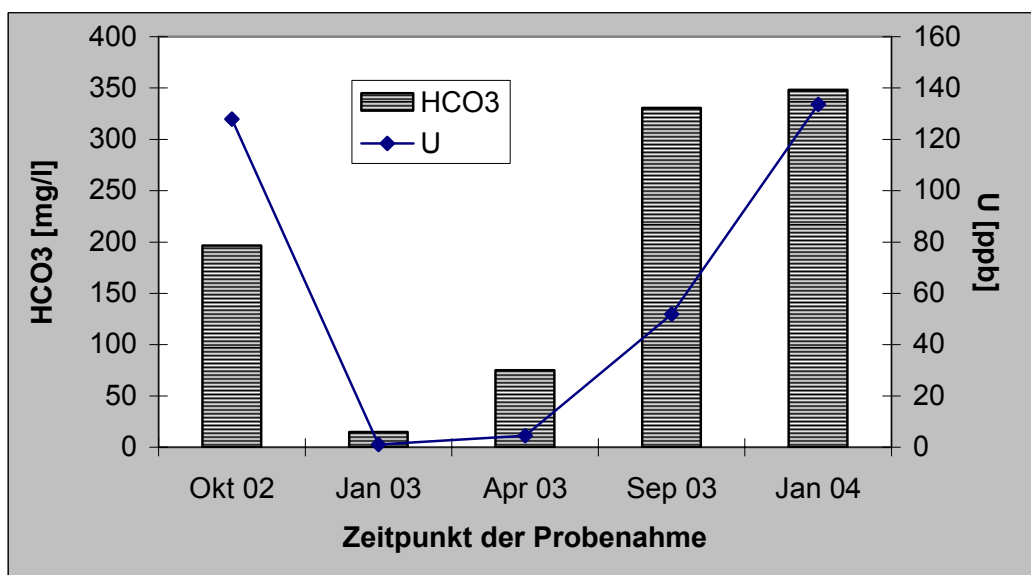
Fig. 57: Uranium und bicarbonate concentrations in well HB03-02 at different dates

The increased CO_2 contents in the Heselbach groundwaters could be due to degradation processes in the coaly sediment layers.

In addition to the standard carbonate analyses, the concentration of the dissolved organic carbon (DOC) in groundwater was determined (Fig. 58). In nature, dissolved humic substances account for 60 - 90 % of the DOC content in groundwaters. Due to their tendency to form strong complexes with morevalent cations, they are of particular interest for the uranium transport.
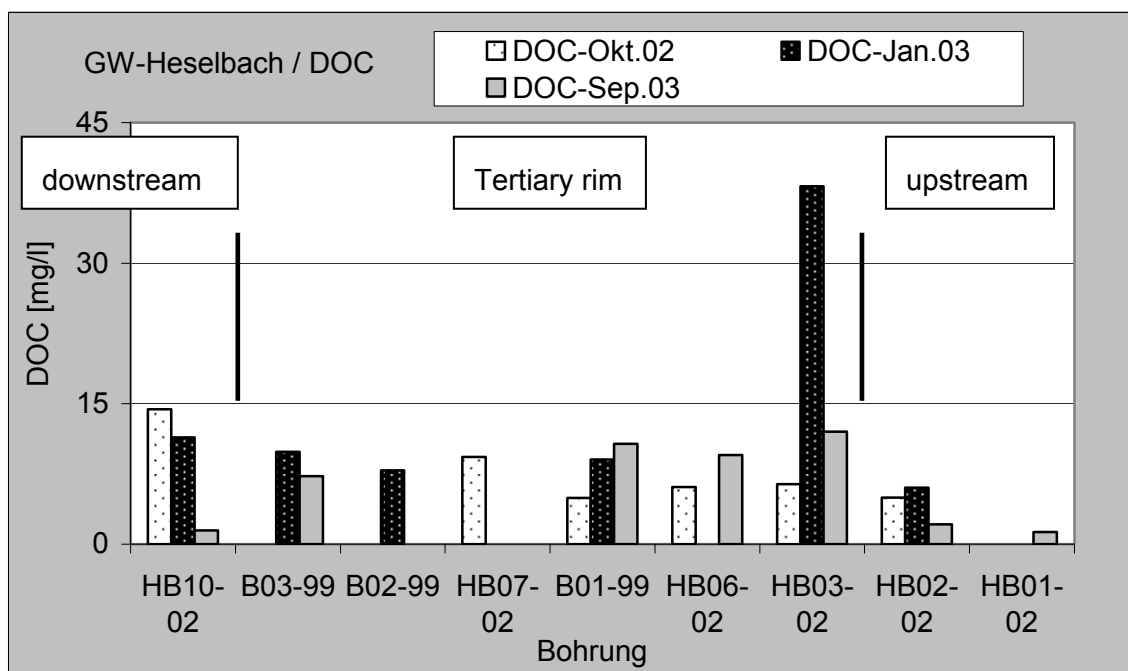
Fig. 58: DOC content in groundwaters from Heselbach wells

The DOC contents of the groundwaters are in the range of 6.05 to 14.4 mg/l. This corresponds with the content of natural groundwaters in or adjacent to humus-containing sediment layers. The unusually high DOC concentration of well HB03-02 in January 2003 (38.2 mg/l) was not confirmed by repeated measurements, but corresponds with high DIC value for the same sample (cf. Fig. 56). This is interpreted as additional indication for a singular degradation process (anthropogenic origin).

Table 33: Uranium and thorium contents [ppb] in groundwaters and water from a detention pond at Heselbach; PL = Pond Lohbauer

Well	HB10-02	B03-99	B02-99	HB07-02	B01-99	HB04-02	HB06-02	HB11-03	HB03-02	HB01-02	HB02-02	SL8	Bk6a	PL
Sampling date	^{238}U [ppb]													
Oct 02	0.35			0.81	1.25		1.31		127.88		1.73			
Jan 03	0.10	0.13	0.46		1.05				1.09		0.69			
Apr 03				0.17	3.19	0.18	0.39		4.47		0.26			
Sep 03	0.10	0.10			1.02		1.09		51.89	0.13	1.46			1.87
Jan 04		0.11			2.22		0.66	1.05	133.58	0.08				
Jul 04		0.34					0.66	10.75		0.01	0.41	0.20	0.93	
	^{232}Th [ppb]													
Oct 02	0.74			0.01	0.21		0.45		0.28		0.26			
Jan 03	0.38	0.20	0.23		0.27				0.19		0.18			
Apr 03				0.08	0.24	0.11	0.09		0.11		0.12			
Sep 03	0.12	0.08			0.14		0.09		0.14	0.09	0.09			0.78
Jan 04		<0.01			0.16		0.03	0.41	0.02	0.04				
Jul 04		<0.01					<0.01	<0.01		<0.01	<0.01	<0.01	<0.01	

Table 34: Bicarbonate und CO_2 concentration in groundwaters from Heselbach wells

Well	HB10-02	B03-99	B02-99	HB07-02	B01-99	HB04-02	HB06-02	HB11-03	HB03-02	HB01-02	HB02-02
Sampling date	HCO_3 [mg/l]										
Oct 02	39.48			10.25	12.45		8.24		196.50		9.89
Jan 03	58.03	10.68	12.21		15.31				14.95		15.08
Apr 03				12.64	8.60	6.96	9.95		75.24		9.76
Sep 03		9.945			11.35		14.53		330.50	3.97	35.02
Jan 04		11.11			33.32		15.93	43.75	348.20	16.29	
Jul 04											
	CO_2 [mg/l]										
Oct 02	248.20			129.60	122.70		123.50		50.44		88.29
Jan 03	263.50	65.79	104.30		119.30				60.16		89.95
Apr 03				117.200	92.20	57.04	87.10		155.50		125.50
Sep 03	215.90	77.64			105.80		109.70		20.20	79.31	50.88
Jan 04		64.35			46.17		106.10	25.48	43.27	148.90	
Jul 04											

Nitrate is a potential electron acceptor and thus plays an important role with regard to redox reactions. In sediments, nitrogen is generally bound to organic matter /DVW 96a/ and exists in form of ammonia or ammonium ions. In the presence of oxygen, nitrate is formed from ammonium, catalysed by microbial activity (nitrosomonas, nitrococcus), via the intermediary product nitrite (nitrification). This process can be observed in the Heselbach groundwater. With increasing seam thickness towards the centre of the basin, the nitrate content in the groundwater increases correspondingly (Fig. 59). The relative decrease of the seam thickness in well B03-99 is to be explained by partial thinning during surface mining and filling with backfill material in this area.
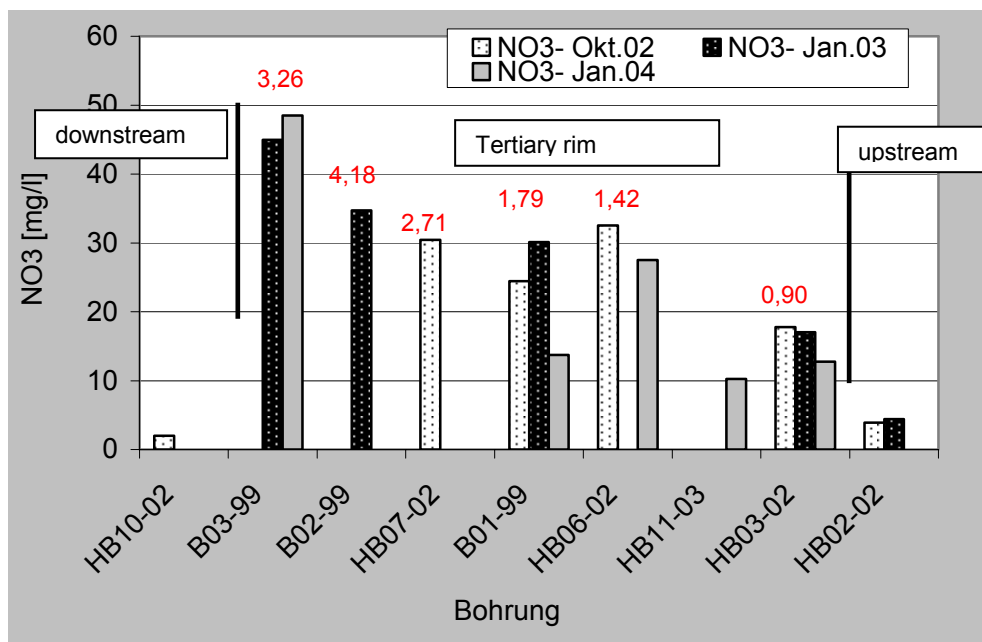
Fig. 59: Nitrate content in groundwaters from Heselbach wells; red numbers = seam thickness [m]

However, under anaerobic conditions, nitrate ions are also reduced in the presence of bacteria (denitrification) where ammonium ions or elemental nitrogen gas can be formed as final products. One example for occurrence of denitrification is well HB10-02 which is characterised by low to non-detectable nitrate concentrations and high CO_2-concentrations. As shown in Fig. 60, ammonium only exists in the groundwater in very low concentrations with a maximum of 1 mg/l. This confirms that an oxidising environment prevails at the Heselbach site.

$$[CH_2O] + \frac{4}{5}NO_3^- + \frac{4}{5}H^+ \rightarrow CO_2 + \frac{2}{5}N_2 + \frac{7}{5}H_2O \qquad (6)$$
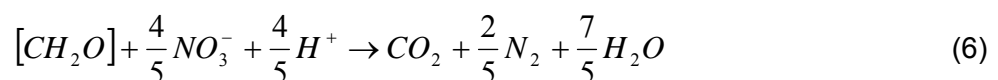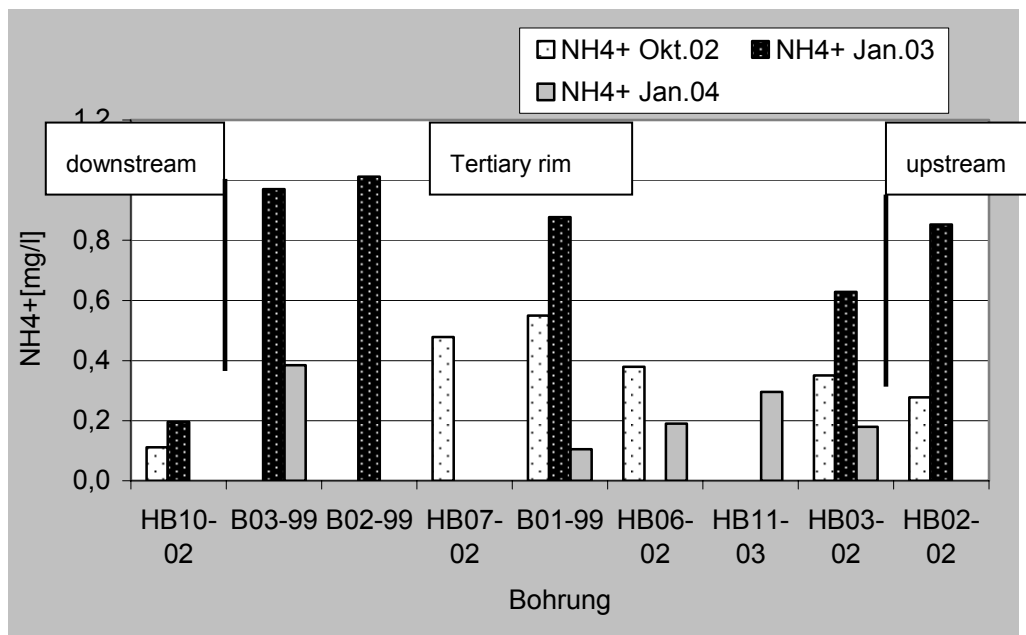
Fig. 60: Ammonium concentration in groundwaters from Heselbach wells

While denitrification already starts with oxygen deficit (< 5 mg/l), the process of desulphurisation only starts at lower oxygen concentrations /HOE 96/. In the Heselbach groundwaters, the occurrence of this process becomes apparent by the high sulphate contents (see on-site parameters).

The representation of the groundwater analyses by means of a Piper diagram gives an overview of the main element composition of the Heselbach groundwaters. Due to comparable sampling methods, water analyses from October 2002 to July 2004 were evaluated. The Keuper groundwaters characterise the upstream zone, HB10-02 the downstream zone (Fig. 60). It becomes clear that the near-surface Keuper aquifer directly reacts on changes while the downstream zone is protected by the backfill layer so that variations of the groundwater chemistry don't occur. According to the main element composition, the downstream groundwater of the Tertiary basin is to be assigned to Ca-SO_4^{2-} type.
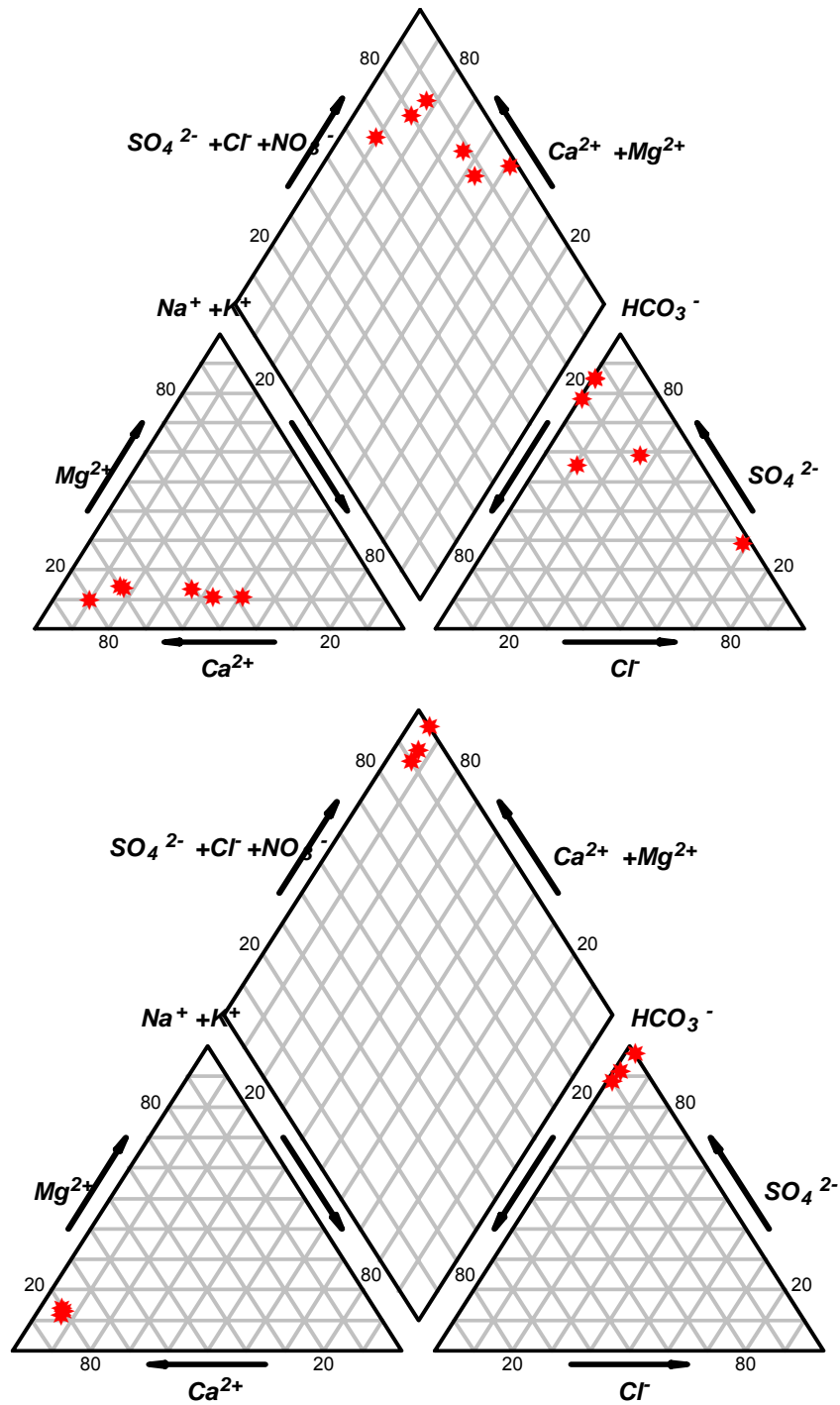
Fig. 61: Piper diagram of upstream (Keuper) groundwaters (top) and downstream (HB10-02) groundwater (bottom)

The analyses of the groundwaters of the Tertiary basin are represented in three separate Piper diagrams. The undisturbed waters (Fig. 62) are compared with disturbed water samples (Fig. 63). The classification was made on the basis of available stable isotope data which, depending on the location of the well, indicate mixing processes with surface waters.

Undisturbed groundwater samples were taken from wells B02-99 and B03-99 for which no influences of surface water could be detected. They exist in the form of Ca-SO_4^{2-}-Cl^- waters. The wells directly located at the rim border are categorised as disturbed groundwaters, i. e. wells B01-99, HB06-02, HB11-03 and HB03-02. The analyses of these groundwater samples vary over a wide range. Particularly striking is the variation of groundwater composition in well HB03-02 (Fig. 63). This well directly located at the rim border shows a strongly varying chemical composition. The input of hydrogen carbonate from the covering gravel material alterates the original chemism of this well to such an extent that uranium from the sediment goes into solution recently.

In periods with high precipitation, as e. g. in January 2004, the installed drainage cannot discharge the water completely so that groundwaters of the Tertiary rim are diluted with surface water.
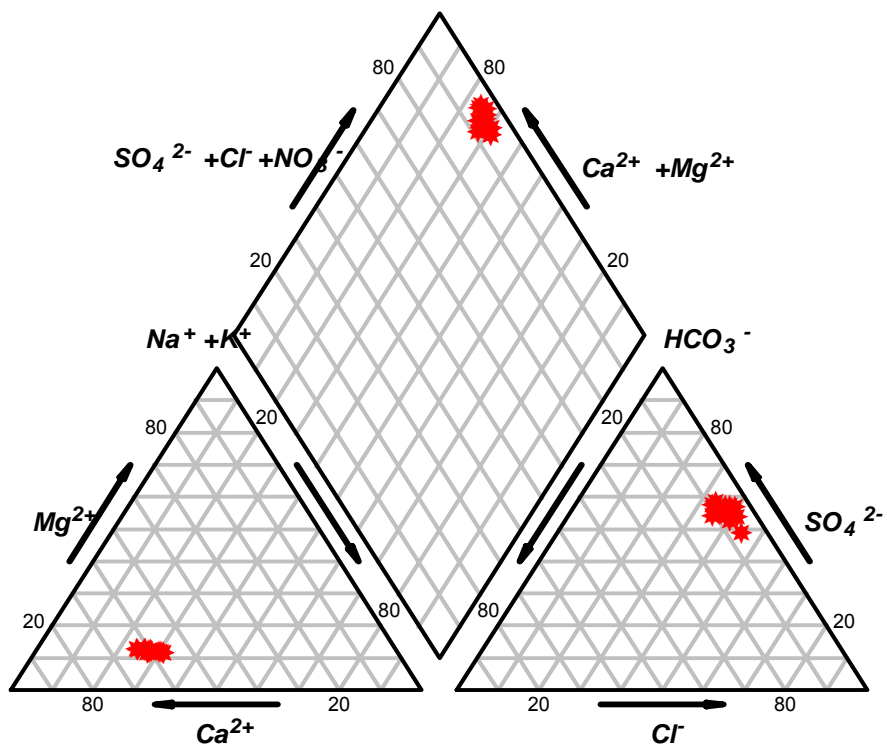
Fig. 62: Piper diagram for groundwater from Tertiary rim
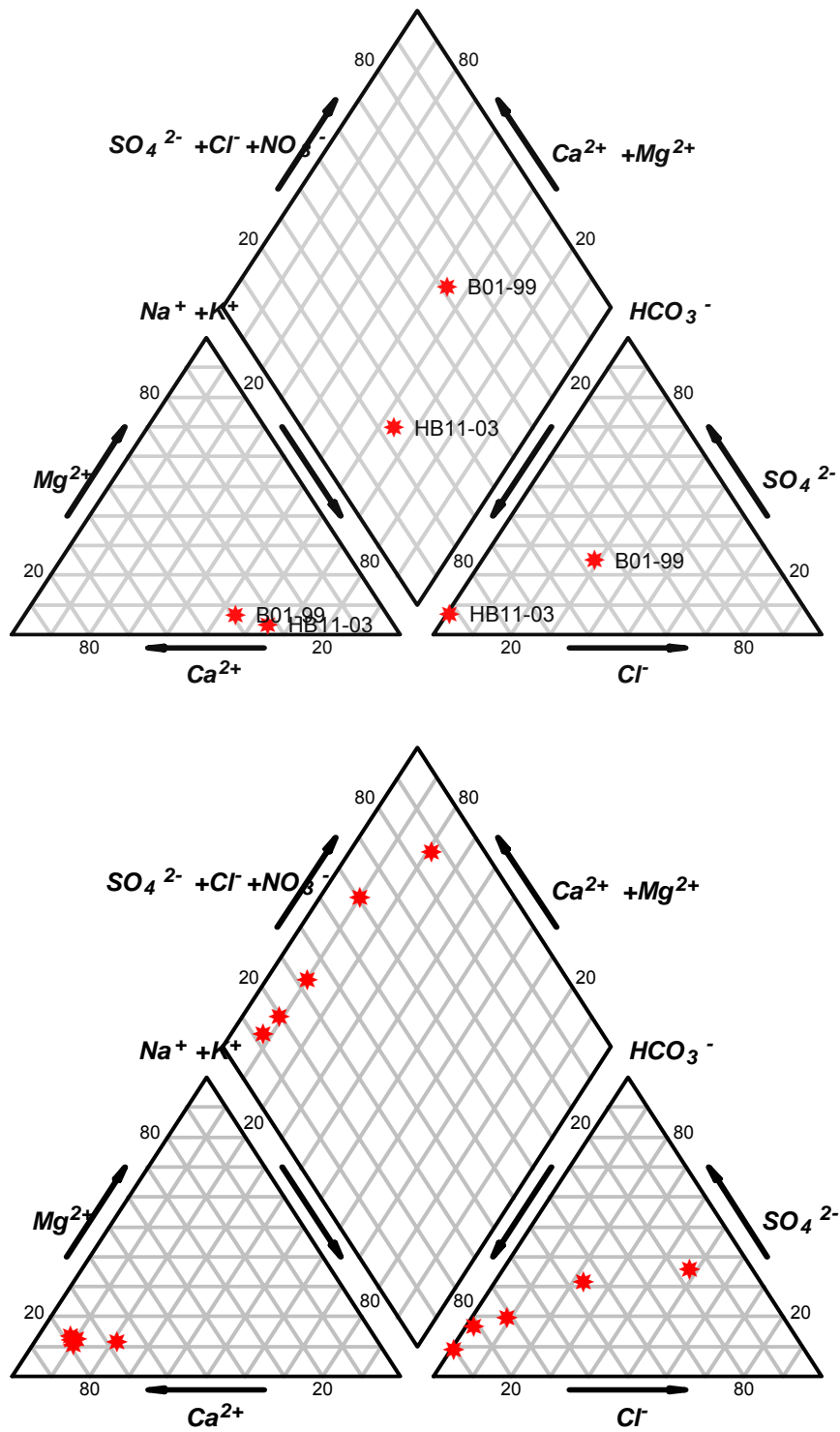
Fig. 63: Piper diagrams of disturbed groundwaters from Tertiary rim; top: variation during single sampling campaign (Jan. 2004); bottom: variation in well HB03-02 within 2 years
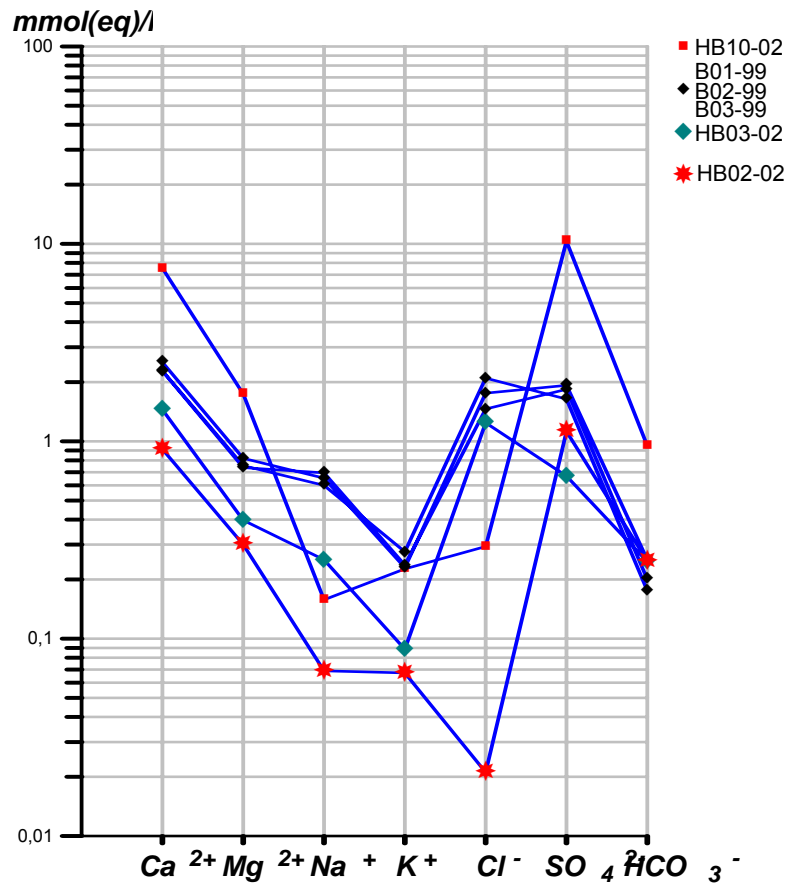
Fig. 64: Schoeller diagram of selected groundwaters from Heselbach wells (Jan. 2003)

The representation of the Heselbach groundwaters in a Schoeller diagram (Fig. 64) clearly demonstrates the different element concentrations in groundwater samples. The Keuper samples (HB02-02) show the lowest concentration of main elements, directly followed by well HB03-02 in the transition area from Keuper to Tertiary (marked in green). All other wells of the Tertiary rim are characterised by an almost identical water chemism. The downstream sample (HB10-02) is enriched in all main elements, but in particular in Ca^{2+} and SO_4^{2-} which is also confirmed by the increased values of the conductivity measurements. Despite different total concentrations, all groundwaters show a similar ion distribution.

Results of groundwater analyses

For a better understanding of the local situation, the analysed wells in the project area Heselbach were classified into different groups. In addition to the down and upstream zone, the wells of the Tertiary rim represent the actual "uranium field" as third group. This

group was again divided into undisturbed (towards the centre of the basin) and disturbed wells (direct transition to the Keuper) to allow characterisation of the original conditions without influence of surface water.

Keuper groundwaters of the upstream zone are classified as Na-Ca-SO$_4$-Cl type according to their chemical composition of main elements. According to the mineralogical composition of the sediments (quartz, feldspars), these waters are characterised by low nitrate and iron concentration. Oxygen contents of 0.1-2 mg/l indicate reducing conditions, at least temporarily. The low uranium and oxygen contents of the Keuper waters do not indicate, as initially assumed, a recent uranium transport into the tertiary sediments. Altogether, the Keuper groundwaters are only low-mineralised (< 280 µS/cm) and hardly vary in their composition. The waters are slightly acid (pH values 5.2 - 6.05) and do not differ from the Tertiary rim wells.

The wells of the Tertiary rim show DOC contents < 12 mg/l, little hydrogen carbonate (up to 15 mg/l) and only low uranium concentrations of 0.1 - 1.3 ppb in groundwater despite high uranium concentrations in sediments. In the Piper diagram, the groundwaters are to be classified as Ca-SO$_4$-Cl waters. The pH values are also in a slightly acid range (4.9 - 5.6); the oxygen content is < 5 mg/l and the specific conductivities vary in the range of 260 - 600 µS/cm. In all wells, nitrate was identified as oxidation product of organic matter.

Regarding a possible today's uranium local re-mobilisation, well HB03-02 is of particular interest. The results of one analysis in January 2003 show increased uranium content [up to 134 ppb] together with a slightly increased oxygen content [4.45 mg/l] and also increased hydrogen carbonate concentration of 348 mg/l as a maximum which exceeds the average concentration of the Tertiary rim wells ($\varnothing$15 mg/l) by a factor of 23. This indicates anthropogenic influence which is limited to place and time. Along the profile line towards the former open pit mining areas, such high hydrogen carbonate and uranium concentrations are never observed.

4.4   Natural isotopes

On the one hand, measurements of natural environmental isotopes in groundwaters serve for characterisation and typecast and, on the other hand, for differentiation of local groundwater catchment areas /MOS 80/. Further, the determination of groundwater age can give indications to duration of storage periods and mixing conditions within an aquifer.

To clarify the question whether the groundwater in the lignite horizon exists as a separated groundwater horizon or is continuously recharged by the Keuper aquifer, the following isotope analyses were performed on selected groundwater samples:

1) stable isotopes: $^2H/^1H$ and $^{18}O/^{16}O$
2) radiogenic isotopes: ^3H
3) radiogenic isotope and its decay product: $^3H/^3He$

4.4.1   Stable isotopes

Results of stable isotope measurements are expressed as ratio of the two most abundant isotopes in nature. Since for the interpretation of groundwaters, the absolute ratios are not decisive but their variations, the measured isotope ratios are referred to an internationally recognised standard (here: V-SMOW = Vienna standard mean ocean water). The enrichment and depletion of the heavy isotopes is expressed in per mil as δ values. Negative deviations from the standard show a relative depletion, positive values a relative enrichment of the heavy isotope. For the hydrogeological interpretation, e. g. analyses of the stable isotopes $^2H/^1H$ and $^{18}O/^{16}O$ which can be easily measured have proven to be suitable in practice. For the determination of $δ^2H$, the uncertainty of the measured values is 1.0 ‰, for $δ^{18}O$ data 0.1 ‰.

Due to seasonal influences, the isotope composition in precipitation waters varies such that in the cold winter months precipitation water is depleted in heavy isotopes. Dansgaard 1964 (in /MAZ 04/) explains this fact by means of different effects. Due to the low temperature, the lighter isotopes are already enriched relatively in the clouds (temperature effect). In addition, colder temperatures lead to weakening of the evaporation during rain. The fact that in case of low temperatures the precipitation intensity generally increases, further leads to depletion of the heavy isotopes due to the amount effect. According to the seasonal cycles, the $δ^2H$ and $δ^{18}O$ contents in rain and snow samples of the weather station Regensburg vary considerably, as shown in Fig. 65.
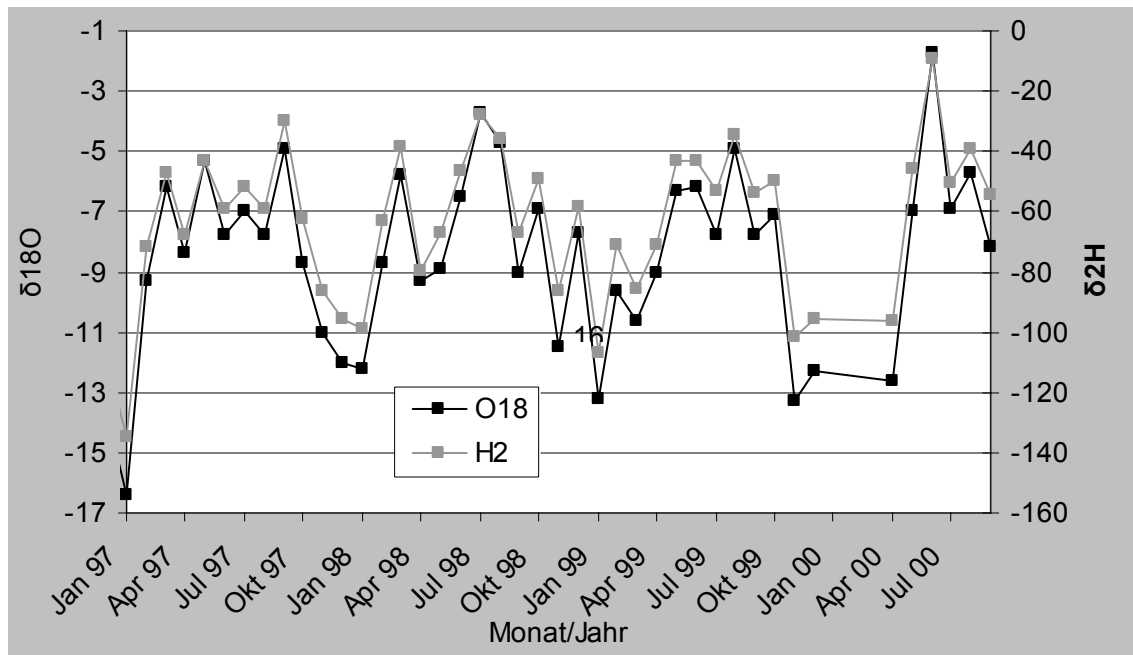
Fig. 65: Seasonal cycle of δ^2H and $\delta^{18}O$ values in monthly precipitation samples of weather station Regensburg in the period 1997 - 2000 (ISOHIS-data base, IAEA)

In addition to the reference values of the Regensburg weather station, Table 35 summarises the results of all stable isotope analyses on Heselbach groundwaters. For comparison purposes, the concentrations of the conservative chloride ion were added. Altogether, samples were taken from seven selected groundwater wells.

In general, the precipitation waters are characterised by the following interrelation of the isotopes:

$$\delta^2H = 8.17 * \delta^{18}O + 11.27 \tag{7}$$

Along this line (WMWL = world meteoric water line) is the typical composition of meteoric groundwaters (according to Craig, in /CLA 97/). Fig. 66 illustrates the isotope data of the groundwaters measured in Heselbach in form of the commonly used graphical representation of the $\delta^2H/\delta^{18}O$ diagram. As expected, all waters are near to the WMWL. The influence of evaporation on near-surface groundwaters can be excluded.

Table 35: Stable isotope values and chloride concentrations in groundwaters from Heselbach wells and reference data from Regensburg weather station

Well	Area	January 2003			January 2004		
		δ^{18}O [‰]	δ^{2}H [‰]	Cl [mg/l]	δ^{18}O [‰]	δ^{2}H [‰]	Cl [mg/l]
HBO2-02	Upstream	-9.33	-64.30	0.75	-9.30	-65.10	-
HBO3-02	Tertiary rim	-10.03	-71.40	44.04	-8.70	-61.50	3.88
HB11-03		-	-	-	-14.10	-104.20	0.37
BO1-99		-9.90	-71.10	62.11	-15.90	-119.20	21.06
BO2-99		-9.95	-70.10	51.68	-	-	-
BO3-99		-9.98	-70.00	74.08	-	-	41.04
HB10-02	Downstream	-9.47	-66.50	10.35	-9.50	-68.40	-
Regensburg weather station January-Ø		-12.27	-93.75	-	-	-	-
Regensburg weather station annual-Ø		-9.60	-71.30				
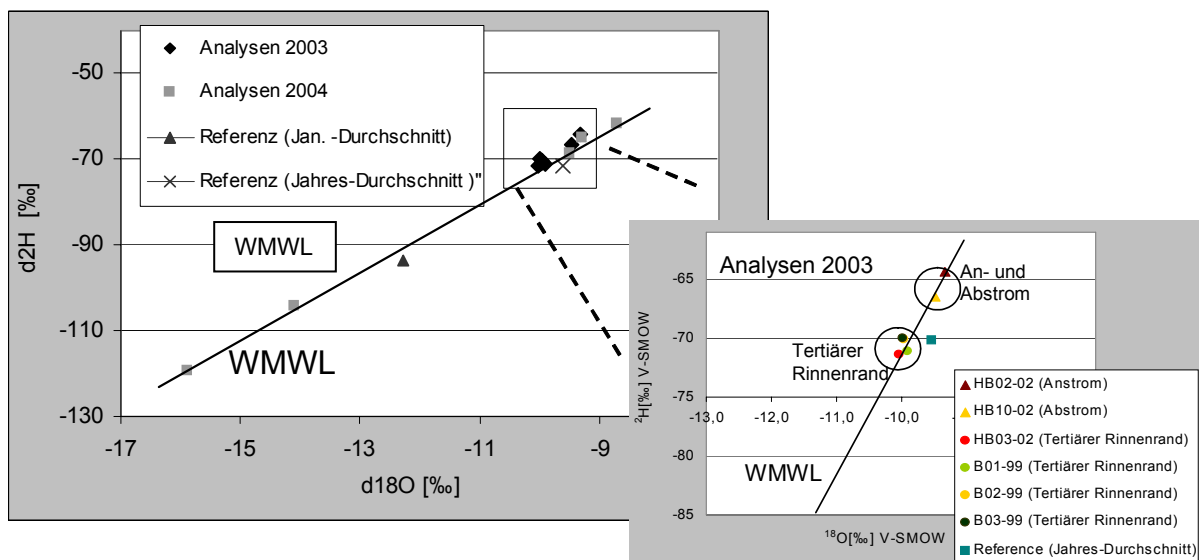
Fig. 66: Stable isotope values of groundwaters from Heselbach wells for 2003 and 2004; reference data from Regensburg weather station (ISOHIS data base, IAEA)

The analyses of the stable isotopes allow a clear classification according to two different groundwater types. On the one hand, there is the groundwater of the Keuper aquifer (HB02-02) that hardly varies in its composition and represents a mixture of recent precipitation waters. The downstream well (HB10-02) can also be assigned to this groundwater type. On the other hand, the Tertiary rim wells whose isotope compositions, compared to the Keuper groundwater, reach more negative δ^{2}H and δ^{18}O values.

This effect becomes particularly striking during the second sampling campaign. Correlations with precipitation data of the project's weather station document heavy rainfalls two days before and during sampling (Fig. 67). The drainage of the sealed surface had not the capacity for complete surface runoff of the water masses from heavy rain events (up to 20 mm/d). Mixing of older groundwater with fresh surface water took place, resulting in changes in the isotopic signature. Tertiary rim samples of this campaign are, on the one hand, exactly on the WMWL. On the other hand, the signature of the stable isotopes and the chloride contents indicates an increase of fresh surface waters towards the pavement slope. Where the surface water accumulates during heavy rainfalls due to the topography, the largest entry of fresh water and thus the strongest change of the original signature occurs (Fig. 68).
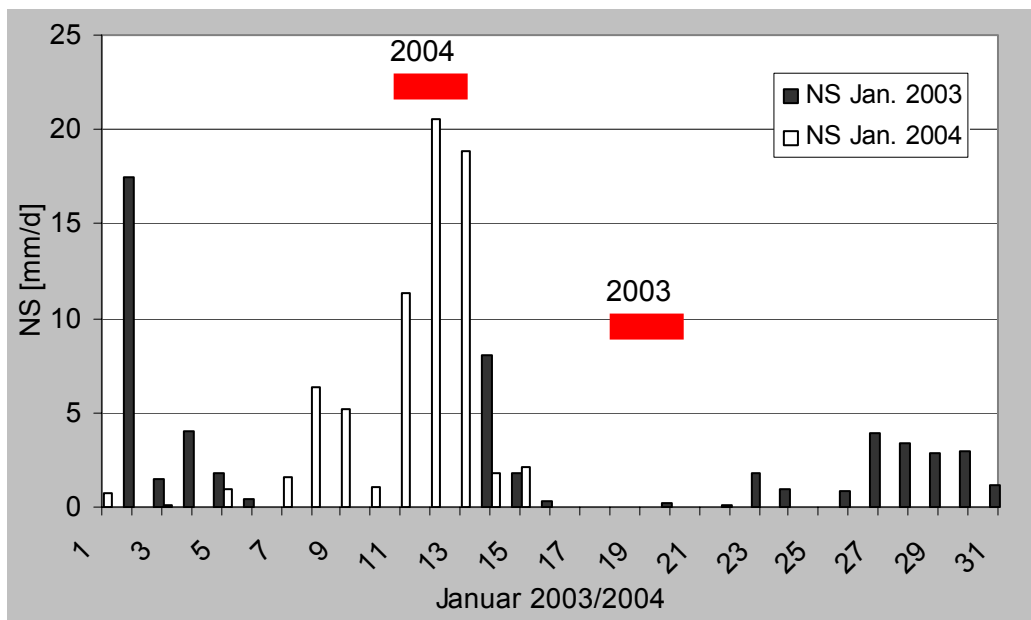
Fig. 67: Precipitation (NS) in Jan. 2003 [black bars] and Jan. 2004 [white bars]; red = period of 3-day groundwater sampling campaign

The mixing fractions of several groundwaters in a known sample can be quantified by the following simple linear calculation:

$$\delta_{\text{Pr}obe} = \chi * \delta_A + (1 - \chi)\delta_B \tag{8}$$

with: δ_A and δ_B as end members of the mixing series

Use of the oxygen isotope data yields for sample HB10-02 a groundwater mixing of 77 % from drilling HB02-02 (Keuper) with 23 % of drilling B02-99 (Tertiary rim). From the dilution of the chloride contents, even a mixing of 87 % groundwater from Keuper and

13 % from Tertiary rim could be derived. This result can only be explained by a hydraulic connection of the downstream well HB10-02 with the Keuper aquifer below the Tertiary basin.
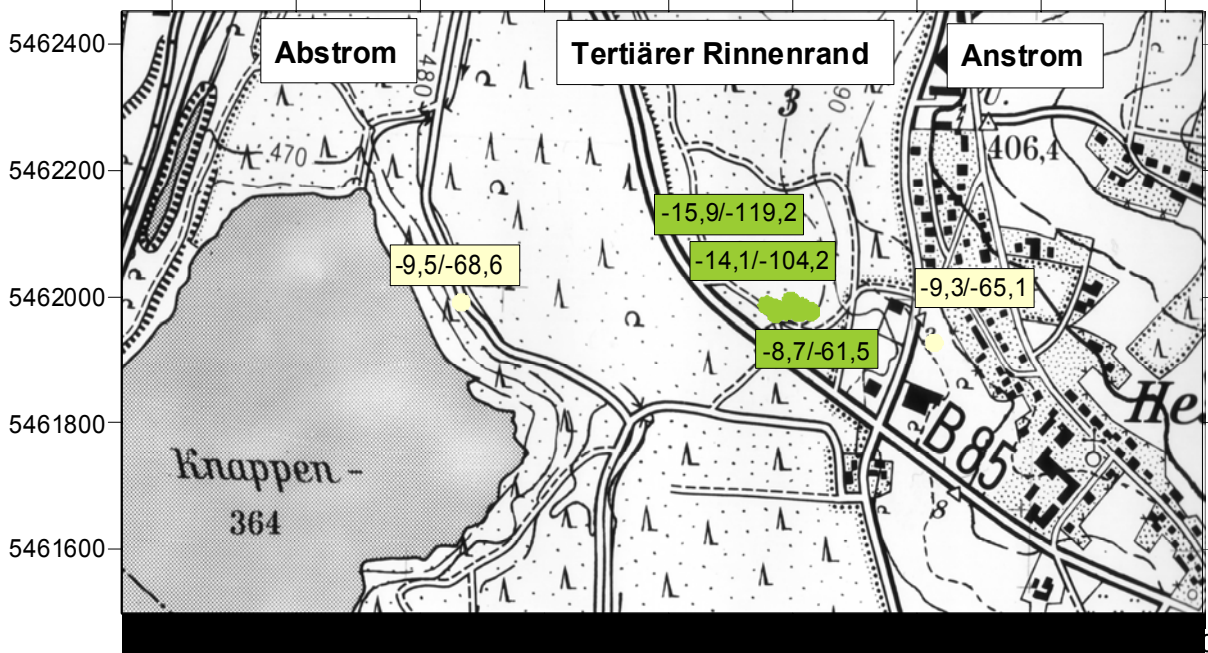
Fig. 68: Stable isotope values (δ^{18}O/ δ^2H) of groundwaters from Heselbach wells (Jan. 2004); yellow = up- and downstream area; green = Tertiary rim

4.4.2 Tritium

For the determination of the age of younger groundwaters (up to 40 years), radiogenic tritium (^{3}H) has been playing an important role for some decades. Small amounts of tritium are produced in the atmosphere by interaction of neutrons with nitrogen atoms (^{14}N), are incorporated there into water molecules and enter the earth's groundwater cycle via precipitation. The nuclear weapon tests performed from 1952/1953 until the beginning of the 1980's led to a manifold increase of the tritium content in the atmosphere. Fig. 69 shows that in 1963 peak values of up to 6090 tritium units (TU) were measured in surface and groundwater in South Germany and since then a decrease in tritium contents is observed. 1 TU equals a concentration of ^{3}H/^{1}H = 10^{-18}.

Due to the short half-life of tritium of 12.32 a, it is possible to determine the groundwater age by means of the tritium content in the groundwater identified if the initial concentration is known. However, this requires knowledge of the time when the tritium entered the groundwater, i.e. the input function c_{in}. With different model approaches, the output

function that is nearest to the ^3H content determined in the groundwater sample can be calculated. The piston flow model and the mixing model are applied. The results are described in the following.
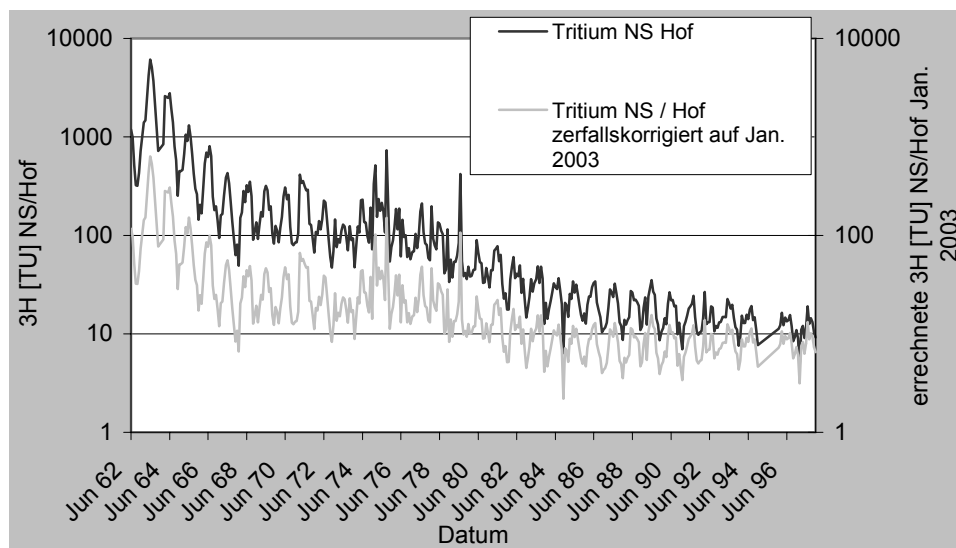
Fig. 69: Tritium content [TU] in rainfall and snow; from Hof weather station (NS) (black) with curve corrected for decay / January 2003 (grey)

Table 36: Tritium contents in groundwater from Heselbach wells

Well	Stratigraphy / area	Sampling depth [m bgl]	Sampling date	^3H [TU] +/- error
HB02-02	Keuper / upstream	8.0	Jan. 2003	9.5 +/-0.5
			April 2004	9.9 +/-0.6
HB03-02	Tertiary / rim	3.4	Jan. 2003	21.7+/-1.0
			April 2004	10.2 +/-0.6
B01-99	Tertiary / rim	3.6	Jan. 2003	19.8+/-0.9
			April 2004	7.4 +/-0.5
B02-99	Tertiary / rim	7.5	Jan. 2003	19.3+/-0.9
			April 2004	9.5 +/-0.5
B03-99	Tertiary / rim	7.5	Jan. 2003	21.9+/-1.0
			April 2004	9.5 +/-0.5
HB10-02	Tertiary / downstream	9.0	Jan. 2003	10.1+/-0.5
			April 2004	0.8 +/-0.4
HB11-03	Tertiary / rim	1.9	-	-
			April 2004	5.9 +/-0.5

The tritium contents of both sampling campaigns listed in Table 36 show a clear discrepancy. While the Keuper groundwater sample confirms the results of the sampling in the preceding year, the samples from Tertiary rim in 2004 show unexpectedly low tritium contents. This effect can be explained by a strong dilution of the groundwater at the

Tertiary rim with recent precipitation water at the time of sampling in January 2004 (see stable isotopes). As a consequence, only the data from 2003 are referred to for the further analysis and subsequent interpretation.
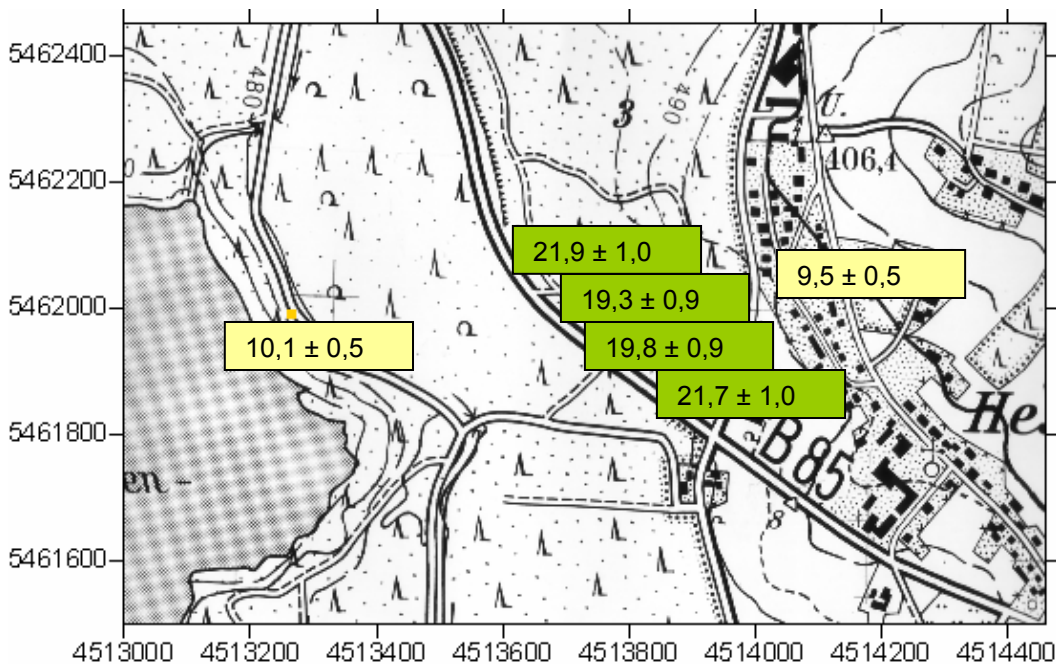
Fig. 70: Tritium contents of groundwaters from Heselbach wells (Jan. 2003); yellow = up- and downstream area; green = Tertiary rim

Model approach 1: piston-flow model

In this approach it is assumed that no dispersion, diffusion and exchange processes take place, i. e. the input function depends solely on radioactive decay. All groundwater particles move with equal velocity. Then:

$$a_t{}^3H = a_0{}^3H * e^{-\lambda t} \tag{9}$$

with:
$a_t{}^3H =$ measured tritium concentration;

$a_0{}^3H =$ initial tritium concentration;

λ = half-life;

t = time in years [a]
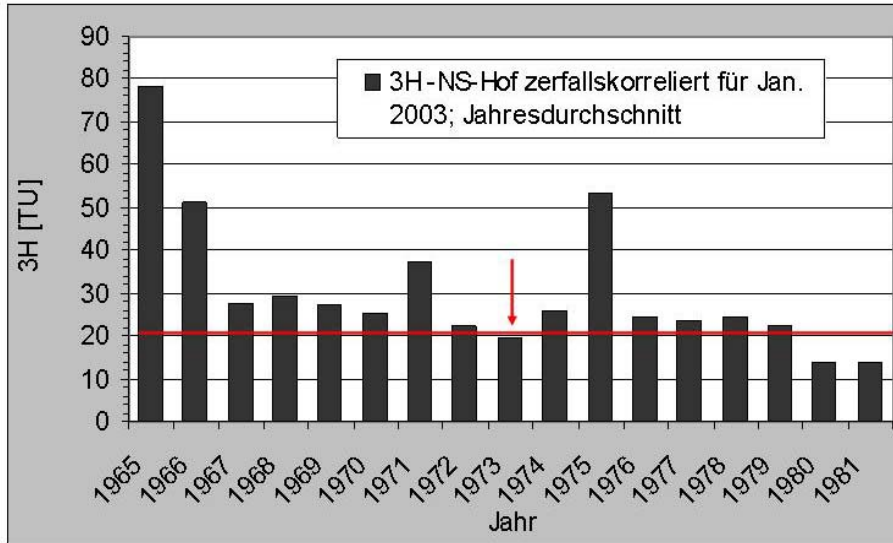
Fig. 71: Annual means of ^3H contents in precipitation (Hof weather station) - decay corrected for year 2003; red line = mean value ^3H content in groundwater samples from wells of the tertiary basin (Jan. 2003)

Today, groundwaters formed after 1980 have tritium concentrations of about 14 TU (Fig. 71) and cannot explain the values of the Tertiary rim waters (20.6 TU on average). For the Heselbach groundwaters of the Tertiary rim wells, an age of at least 24 years is calculated with the piston-flow-model. Without dilution, the concentration of the waters today can be explained by groundwater recharge in 1972/1973 (Fig. 71). Considering a later dilution, the years until 1979 may also be possible. In general, however, groundwater is a mixture of recharge water of different ages. For this reason, an additional model calculation was performed according to the mixing model.

Model approach 2: mixing model

Considering the history of lignite mining in the region, the following hydraulic model can be developed for the investigation area. From historical records it is known that the North field was backfilled in 1970 and mining continued in more southern areas. It is therefore to be assumed that the groundwater level conditions, as they exist today in the investigation area, have only been readjusted after 1970. Further, a lowering of the groundwater level during mining until 1970 is to be assumed. The pore space in the clay and lignite horizons was, at least partly, exposed to the atmosphere. After termination of the mining activities, a new groundwater level was reached and groundwater with isotopic composition of that time gradually filled the pore space of the rock layers from bottom up. Based on the

103

assumption that groundwater from three consecutive years (e. g. 1969 - 1971) was involved in filling up the pore space with one third each, a tritium concentration of 29.4 TU is calculated for this mixed water referred to the year 2003 (Table 37). Filling up of the Tertiary basin with groundwater at the beginning of the 1970's and subsequent dilution may explain the recently measured TU contents of the water.

Table 37: Tritium input function for the years 1969 - 1971 and calculated average tritium content for 2003

Year	a_o	a_t1970	a_t1971	a_t2003
1969	177.2	167.6	158.5	26.6
1970	157.2		148.6	25.0
1971	218.1			36.6
2003				29.4

4.4.3   Tritium-helium measurement

The ^{3}He produced by the decay of tritium allows calculating the time span between precipitation input and sampling so that the age of the groundwater can be determined. For the determination of the tritiogenic ^{3}He (^{3}He trit.), however, it is required to deduct the ^{3}He concentration from other sources from the total helium concentration measured, i. e.:

1) helium in equilibrium with the atmosphere (He_equil.),
2) helium dissolved under pressure as excess fraction (He_excess), and
3) terrigenic helium from the mantle or U/Th decay (He_terr.)

The atmospheric helium (He_equil.) fraction is calculated from temperature, salt content of the water and air pressure (or elevation above sea level). The additionally determined ^{20}Ne content allows calculating the He_excess fraction. From this, a calculable terrigenic component can be derived for ^{4}He. This, in turn, is at a constant ratio with the terrigenic ^{3}He ($2*10^{-8}$) and allows the determination of the ^{3}He_terr. After deduction of these three components from the total helium concentration, the remaining ^{3}He fraction from tritium decay is obtained (Fig. 72).
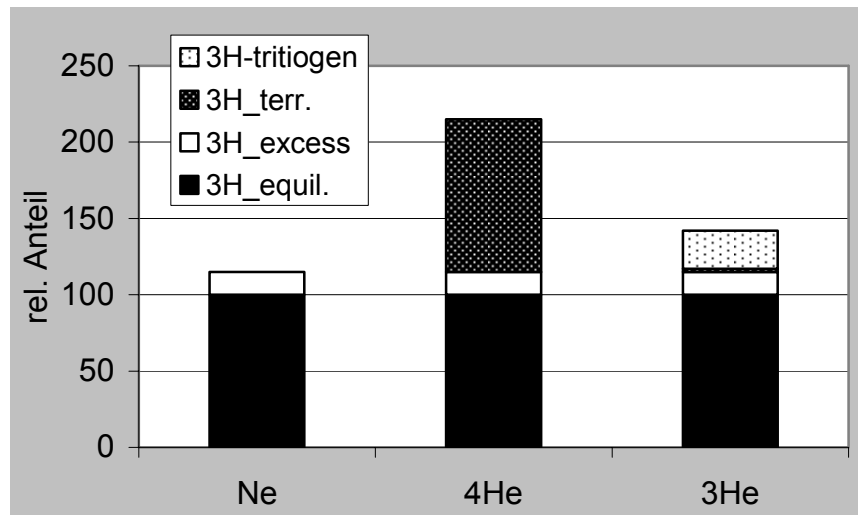
Fig. 72: Content of gases in groundwater sample for ^{3}H/^{3}He dating (www.noblegas.uni-bremen.de)

After the described correction of the measured values, the ^{3}H/^{3}He groundwater age can be calculated according to the following formula /CLA 97/:

$$t = \frac{t_{1/2}}{\ln 2} * \ln\left(1 + \frac{^3He}{^3H}\right)$$

(10)

with:

t = a; $t_{1/2}$ = half-life = 12.43;

^{3}He = calculated helium concentration [TU];

^{3}H = measured tritium concentration [TU]

Age dating according to this method shows an experimental error of 10 % as a maximum (www.noblegas.uni-bremen.de). In January 2004, samples were taken from well B03-99 for ^{3}H/^{3}He age dating. Selection of this well was due to the comparably large filtering depth (6 - 9 m b.g.l.) and its limitation to clayey and lignitic layers of the Tertiary.

Table 38: Calculated tritium-helium age of groundwater sample B03-99

Well	Sampling depth [m b.g.l.]	^{3}H [TU]	^{3}He [TU]	Initial tritium	Tritium-helium age [a]	GW recharge year
B03-99	7.5	21.27	25.00	46.27	13.9	1990

For the groundwater in the Tertiary basin, a ^{3}H/^{3}He age of 13.9 years is yielded which corresponds to 1990 as year of origin. However, to be able to explain this result, the

precipitation in 1990 must have had a TU content of 46.3 (Table 38). For precipitation waters in Europe at the beginning of the 1990's, these high TU contents are unrealistic; the recorded TU values are clearly below 30 TU (e. g. Regensburg weather station in 1990: 22.4 TU). An explanation for this result could be found in mixing processes of very young surface water (^{3}He-free) with older groundwater so that a too young age of groundwater origin is suggested. However, calculations of different mixing combinations do not show any possibility that could explain such a result. Groundwater from the 1970's, which explains the tritium concentration, would have to show a ^{3}He concentration between 80 and 124 TU. The determined ^{3}He content of 25 TU clearly deviates from it and indicates an early degassing of the groundwater sample.

To exclude degassing of the groundwater sample, fast recharge of the groundwater within the horizon from which the samples were taken should generally be ensured so that the groundwater in the well will not come into contact with the atmosphere. In Heselbach, this is not given to the desired extent due to the poor hydraulic conductivity of the lignite horizon so that partial degassing of the groundwater cannot be excluded. This assumption leads to the conclusion that considerable fractions of the ^{3}He content had already diffused out at the time of sampling so that a too young age of groundwater origin was calculated.

5   Radiometric investigations

Radiometric investigations were performed on sediment and groundwater samples. Isotope concentrations of the uranium decay chain were analysed with the aim to determine equilibrium and non-equilibrium conditions between parent and daughter isotopes. An assessment of uranium migration (enrichment or depletion) and dating of the transport processed is possible on the basis of these results. The samples were analysed with regard to the radionuclides ^{238}U, ^{234}U, ^{230}Th and ^{226}Ra:

5.1   Methodology

Alpha-spectrometric analyses with regard to radionuclides on sediment and groundwater samples from Heselbach were performed by the Research Centre Jülich (FZJ) and the Institute for Environmental Technologies IUT Berlin. Depending on the laboratory, sample treatment and evaluation of the results differ.

FZJ

The Research Centre Jülich (FZJ) dissolves the dried, homogenised sediment sample by means of microwave-facilitated pressure digestion. The acidity of solution obtained amounts to 7 mol/l by adding concentrated HNO_3. Afterwards the solution is extracted in n-heptane with a 0.25 M TOPO solution. 1 ml of this extract is evaporated on a stainless steel dish (diameter of 20 cm) together with 2 ml cellulose lacquer/acetone (1:100) and analysed for uranium and thorium by alpha-spectrometry. Subsequent separation of the overlapping ^{234}U/^{230}Th spectra by deconvolution was performed with the ALPS software of Westmeier company.

For the determination of radium, the sample solution was mixed with 100 µl $BaCl_2$ solution and 1 ml of concentrated HNO_3. $BaSO_4$ and $RaSO_4$ is obtained as purified precipitation and then brought into solution again at about 100°C with NH_3-EDTA solution (0.5 g titriplex II in 7 ml NH_3 solution). After addition of 3 ml saturated NH_3 solution and 2 ml 8 M HNO_3, the solution was evaporated on stainless steel dishes and ^{226}Ra was subjected to an α-spectrometric measurement. The α-spectrometric measurements of the uranium, thorium and radium isotopes were performed with sample carriers sized 20 cm in a grid ionisation chamber of the company MAB. With a measurement time of 24 h, a detection limit of 0.003 Bq is reached.

Regarding the error analyses, distinction is to be made between systematic errors and statistical uncertainties of the measurement method. Errors during weighing, volume measurements etc. are summarised as systematic errors and stated with a value of 10.3 % as a maximum. The statistical uncertainty for the isotopes ^{226}Ra, ^{228,232}Th and ^{235,238}U was assumed to be n$^{0.5}$ (n = counting rate). Since the α-spectra of the isotopes ^{234}U and ^{230}Th are overlapped and the areas were separated by deconvolution, the error of the isotope is given by 2n$^{-0.5}$. The total error is obtained by addition the two error types and rounding to a whole number.

IUT Berlin

At the Institute for Environmental Technologies IUT Berlin, the elements uranium and thorium are separated before α-spectrometric measurement by a TRU ion exchange column. Therefore, subsequent separation of the spectra by deconvolution is not required. By addition of 2 ml 9 M and 10 ml 4 M HCl, the REE are eluted. After that, the thorium is brought into solution selectively with 1 M HCl. The thorium eluate is nearly evaporated to dryness and mixed with H_2SO_4. By addition of cerium nitrate solution and concentrated H_2F_2, thorium precipitates together with the cerium fluoride produced. After 30-minutes ageing, the precipitation < 0.1 µm is filtrated, the filtrate dried and the sample analysed for thorium by α-spectrometry. The subsequent elution of uranium is performed with a mixture of 0.1 M HCl and 0.1 M H_2F_2. The uranium eluate is mixed with diluted H_2SO_4 and carefully concentrated until formation of sulphuric acid fumes. After addition of 20 - 30 ml distilled water and titanium trichloride solution until change of colour, cerium nitrate solution and concentrated H_2F_2 is added, analogously to the separation of thorium. As internal standard, ^{229}Th and ^{232}U were added to the samples. The activity measurements are performed with an alpha spectrometer (Solist Ortec EG&G). The detection limit of this method is 0.0005 Bq, the relative error is given by a total of 15 %.

Groundwater samples of selected wells were also analysed at the IUT Berlin. The sample processing method (separation of the elements) corresponds to that of the digested sediments.

5.2 Radiometric investigations on sediments

By means of the ^{230}Th/^{234}U and ^{234}U/^{238}U activity ratios (AR), immobilisation and mobilisation processes within a sediment can be identified. Further, the AR of the sediment samples shows whether it is a fast or slow process and whether a singular or multivariant process took place. Radiometric analyses were performed on six sediment samples from Keuper and 21 sediments samples from the Tertiary rim.

5.2.1 Activity ratios of Keuper sediment samples

The uranium concentrations and ^{234}U/^{238}U activity ratios (AR) of the Keuper samples are listed in Table 39.

Table 39: ^{234}U/^{238}U activity ratios (AR) and uranium concentrations of sediment samples from Keuper sandstone

Drilling	Depth [m bgl]	U [ppm]	$\pm \delta$	^{234}U/^{238}U-AR	$\pm \delta$
HB01-02	1.10-1.15	0.236	0.019	0.95	0.11
HB01-02	5.20-5.25	0.148	0.008	1.02	0.08
HB02-02	10.90-10.92	0.214	0.011	0.89	0.06
HB08-02	3.30-3.35	0.658	0.023	0.79	0.04
HB01-02	9.15-9.17	1.146	0.270	0.75	0.02
HB02-02	3.40-3.45	1.812	0.048	0.79	0.03

Five of the six samples analysed show ^{234}U/^{238}U activity ratios of clearly < 1 which can be explained by a preferred dissolution of the ^{234}U isotope. Responsible for the different dissolution behaviour of the two uranium isotopes are processes connected with the radioactive decay of ^{238}U via ^{234}Th and ^{234}Pa to ^{234}U. ^{234}Th and ^{234}Pa with half lives of 24.1 d and 1.18 m are very short lived isotopes. During the α-decay of ^{238}U a recoil energy is transferred to its direct daughter ^{234}Th.

The recoil energy causes breaking of chemical bonds and/or or leads to local lattice defects so that the daughter isotope ^{234}U can be mobilised more easily than ^{238}U /OSM 83/. In addition to this physical effect, the chemical reactions along the trajectories also can play a decisive role. In case of an original tetravalent ^{238}U the hexavalent, chemically more mobile daughter isotope ^{234}U is produced by oxidation with oxygen radicals, which are generated along the trajectory.

Recent low $^{234}U/^{238}U$ activity ratios are only possible if uranium had been fixed in the Keuper sandstone over several million of years and so the depletion process of ^{234}U was sufficiently long. Consequently, uranium must have been interbedded in the Keuper sandstone over long time periods before it was remobilised again and transported to the lignite horizon. For reaching an AR around 0.75, the physical alpha-recoil process alone is not sufficient. Therefore, the α-recoil process was accompanied by uranium release due to oxidation from $^{238}U(IV)$ to $^{234}U(VI)$ /SUK 05/. This statement means, that uranium exists in the Keuper sandstone in the tetravalent state due to locally reducing areas (this assumption is currently being verified).

For a remobilisation of the uranium from the Keuper sandstone, changes of the chemical environment are necessary. A distinctive change in climate and groundwater flow direction took place in the Bodenwöhr basin during the Quaternary /TIL 56/. The flow regime, as it exists today, was formed about 800'000 y ago. Since that time, 4 to 5 ice age cycles took place in the investigation area as river gravel and mud deposits show. It might therefore be possible that cold, fresh meltwaters with an increased oxygen content led to a remobilisation of the uranium fixed in the Keuper. During the warm periods towards the end of the ice age cycles, massive water masses might have flown through Keuper that caused oxidation of the uranium due to the change of the chemical environment and transported mobile uranium into the sediment layers of the Tertiary basin.

5.2.2   Activity ratios in Tertiary rim sediments

The results of all activity ratios determined for Tertiary sediment samples are presented in Fig. 73 and Fig. 74. In all samples of the Tertiary rim, the $^{234}U/^{238}U$ activity ratio is near 1. Significant differences between lignite and clay samples could not be identified. The $^{230}Th/^{234}U$ ratio varies, dependent on lithology, over a wide range (0.36 to 1.42). The major part of the samples has an activity ratio of < 1. The $^{226}Ra/^{230}Th$ ratio shows the largest deviation from equilibrium and is, for most of the samples, clearly > 1.

For a better illustration, the activity ratios of the three long-lived nuclides ^{234}U, ^{238}U and ^{230}Th are usually represented in a Thiel diagram (Fig. 75). Dissolution and accumulation processes of uranium can be derived from it. Samples localised in the centre (AR = 1) do not show enrichment or depletion and are in secular equilibrium. Analyses above the $^{230}Th/^{234}U$ equilibrium lines, thus showing $^{230}Th/^{234}U$ activity ratios

< 1, indicate uranium enrichment; ^{230}Th is not yet in secular equilibrium with its parent isotope ^{234}U. Samples below this line indicate dissolution of uranium. The ^{230}Th/^{234}U activity ratios reach values of > 1 because immobile thorium remains in the sediment.
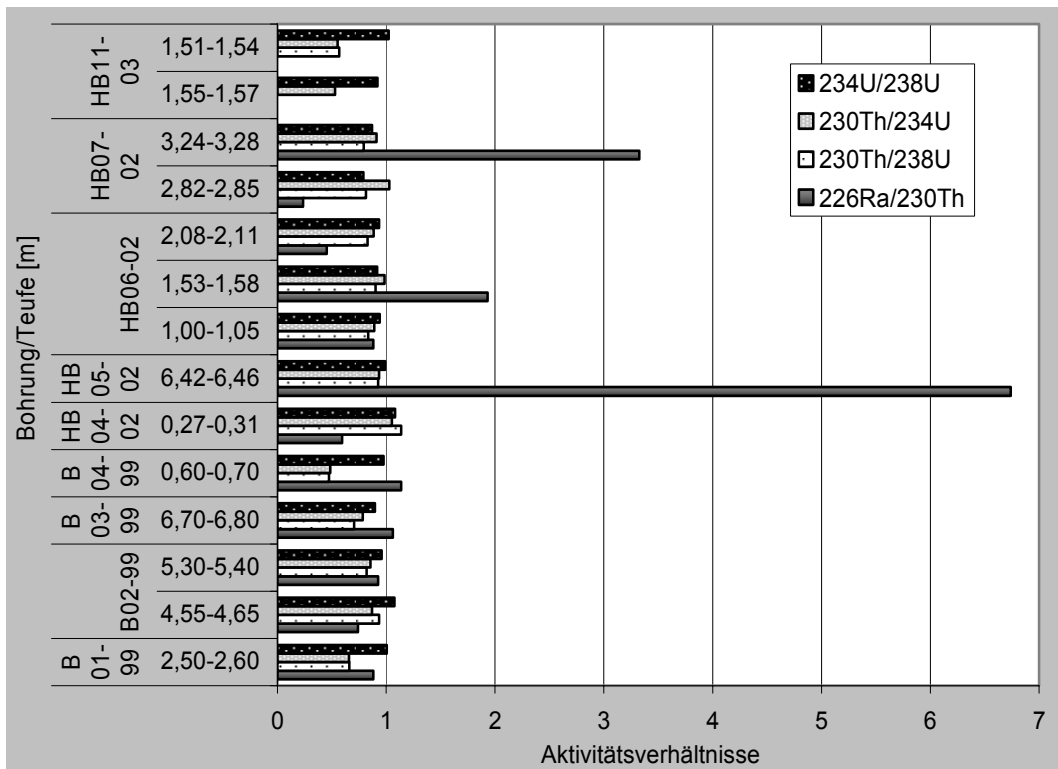
Fig. 73: Activity ratios of isotopes from the uranium decay chain in sediment samples from lignite horizon (Tertiary)
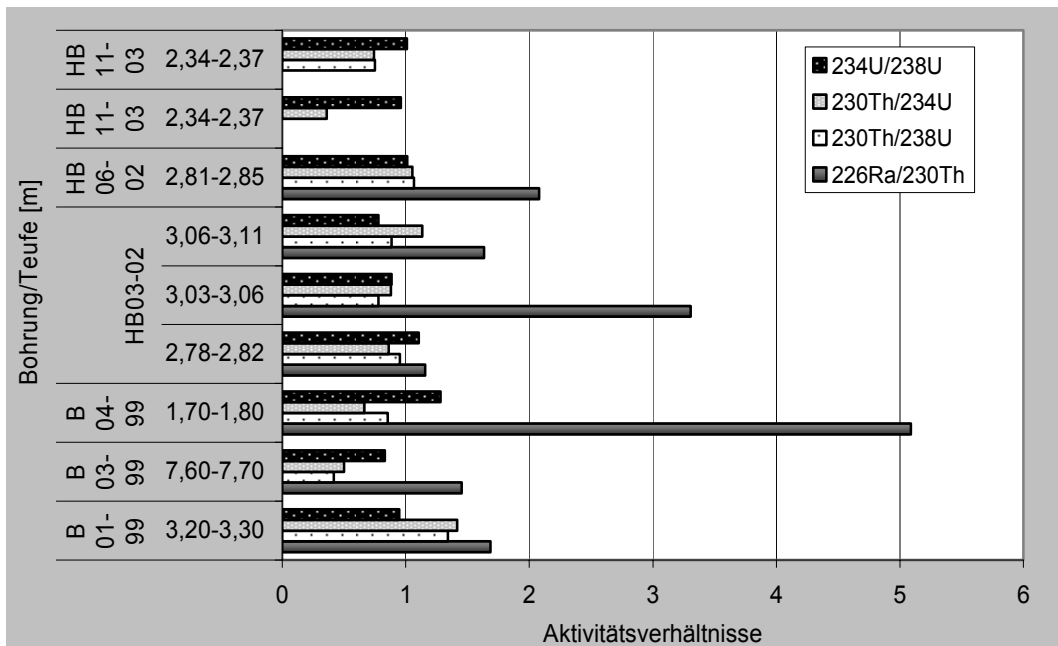
Fig. 74: Activity ratios of isotopes from the uranium decay chain in sediment samples from interbedded clay (Tertiary)
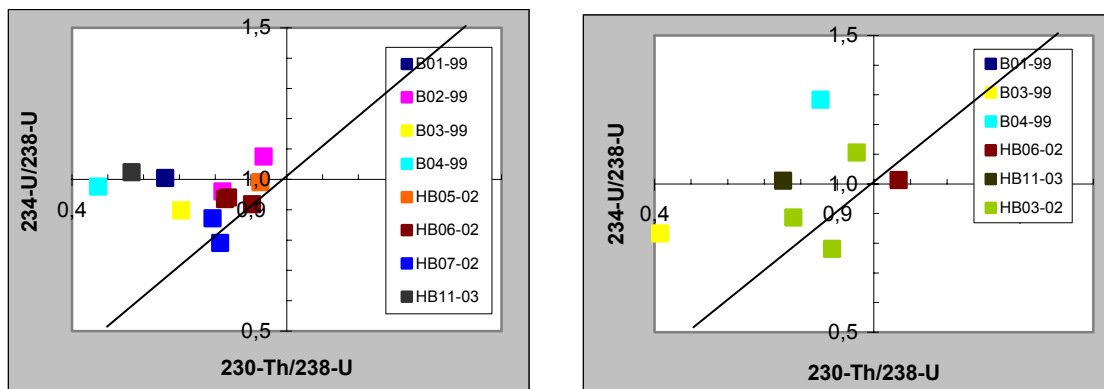
Fig. 75: Thiel diagram with values of sediment samples from Heselbach; left = samples from lignite horizon; right = samples from interbedded clay

The samples from the lignite horizon are mainly in the left, lower quadrant above the ^{230}Th/^{234}U equilibrium line and document a young, rapid accumulation process for uranium in this layer.

Within the interbedded clay, the activity ratios vary over a large range which indicates that different processes took place. The samples in the right diagram field below the ^{230}Th/^{234}U equilibrium line represent discharge processes of the uranium from the sediment. At these samples, oxidation of the sediments might have occurred, leading to the remobilisation of uranium. Two of the five analyses in the left, upper diagram field (^{234}U/^{238}U activity ratios > 1) indicate that uranium accumulation in the clay took place more slowly compared to the lignite horizon. In addition to the advective transport of the uranium with the groundwater, diffusion might be possible here as another uranium migration process.

5.2.3 Age determination of uranium enrichment

For determination of the time frame of uranium input only uranium, which was transported post sedimentary via groundwater into the tertiary rim sediments, has to be considered. For this purpose the so-called detritus fraction, which occurred in the sediment before uranium input, needs to be substracted from the total uranium content of the samples. It is possible to calculate the detritus concentration of uranium from the ^{232}Th-concentration, since thorium can be considered as immobile and therefore the original ^{232}Th/^{238}U concentration ratio can be assumed as constant. Usually the average ^{232}Th/^{238}U concentration ratio of 4.26 for granite /CHE 71/ is used for detritus correction. For the Tertiary sediments from Heselbach site the local ^{232}Th/^{238}U ratio

could be calculated from the background concentrations of [232]Th and [238]U in the downstream area (HB09-02 und HB10-02), where no uranium enrichment occurred. The average [232]Th/[238]U concentration ratio is 3.41. The value is calculated from the relation between activity A, mass m, decay constant λ and concentration c

$$A = \frac{c * \lambda}{m} \tag{11}$$

by:

$$\frac{A\left(^{232}Th\right) * \dfrac{m_{232}}{\lambda_{232}}}{A\left(^{238}U\right) * \dfrac{m_{238}}{\lambda_{238}}} = 3.41 \tag{12}$$

$$\frac{A\left(^{238}U\right)}{A\left(^{232}Th\right)} = \frac{1}{1.116} = 0{,}896 \quad \text{(detritus factor)} \tag{13}$$

Table 40: Detritus corrected [238]U-, [234]U-, [230]Th-activities [Bq/g] and activity ratios in sediment samples from Heselbach

sample	depth [m b.g.l.]	[238]U	[234]U	[230]Th	[234]U/[238]U	[230]Th/[234]U
B01-99	2.50-2.60	8.22	8.25	5.40	1.004	0.654
B02-99	4.55-4.65	2.83	3.05	2.64	1.078	0.866
	5.30-5.40	3.89	3.73	3.18	0.959	0.853
B03-99	6.70-6.80	1.78	1.59	1.24	0.894	0.779
	7.60-7.70	4.58	3.79	1.84	0.828	0.485
B04-99	0.60-0.70	8.58	8.37	4.04	0.975	0.482
	1.70-1.80	1.28	1.65	1.08	1.294	0.656
HB03-02	2.78-2.82	2.39	2.65	2.28	1.108	0.859
	3.03-3.06	2.32	2.05	1.80	0.883	0.876
HB05-02	6.42-6.46	0.24	0.24	0.22	0.987	0.920
HB06-02	1.00-1.05	5.53	5.20	4.62	0.939	0.888
	1.53-1.58	3.79	3.47	3.42	0.917	0.984
	2.08-2.11	4.88	4.53	3.96	0.929	0.873
HB07-02	3.24-3.28	1.12	0.97	0.88	0.866	0.906

The measured activities are reduced according to the calculated detritus factor F_d as demonstrated exemplary for the sample B01-99/2,50-2,60. All corrected values are shown in Table 40.

$$^{238}U_{corr}[Bq/g] = ^{238}U_{meas}[Bq/g] - F_d * \,^{232}Th \; [Bq/g] \qquad (14)$$

$$^{238}U_{corr}[Bq/g] = 8.310 - 0.896 * 0.103 = 8.2177 \; [Bq/g] \qquad (15)$$

Determining the age of sediment samples by means of the uranium decay chain uses the fact that the daughter isotope is also radioactive. In case of a natural system having been undisturbed over a long period of time, the parent/daughter activity ratio tends towards secular equilibrium. When secular equilibrium is reached, the activities of parent and daughter isotopes are identical and the activity ratio reaches the value 1. The accumulation of the daughter isotope or the degree of deviation from secular equilibrium can be used for dating the last uranium input. This only applies under the assumption that uranium was rapidly transported into the sediment compared to the half-life of the daughter isotope produced and that since then the system is closed. Under this assumption, the uranium enrichment can be calculated back on the basis of the $^{230}Th/^{234}U$ activity ratios as follows:

$$^{230}Th/^{234}U = \frac{1-e^{-\lambda_{230}*t}}{^{234}U/^{238}U} + \left[1 - \frac{1}{^{234}U/^{238}U}\right] * \frac{\lambda_{230}}{\lambda_{230}-\lambda_{234}} * \left[1 - e^{-(\lambda_{230}-\lambda_{234})t}\right] \qquad (16)$$

Table 41: Calculated uranium/thorium age of uranium enriched sediments at Heselbach site; light grey = interbedded clay; others = lignite

Drilling	Depth [m bgl]	Model age [k y] $^{230}Th/^{234}U$	Error ±
B01-99	2.50-2.60	116	57
B02-99	4.55-4.65	210	110
	5.30-5.40	220	130
B03-99	6.70-6.80	180	120
	7.60-7.70	75	38
B04-99	0.60-0.70	72	35
	1.70-1.80	110	51
HB03-02	2.78-2.82	200	230
	3.03-3.06	260	460
HB05-02	6.42-6.46	290	930
HB06-02	1.00-1.05	260	330
	2.08-2.11	240	330
HB07-02	3.24-3.28	300	1700
HB11-03	1.55-1.57	83	4.8
	2.34-2.37	49	1.7

The results presented in Table 41 show an uranium accumulation age of 49 - 300 ky. Despite large fluctuations and broad error variations this demonstrates the uranium enrichment in Heselbach being a geologically young process. Assuming that during the Quaternary uranium was transported into the Tertiary basin intermittently the uranium/thorium age of the sediment samples determined cannot reflect the absolute enrichment age. In this case, it cannot be assumed that the system is closed. Older uranium (about 800 ky) is already in equilibrium with [230]Th while very young uranium (about 10 ky) is in a clear non-equilibrium with its daughter isotope. Samples whose uranium enrichment was calculated to be, e. g., 250 ky can thus contain older uranium in combination with very young uranium. However, it is certain that uranium was transported into the Tertiary basin within the last 300 ky. This result leads to the model assumption that uranium reached the Tertiary rim by Quaternary meltwaters.

5.3 Radiometric investigations on groundwater samples

Activity ratios of surface- and groundwaters are presented in Table 42 and Fig. 77.

Table 42: Activity ratios in surface- and groundwater samples from Heselbach site

Drilling	Year	$^{234}U/^{238}U$	±	$^{230}Th/^{234}U$	±	$^{230}Th/^{238}U$	±
Steinbergsee							
OW-SBS	**2001**	0.91	0.19	1.93	0.30	1.75	0.28
	2003	-	-	-	-	-	-
Tertiary basin							
B01-99	**2001**	0.69	0.18	0.28	0.17	0.19	0.17
	2003	1.16	0.29	0.19	0.28	0.22	0.28
B02-99	**2001**	1.15	0.23	0.59	0.18	0.68	0.18
	2003	-	-	-	-	-	-
B03-99	**2001**	1.10	0.23	0.58	0.25	0.64	0.25
	2003	1.85	0.78	0.40	0.44	0.73	0.51
HB03-02	**2001**	-	-	-	-	-	-
	2003	0.89	0.14	0.002	0.62	0.002	0.62
HB06-02	**2001**	-	-	-	-	-	-
	2003	0.92	0.24	0.17	0.64	0.16	0.64
HB10-02	**2001**	-	-	-	-	-	-
	2003	1.65	0.57	0.70	0.60	1.15	0.66
Keuper groundwater							
HB01-02	**2001**	-	-	-	-	-	-
	2003	0.92	0.58	0.67	0.60	0.62	0.53
HB02-02	**2001**	-	-	-	-	-	-
	2003	1.03	0.32	0.23	0.63	0.24	0.63

The $^{234}U/^{238}U$ activity ratios in groundwaters of the Tertiary basin vary in a range from 0.69 to 1.85, the $^{230}Th/^{234}U$ ratios from 0.002 to 0.70. Towards the centre of the basin, a tendency to higher activity ratios was identified (Fig. 76). The samples extracted in September 2003 show lowest $^{234}U/^{238}U$ ratios at the transition to the Keuper sandstone directly at the rim. In these samples, thorium hardly exists. Since hydrogeological investigations confirm that the groundwater within the Tertiary basin originates from the same source and that the lignite was filled up evenly, the activity ratios of the groundwaters within the Tertiary basin should not differ significantly. It is therefore to be assumed that the different activity ratios are due to mixing processes with fresh surface waters.
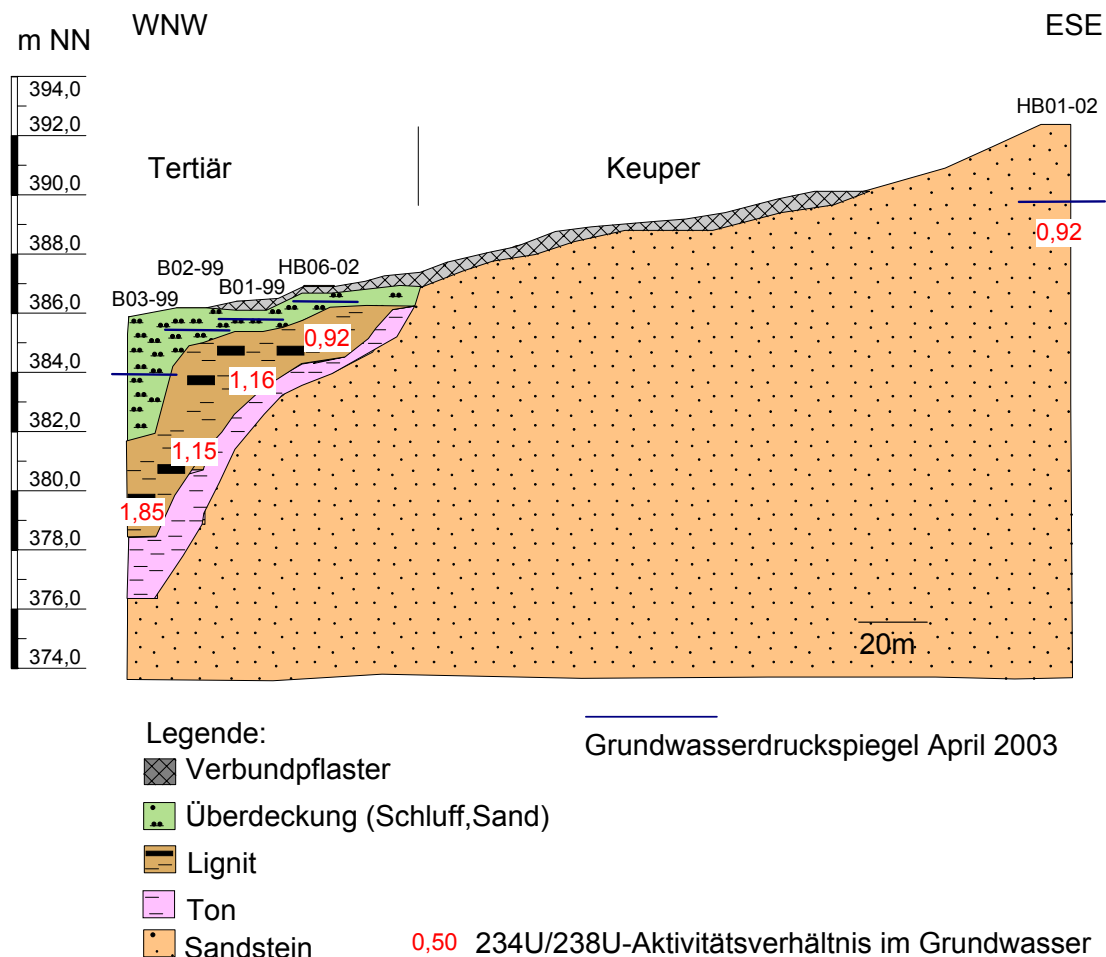
Fig. 76: Cross section of Tertiary rim with $^{234}U/^{238}U$ activity ratios (red numbers) in selected groundwater samples (Sep. 2003)

116
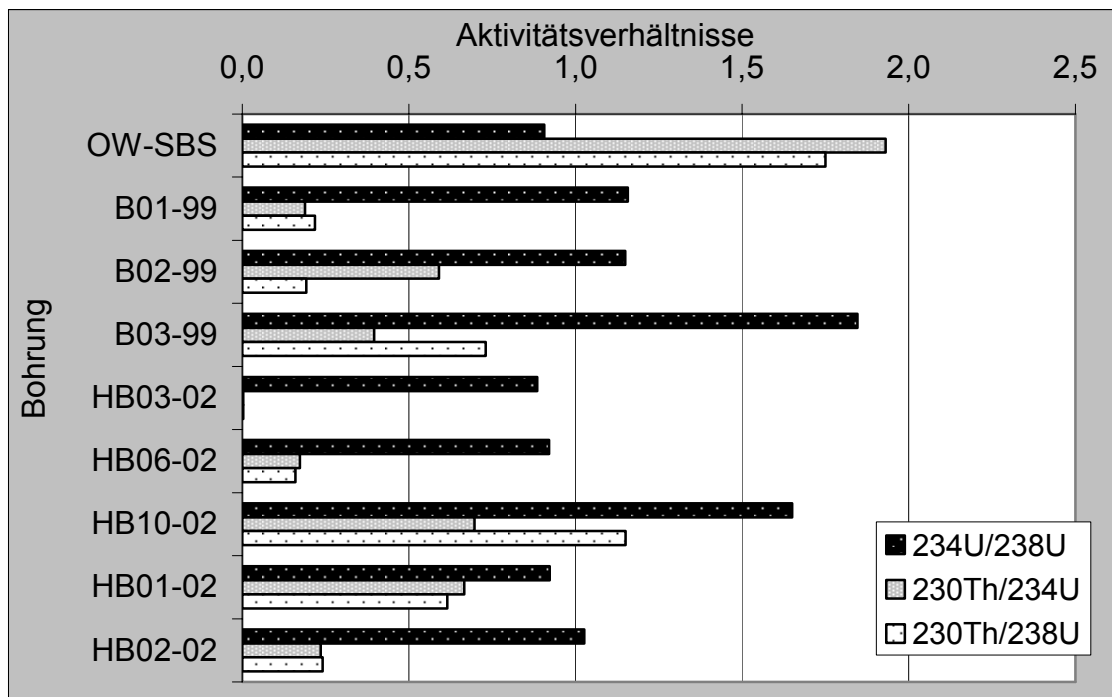
Fig. 77: Activity ratios of isotopes from the uranium decay chain in surface water and groundwater samples from Heselbach site

The $^{234}U/^{238}U$ activity ratios of the groundwaters from the Keuper sandstone are around 1 and < 1 which is equivalent to the ratio determined in the sediment. In general, groundwaters show $^{234}U/^{238}U$ activity ratios > 1 (e. g. seawater 1.14) due to the preferred dissolution of the ^{234}U isotope. Ratios < 1 document prior fixing of the uranium over a long period of time in the catchment area. Only after reaching $^{234}U/^{238}U$ activity ratios < 1, the uranium of the Keuper sandstone was remobilised.

6   Conclusions of the experimental investigations

In the following the main results of the experimental investigations are summarized with regard to the characteristics of the site and the development of uranium enrichment scenarios.

Characterisation of hydraulic conditions

From grain size investigations a value of $1.5 \cdot 10^{-5}$ m/s was determined for the hydraulic conductivity of the Keuper sandstone. This value characterises the inflow region of the investigation area and lies in the range generally observed for sandy aquifers. Based on the hydraulic gradients of the site the advective velocity in the Keuper sandstone was determined to max. 47 m/y.

The clay layers in the tertiary rim are low permeable; laboratory measurements yielded a hydraulic conductivity of about $3 \cdot 10^{-9}$ m/s. The same accounts for argillised parts of the lignite layer. These low hydraulic conductivities are supported by the result of a tracer test in the argillised lignite layers at the tertiary rim. Therefore, underlying clay layers and the argillised lignite layers at the tertiary rim are acting as a hydraulic barrier. This assumption is supported by very low changes in the water head at the tertiary rim. Furthermore, Tritium analyses show that the groundwater at the Tertiary rim originates from the 1970's in contrast to recent groundwater from the Keuper. The less argillised lignite layers with higher thickness downstream in the Tertiary basin exhibit higher hydraulic conductivities.

In the overlying Tertiary advective transport may take place due to hydraulic conductivities of 10^{-5} to 10^{-6} m/s, i.e. uranium input via the covering layers of the tertiary rim is possible.

Groundwater chemistry

The groundwater from Keuper sandstone in the upstream area can be categorized as $Na-Ca-SO_4-Cl$ type. They are low mineralised (<280 µS/cm) and hardly vary in their composition. The pH-values are in a range of 5.2 to 6.05 and are only slightly higher than the values in the Tertiary rim. Low oxygen contents of about 0.1 – 2 mg/l indicate at least partly reducing conditions.

The groundwater from the Tertiary rim show DOC concentrations < 12 mg/l, low bicarbonate contents (<15 mg/l) and in spite of high U contents in the sediments only low uranium concentrations of 0.1 to 1.3 ppb. In the Piper diagram they are classified as Ca-SO_4^{2-}-Cl^- type waters. The pH-values of 4.9 to 5.6 are in the slightly acid range, the oxygen content is < 5 mg/l and the specific electrical conductivity ranges from 260 to 600 µS/cm. In all wells nitrate was found as oxidation product of organic matter.

In addition it is possible to group the groundwaters from Heselbach site due to their different content of stable isotopes. The isotope signature of Keuper groundwater with $\delta^{18}O$-values of -9.30 [‰] and δ^2H of -64.70 [‰] complies with typical recent precipitation waters. The Tertiary rim waters on the other hand show significantly lighter isotope compositions ($\delta^{18}O$ values from -9.95 to -15.90 [‰]; δ^2H values from -70.0 to -119.2 [‰]).

This decrease in heavy isotopes documents the different age of the waters and an additional anthropogenic activity in the investigation area. After strong precipitation events groundwater and therewith the original isotope signature become diluted by surface run-off. It is very likely that the capacity of the drainage system of the newly constructed pavement is not high enough so that precipitation water gets from the surface via the overlying Tertiary into the wells. The effect is highest at the lowest niveau of the area. A dilution with isotopically light water mainly occurs in winter months where temperature effect causes enrichment of light isotopes in precipitation water. The strong precipitation events in January 2004 are probably responsible for very low values for $\delta^{18}O$ und δ^2H in this measuring campaign.

Characterisation of sediments

The sandy sediments from Heselbach site are characterised by SiO_2 contents of 46-90 % and by occurrence of orthoklas, muscovite and in more altered areas also kaolinite. The content of Al_2O_3 varies between 4.9 and 32.5 %.

Samples from the lignite horizon contain up to 44 % of SOC. Inorganic carbon is only found in traces (< 1.3 %). Beside isolated gypsum minerals the lignite horizon shows different contents of iron minerals, which are mainly pyrite, marcasite and jarosite. The occurrence of iron(II) and iron(III) minerals documents the variability of redox conditions on a small spatial scale.

Highest iron concentrations (up to 7 %) are found in the underlying clays. This clay consists of kaolinite and illite, halloysite in lower amounts. Mineral analyses together with analyses of their cation exchange capacity indicate a comparably low sorption capacity.

Characterisation of the uranium phases

The background values of uranium and Thorium in Keuper sandstone, derived from a number of samples are 2.64 and 13.84 ppm, respectively, resulting in a Th/U-ratio of 5.24. The average Th/U-ratio for sandstones is 4.2 /MEY 93/. Compared to this uranium seems to be decreased in Keuper sandstone in agreement with the assumption, that secondary uranium was mobilised from the Keuper sandstones and transported into the Tertiary basin. ^{234}U/^{238}U activity ratios of ~0,8 support this theory. In order to obtain such low activity ratios in the Keuper sediments, a preferred mobilisation of ^{234}U must have occurred over a long time frame, i.e. by α-recoil processes and subsequent oxidation of ^{234}U.

The uranium contents in sediment samples from the tertiary rim reach maximum values of 1128 ppm. The strong variations of more than 500 ppm in one sample (HB11-03/2,34-2,37) are indications for the high heterogeneity of the sediments. It is noticable, that in all drillings uranium enrichment is significantly lower at the bottom of the lignite horizon. Furthermore, uranium is mainly enriched in the upper third of the clay layer. Therefore, uranium input from the bottom of the tertiary basin is not likely.

The immobile uranium in the clay lignite layers of the tertiary rim was characterised in more detail by chemical and spectroscopic analyses. Sequential extractions have been performed with two different methods. The first method according to Percival resulted in a major amount of uranium bound to the organic phase. With this method an unexpected high content of easily accessible uranium of some 10 % was observed. For the extraction of this phase 1 M sodium acetate, pH 5 was used. In order to check this result, a second, modified, sequential extraction procedure was applied. A milder agent in phase 1 (1 M NH_4NO_3) yielded an easily accessible uranium fraction of less than 1 %. Therefore, it is very likely that sodium acetate as a slightly acid solution already dissolved uranium containing phases as iron(III) minerals. This is also indicated by high amounts of iron in the easily accessible phase of the procedure according to Percival. Iron(III) phases like markasite have been detected by XRD. Therefore, we assume that part of uranium is bound to oxidised, easily soluble iron minerals (secondary phases).

It was not possible to identify crystalline uranium phases by BSE images in the sediment samples from Heselbach, neither by punctual element analysis at mineral grains of pyrite or coal nor by long-term mapping of several sample segments of high uranium content. However, the spatial resolution of the method is limited to mineral sizes of 1 µm. This means, uranium does not occur in crystalline form or mineral grains are << 1 µm in size. This statement is confirmed by autoradiographic measurements, which show a highly homogenous distribution of α-activity without any hot spots.

XANES investigations identified uranium exclusively as U(VI). This is in good agreement with U(IV)/U(VI) separation experiments by wet chemical method, where more than 99 % of uranium was observed as U(VI). A third argument for existence of uranium in oxidation state U(VI) is derived by EXAFS spectra, showing bonding lengths of uranium with oxygen atoms of 1.78 and 2.42 Å which are typical for the uranyl ion UO_2^{2+}. A third bonding length of 3.08 Å measured by EXAFS probably represents bonding of uranyl to functional groups of sedimentary organic matter.

Spectroscopic analysis and chemical extraction experiments show a unique picture for the uranium enriched sediments in the Tertiary basin: Reduction of U(VI) to U(IV) did not occur. This is furthermore supported by rather high Eh-values in this surface-near groundwater, where uranium is expected to occur in the hexavalent form. The existence of U(VI) minerals could not be observed. Thermodynamic calculations with PHREEQC confirm that saturation of U(VI)-phases will not occur under the observed geochemical conditions and the low uranium concentrations of max. 1.3 ppb.

The combined evaluation of all results let us conclude that the major fraction of uranium is homogeneously bound to organic substances but not easily accessible. It is likely that additional co-precipitation with iron(III) minerals plays a role.

Characterisation of enrichment processes by radiometry

All activity ratios of isotopes from the uranium decay chain of samples from the lignite horizon indicate a young accumulation process of uranium in this layer. An advective transport via the overlying Tertiary into the Tertiary rim is one possible process. Assuming, that uranium enrichment occurred as one single process in the past the dating by evaluation of ^{230}Th/^{234}U activity ratios yields uranium ages of 72-300 ky. Therefore, a pure syn-genetic uranium enrichment can be excluded. This is supported by the fact, that the observed uranium enrichment occurs not stratiform. /ZIE 57/

7　　　Scenarios for site evolution

Resting upon experimental investigations, firstly a description of the hydrogeological situation of the site under today's disturbed conditions is given. Based on this a hydrogeological model is developed for the pre coal mining situation, i.e. under undisturbed conditions, which represents the hydrogeological situation during the time of uranium input into the Tertiary rim. Concerning this uranium input two different scenarios are developed. Finally, for both scenarios flow and transport calculations are performed.

7.1　　　Site under disturbed conditions

As basis for the description of the hydrogeological situation today, data from very different sources were used. The following data bases were available:

1) Topographical data (1:10'000 topographical map, digitalised surface, relief, location of receiving stream, watersheds)

2) Geological data (1:25'000 geological map, lithology and stratigraphy from 14 drillings, cross-section profiles)

3) Hydrogeological data (1:50'000 hydrological map, hydraulic parameters, groundwater recharge, groundwater dynamics, groundwater chemistry, isotope analyses)

For the investigation area, three cross-section profiles were developed which cover all drilled stratigraphic units and illustrate their positioning to each other. The locations of the different profiles are shown in the section of the geological map (Fig. 78).

Within the investigation area, a Keuper spur has been mapped at the surface (south of the interstate road B85), but also subducts the Tertiary basin in westward direction and subdivides the investigation area south and north of this spur into two subbasins. Fig. 79 shows the revealed Keuper surface and reflects the spatial orientation of the two subbasin areas. The data selectively acquired in the relevant boreholes were applied to the entire model area by means of kriging interpolation (Surfer 8.0). In addition to the actual borehole data, digitalised outcrop data as well as cross-section profile data are also taken into consideration.
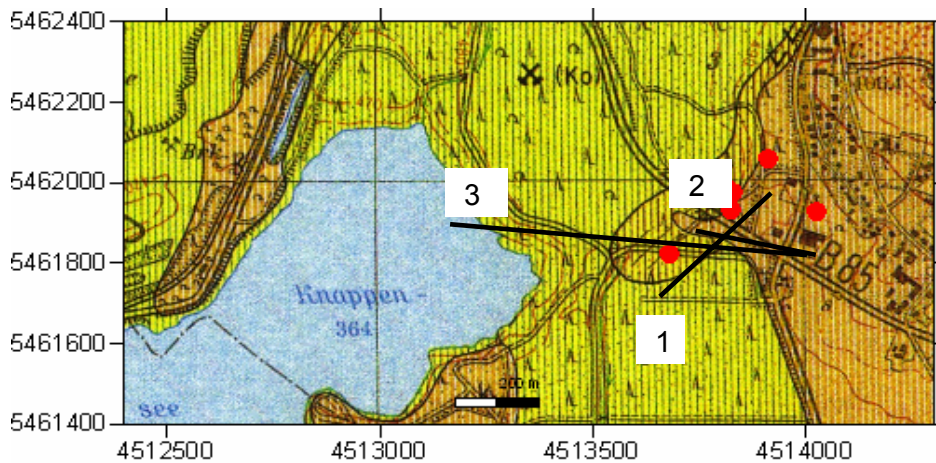
Fig. 78: Excerpt from geological map (GK25, 1995) with location of boreholes (red) und profile lines 1 - 3
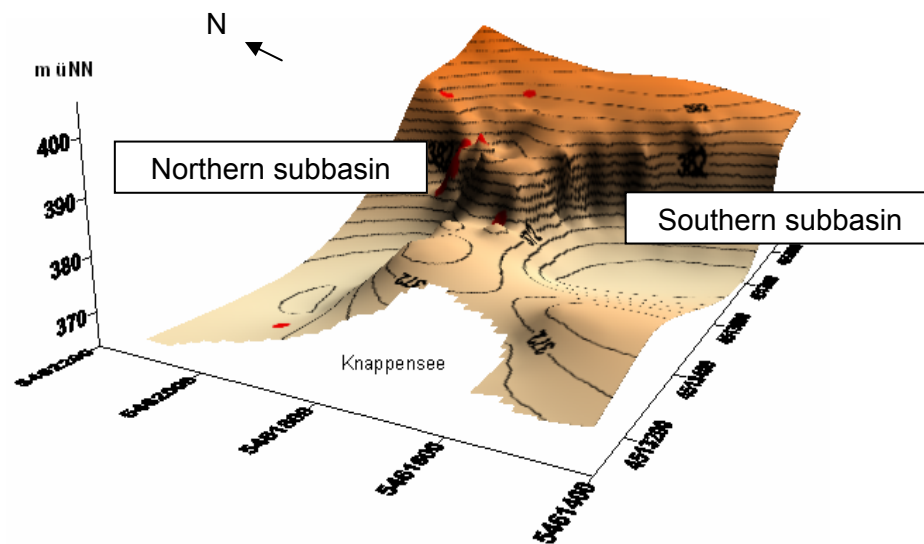
Fig. 79: Surface of Keuper sandstone at the Heselbach site (revealed); boreholes (red).

Profile 1 (Fig. 80) runs through both subbasins and documents their different filling. While in the northern subbasin, interbedded clays and lignites of the upper seam with increased uranium concentrations in their original bedding were obtained, the southern subbasin has been excavated by open-cast mining and is now backfilled with mainly clayey sediments.
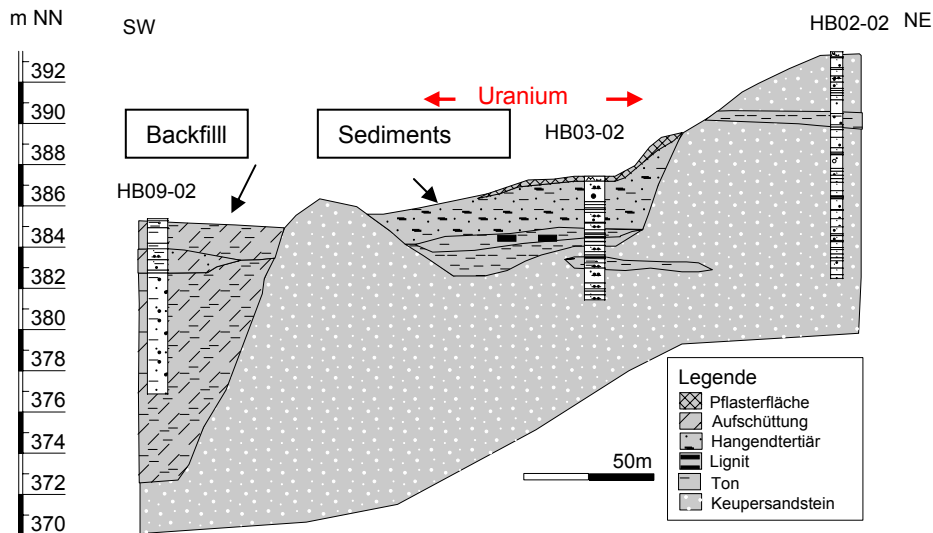
Fig. 80: Profile 1: SW-NE profile through investigation area with northern (right) and southern (left) subbasins
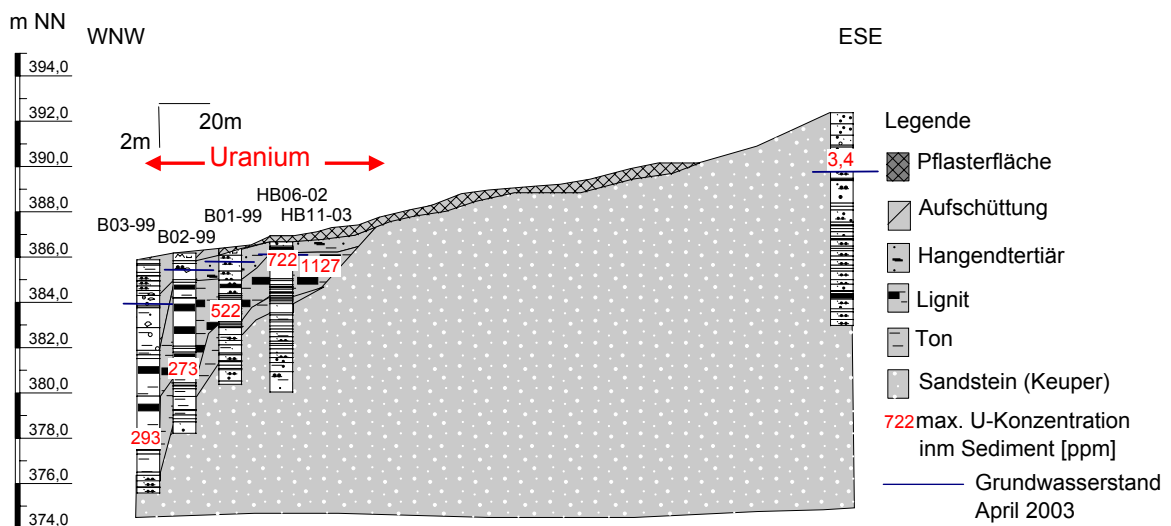
Fig. 81: Profile 2: WNW-ESE profile through the northern subbasin with transition from Keuper (right) to Tertiary basin (left)

Profile 2 (Fig. 81) displays the uranium-containing Tertiary rim of the northern subbasin and shows the transition from Keuper sandstone in the east to the basin sediments in the west. Further, it shows the lensing-out of the Tertiary main interbedded clay sediment and the lignite horizon of the upper seam. It also illustrates the overlap of the overlying Tertiary layer. The "overlying Tertiary" was identified within seven drillings at the property of Lohbauer company but no more in drilling B03-99. Hence, the transition between excavated and backfilled basin and the undisturbed rim with still existing overlying Tertiary is located between drillings B03-99 and B02-99.

125

Profile 3 displays a W-E cross-section through northern subbasin reaching from Keuper outcrop in the E to lake Knappensee in the W and covers nearly the entire investigation area. The sketch (Fig. 82) also evinces the relatively shallow relief at the basin rim as well as the steep decline towards lake Knappensee.
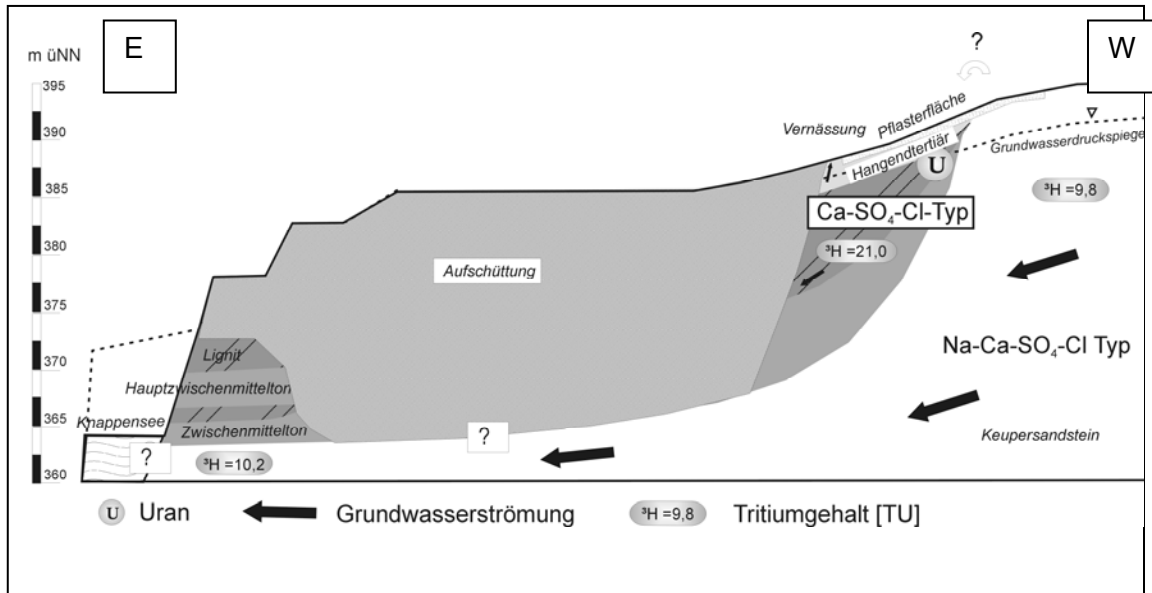
Fig. 82: Profile 3: Schematic W-E cross-section through the northern subbasin. This figure especially points out the extent of anthropogenic backfill (light grey) in the investigation area. Remnants of natural Tertiary sediments (clay, lignite) are marked by dark grey colours

In drilling HB10-02 (close to lake Knappensee), Keuper sandstone was found at the base. In addition, groundwater isotope analyses confirm a hydraulic connection between upstream area in the east and HB10-02 which is assumed to exist below the Tertiary basin. Due to the open pit mining until the end of the 1960's, the area of today's lake Knappensee and areals of the investigation area were excavated and partly backfilled up to the former surface level. The dashed line in left part of Fig. 82 corresponds to the former topography. Whether the Keuper sandstone is really connected to lake Knappensee or not cannot be verified due to lack of drillings. Further, the extension of the lower backfill level to the Keuper is also uncertain. Tertiary interbedded clays, not having been removed by mining, possibly seal the Tertiary basin towards the deeper basement, or clayey backfill material directly covers the Keuper sandstone, as shown in the profile. In both cases, it can be assumed that at least the basin rim is sealed towards the deeper basement. This assumption is substantiated by the clearly different chemism of the waters. Further, the measured tritium contents and

the tracer test performed indicate older, stagnant groundwater in drillings at the basin rim area, while the Keuper aquifer contains recent water, which is confirmed by today's isotope signature. Another indication for a sealing function of backfill material are episodic wet areas at the transition from overlying Tertiary to the backfill (Fig. 82).

7.2   Site under undisturbed conditions

The model presented in this chapter describes the groundwater conditions as they probably have been at the time of uranium input into the Tertiary rim. It represents undisturbed conditions in the region before the mine operation caused changes in topography, lithology and flow regime.

7.2.1   Scenarios for uranium enrichment

Based on all informations available for the site two different scenarios for uranium enrichment in the Tertiary rim sediments have been developed. For both scenarios flow and transport calculations are performed in order to test, whether uranium enrichment and uranium distribution observed today can be described and explained.

The stratigraphic distribution of the immobile uranium in sedimentary layers argues against a syngenetic uranium enrichment. Uranium does not exist stratiform, but extends over different layers and depths /ZIE 61/, indicating subsequent uranium input. Further, the evaluation of the analyses isotope activity ratios showed a recent uranium input into the sediments of the Tertiary basin during the last 300 ky up to recent periods (app. 40 ky). An older uranium input (e.g. 1 My) in combination with a young enrichment (e.g. 10 ky) could also have led to the activity ratios determined. Therefore, the uranium input must not be limited to the last 300 ky but may have started already before. But, a single uranium input phase during Tertiary can be excluded.

Scenario 1

Scenario 1 (Fig. 83, top) describes a continuous uranium input into the Tratiary rim sediments and assumes that a permanent groundwater flow originating from Keuper sandstone occurred in the past and even occurs today. Since the today's groundwater system was formed during the Quarternary, about 800 ka ago /TIL 56/, this date is taken as the starting point. Since then uranium has been mobilised in the Keuper

sandstone, transported and finally enriched in the lignitic sediments of Tertiary rim by a more or less constant precipitation rate.
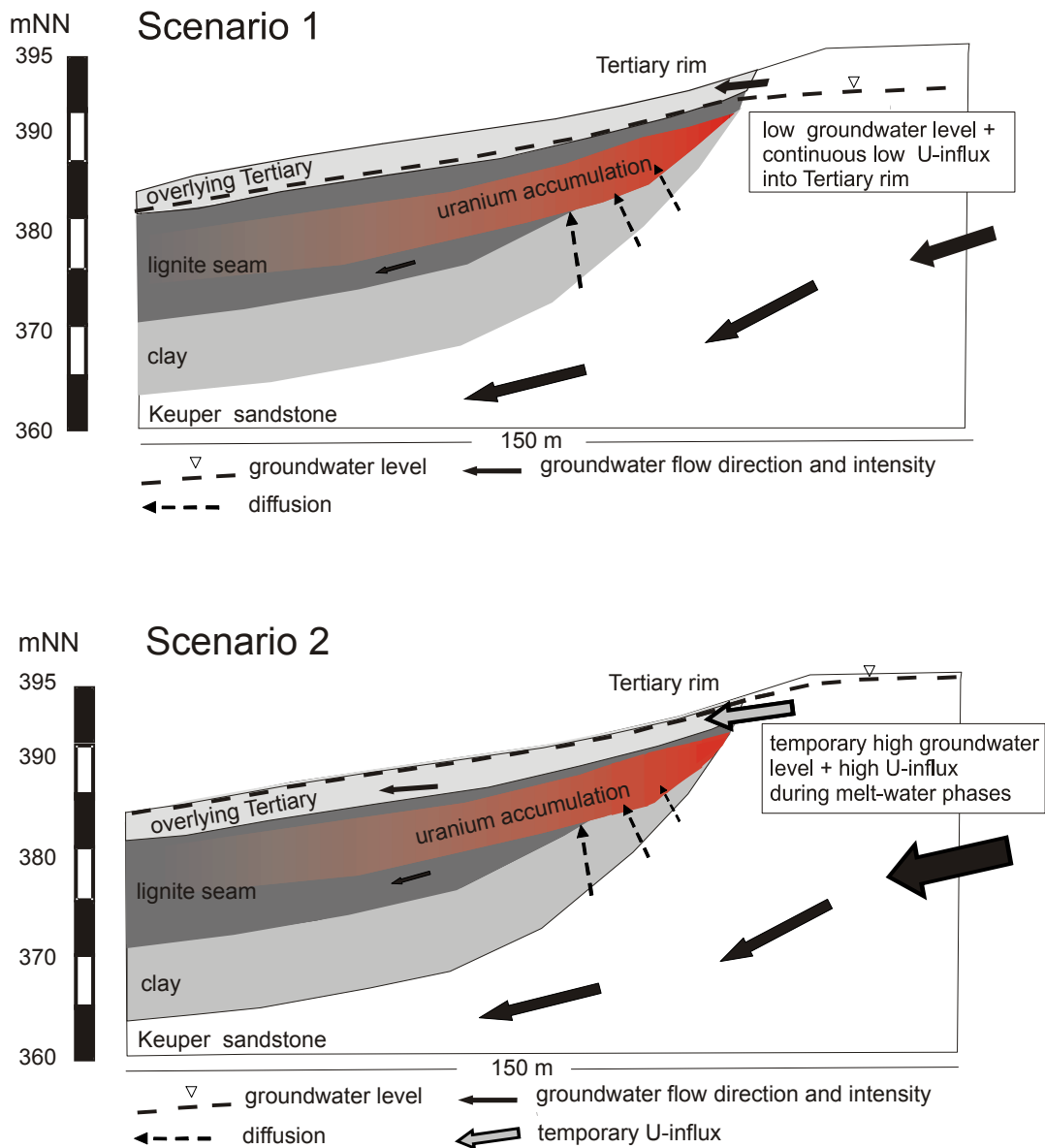
Fig. 83: Main characteristics of Scenario 1 and Scenario 2

Scenario 2

However, radiometric measurements gave indications, that uranium was fixed in the Keuper sandstone as U(IV) and mobilization occured via changes in redox conditions. This observation lead to the development of a second scenario (Fig. 83, bottom), where uranium enrichment in lignitic sediments occurred not by continous but periodic input of uranium. Climatic changes are supposed to have changed the chemical conditions in the Keuper sandstone during the last several hundred thousand

128

years. It is known from literature that during the last 800 ky, four to five ice age cycles covered the region with huge masses of snow /TIL 56/. It is to be assumed that after melting of these snow masses at the beginning of warm periods the aquifers were filled up with fresh, cold, very oxygen-rich groundwater and - beside generally high groundwater levels - an oxidising environment developed abruptly. Under such conditions, the interbedded uranium of the Keuper sandstone could have been leached and transported into remote areas via groundwater. Some time after the melting of glaciers, the groundwater levels normalised and the former hydraulic and chemical conditions were reached again until the next cycle of glaciation.

In the Bodenwöhrer Senke the occurence of 4 to 5 glacial periods is documented by river gravels and mud. According to the model assumption, an uranium input would have taken place within the last 800 ky four to five times over a period of about 1000 y each. This is summarised in Table 43.

Table 43: Structuring of Quaternary with alpine classification with assignment of uranium input phases at Heselbach acc. to scenario 2

Geological epoch		Age [ky]	Duration of interglacial [ky]	Alpine classification	Uranium input phases
Holocene	Late Holocene	0		post glacial	
	Middle Holocene				
	Early Holocene	~10			
Pleistocene	Late Pleistocene	~15	10	**Würm Interglacial** Würm ice age	5th input
		~115			
		~130	15	**Riß-Würm Interglacial**	4th input
	Middle Pleistocene	~130		Riß ice age	
		~300			
		~300	30	**Mindel-Riß Interglacial**	3rd input
	~380 [ky]	~330			
	Early Pleistocene	~330		Mindel ice age	
		500	?	**Haslach-Mindel Interglacial**	2nd input
		~500		Haslach ice age	
	~780 [ky]	700	?	**Günz-Haslach Interglacial**	1st input

7.3   Flow and Transport modelling

Primary objective of flow and transport modelling consists in reviewing quantitatively the geological interpretations of the gained site data on the one hand and understanding the presented scenarios of uranium enrichment in the Tertiary rim on the other hand. For this purpose, an abstracted cross section along the main flow direction - based on drilling data - is transferred to a vertical 2D flow model. Based on the flow model considering the original stratigraphy, transport calculations were carried out for the two uranium transport scenarios presented in section 7.2.1 and the uranium input was described quantitatively.

Scenario 1 describes a continuous uranium input into the tertiary rim over a period of 800'000 years. It is assumed that the chemism of the groundwaters as well as the upstream boundary conditions are the same as today. In Scenario 2 apriori a period of 20'000 years is considered. This period complies with an average interglacial period during the Quaternary. For the beginning of this period an increased water recharge is assumed due to the melt water inflow from the hinterland. The Keuper pore aquifer is filled up with cold oxygenated waters. This effect is considered by means of an increased upstream flow in the model for the first 1'000 years. Due to the variation of the Redox environment of the waters an increased uranium concentration is also assumed. For the remaining 19'000 years, a sedation of the hydraulic conditions is presumed, the boundary conditions to be determined according to the present (original) conditions. These boundary conditions are defined in the following as a *'moderate upstream'*.

The calculated amount and distribution of the irreversibly bound uranium phase documents the uranium enrichment within the interglacial period. In order to make a statement on the accumulated overall uranium concentration, the calculated immobile uranium concentration according to the amount of ice age cycles assumed for the area under investigation is multiplied by a factor of five. During the ice-ages itself no groundwater flow and therefore no uranium transport take place.

7.3.1   Model Assembly

The flow- and transport calculations were carried out by Wasy with the *Finite-Element-Subsurface Flow und Transport Simulation System* (FeFlow) Version 5.2 /DIE 05/. The first step consisted in summarizing the   encountered   stratigraphic   units   and

implementing them in a geometric model assembly. The discretisation of the model is done subsequently by using the triangle grid generator /SHE 06/. In order to recreate the thinning out layers at the tertiary rim edge as exactly as possible triangle-shaped elements were chosen. A manual grid refinement allows a high resolution of the uranium-bearing Tertiary rim area. The edge length of each element varies from 0.08 m at the Tertiary rim and max. 1.5 m in the Keuper sandstone area, depending on the refinement level. Alltogether 65'973 knods were produced with 130'154 elements. With an East-West extension from 853 m and a height difference of max. 32.5 m the model comprises a total area of 20'095 m².

The model is made up by altogether 4 stratigraphic units. The bottom model layer emulates the Keuper sandstone (1). Within the Tertiary basin structure, clay (2) and lignite (3) horizons follow which are covered by the overlaying tertiary layer (4) on the top. (Fig. 84). Observation points exist on each of four knods within the uranium-bearing lignite layer. At these points simulated element concentrations can be illustrated in form of time series or for defined time periods. Three of this four observation points represent the boreholes B03-99, HB06-02 and HB03-02. In order to receive further information on the not encountered rim edge area, a fourth observation point (ZP) was added at the border between Keuper sandstone and Tertiary rim edge.
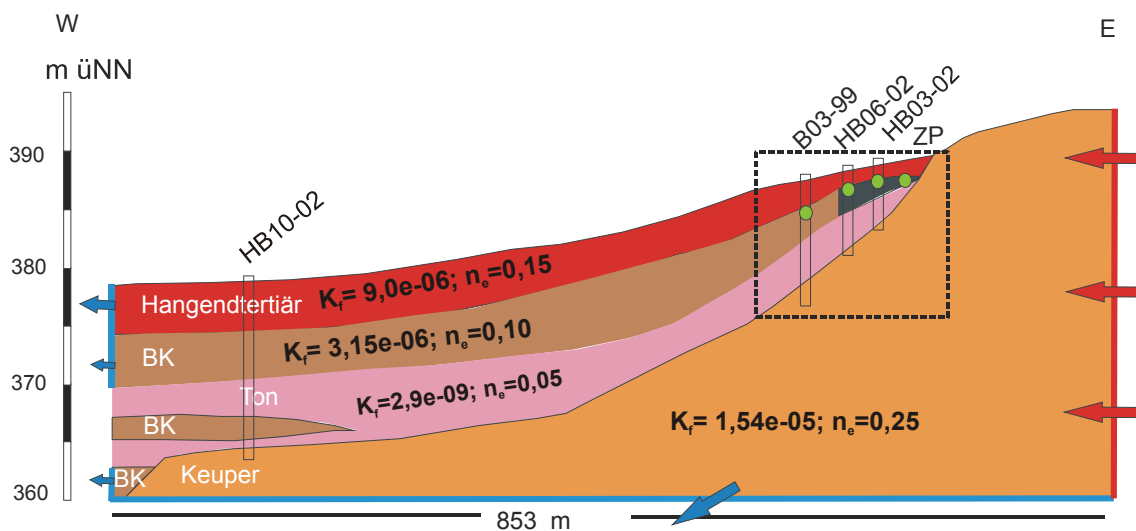
Fig. 84: Schematical 2D-Vertical Model (vertical exaggeration: 10x) demonstrating the refined discretisation area at the Tertiary rim edge (dashed rectangle), the hydraulic parameters of the model layers as well as boundary conditions for flow modelling. The red arrows present the upstream Dirichlet-, the blue arrows the downstream Neumann-boundary condition. The observation points in the uranium-containing lignite horizon are marked by green dots

131

7.3.2 Flow parameter and boundary conditions

The classification of the hydraulic material parameters to single model elements is effected according to hydrostratigraphic units defined beforehand (Table 44). The assignment herewith is based on the hydraulic permeability results from field slug & bail tests, as well as from laboratory testing (section 3.1.3). It was assumed that the k_f-values are not subjected to anisotropy.

A special characteristic is related to the Tertiary rim edge directly bordering the Keuper: the top soil layers of the lignite horizon are featured by very high clay content. For this reason the k_f-values of the model elements at the rim edge were not refered to lignite, but to clay type material. This area is highlighted in Fig. 84 by dark grey colouring.

Table 44: Material parameter for the flow model

Hydrostratigraphic Unit	k_f-value [m/s]
Overlying Tertiary (‚Hangendtertiär')	$1.00 \cdot 10^{-6}$
Lignite (BK)	$3.15 \cdot 10^{-6}$
Clay (Ton)	$2.90 \cdot 10^{-9}$
Keuper	$1.54 \cdot 10^{-5}$

The surface of the territory forms the top edge of the balance volume, a levelling of 390 m a.s.l. is assumed at random. The eastern groundwater inflow is defined via the Keuper sandstone by means of a Type 1 boundary condition (Dirichlet) and forms the model limit there. A Type 2 boundary condition (Neumann) describes the outflow. At the outflow border, it is distinguished between different hydrostratigraphic units within the Tertiary. Clay units are estimated as impermeable, whereas lignite as well as the overlying Tertiary are pearmeable and facilitate outflow at the western border. Table 45 gives an idea of the two boundary conditions for flow modelling.

Table 45: Overview of constant and temporally varying boundary conditions of the flow modelling

	Boundary conditions	Scenario	
		1	2
Inflow	Dirichlet	Constant: 390 m a.s.l.	1000 y increased inflow: 392 m a.s.l. 19 000 y moderate inflow: 390 m a.s.l.
Outflow	Neumann	Constant, mainly via overlying tertiary layer and Keuper, secondarily via lignite	

The groundwater recharge was not considered in the flow modelling. Data on site-specific groundwater recharge rates are available for the present, but no statements can be made for the geological past. In fact, it can be assumed that during the Quaternary - in times of permafrost - no groundwater flow and no groundwater recharge took place in the investigation area. During the warm periods of the ice age cycles a groundwater recharge is likely; however it is still not considered in the model, as the influence of groundwater infiltration via ground surface is seen to be negligible, compared to sidewise inflow.

First of all a flow model under constant boundary conditions was prepared for the investigation area. The result of this modelling gave the initial conditions for the following transport calculations. In Scenario 1, the boundary conditions were not varied. For the calculations regarding Scenario 2 a dynamic operational behaviour flow model was used according to Table 45.

7.3.3   Transport parameters

The transport modelling was performed for the element uranium. A fluid phase $^{238}U_{fl}$ and a solid phase $^{238}U_s$ are considered. The fluid phase is subject to an element specific linear sorption based on the K_d-concept. For the solid uranium phase it is considered to be irreversibly bound $^{238}U_s$ in the sediment. In the model the formation of the new, solid uranium phase is assumed to occur in the lignite horizon. In Table 46 the defined material parameters for the transport modelling of the model area are summarized.

Table 46: Material parameters for the transport

Hydrostratigraphic unit	Effective porosity (n_e)	Sorption-coefficient U [m^3/kg]	Dispersion length [m]		Diffusion coefficient [m^2/s]
			L	T	
Overlying Tertiary (4)	0.15	n.c.			
Lignite (3)	0.10	0.18	5	0.5	10^{-9}
Clay (2)	0.05	0.70			
Keuper sandstone (1)	0.25	n.c.			

with L= longitudinal; T= transversal;   n.c. = not considered

The effective porosity data for the hydrostratigraphic units are based on informations on particle size measurements of the respective material and deduced from literature average values according to /HOE 96/.

The sorption data for uranium are calculated from the sorbed phase determined by sequential extraction and the dissolved uranium concentration in the relevant groundwater. The resulting K_d-value amounts to 0.18 m^3/kg for lignite and. 0.70 m^3/kg for clay.

Sediment specific dispersion and diffusion values are not available from Heselbach site and therefore are also taken from literature /KIN 92/. The dispersion length is scale dependent. For the area investigated the longitudinal dispersion D_L is fixed on 5 m. The transversal dispersion usually corresponds to 1/10 of D_L and therefore a value of 0.5 m is assumed for the model. The diffusion coefficient is assumed to be 10^{-9} m^2/s.

Due to fact that exact initial and boundary conditions for the uranium input in the past are not known, plausible assumptions have to be made. Especially the uranium upstream concentration and the parameters for the uranium retention have influence on the extent and expansion of the irreversibly bound uranium phase.

For the constant uranium input (Scenario 1) the average upstream uranium concentration was based on the Keuper-groundwater according to present content of 1 ppb. With the intermittent input (Scenario 2) it is assumed that the increased redox-value of the melt waters results in an increased uranium mobilisation. For this reason the first 1'000 years are modelled with an increased uranium concentration in the upstream groundwater over a concentration range which can occur in natural groundwaters. For the period after 1'000 years it is assumed that the hydraulic conditions settle again and a constant uranium concentration of 1 ppb uranium in the upstream water will occur over the remaining 19'000 years of the warm period (Table 45).

The calculation of the irreversibly bound uranium phase is carried out, assuming that above a maximum uranium concentration in the groundwater (C_{max}) the fixation of uranium in a solid phase takes place. Further, it is assumed that it will not be dissolved again after drop of the dissolved uranium concentration in the groundwater below C_{max}. Since the radiometric analyses of sediment samples show an accumulation of uranium in the lignite horizon but no depletion and uranium concentrations in groundwater are

very low, it is assumed that under natural conditions no mobilisation of this uranium takes place. Correspondingly C_{max} of 1.0 ppb is chosen according to the present average value of the uranium concentration in the groundwater of the Tertiary basin.

A further matter of influence on the retention are the reaction kinetics, where a dissolved substance migrates to a solid substance. As lignitic clay presents an efficient barrier, a rapid accumulation can be expected. The precipitation rate of 31.5 mg/l per year that was assumed for the model calculations is estimated accordingly high.

Sensitivity Analysis

One important uncertainty of the modelling is the fact that hydrogeological as well as the hydrochemical conditions of the past are not known exactly. In order to better estimate the influences of several parameters regarding the modelling results, sensitivity analyses are carried out changing one parameter respectively compared with the reference. Table 47 shows a summary of selected parameters for various calculation runs.

Table 47: Varying uranium transport parameters of the sensitivity analysis for Scenario 1 and Scenario 2

Scenario 1				Scenario 2				
run	Upstream [ppb] 800 ky	C_{max} [ppb]	Precipitation rate [mg/l/y]	run	Upstream [ppb] 1 ky	Upstream [ppb] 19 ky	C_{max} [ppb]	Precipitation rate [mg/l/y]
1	1.5	1.0	31.5	3	5	1.0	1.0	31.50
2	1.0	0.5	31.5	4	10	1.0	1.0	31.50
				5	20	1.0	1.0	31.50
				6	30	1.0	1.0	31.50
				7	50	1.0	1.0	31.50
				8	30	1.0	0.5	31.50
				9	30	1.0	1.5	31.50
				10	30	1.0	1.0	3.15

The runs 1 and 2 as well as 3 to 7 illustrate the effect on different higher uranium upstream concentrations. The runs 8 and 9 show the influence in case of modifications regarding the maximum dissolved uranium concentration C_{max} and in run 10 the impact of a decreased precipitation rate (factor 10) is analysed.

7.3.4   Results and plausibility considerations

7.3.4.1   Flow modelling

A calibration of the flow model was carried out by means of a groundwater measurement on 23rd January, 2003. Fig. 85 shows the difference between measured groundwater levels (GWDS) and those calculated by the model.
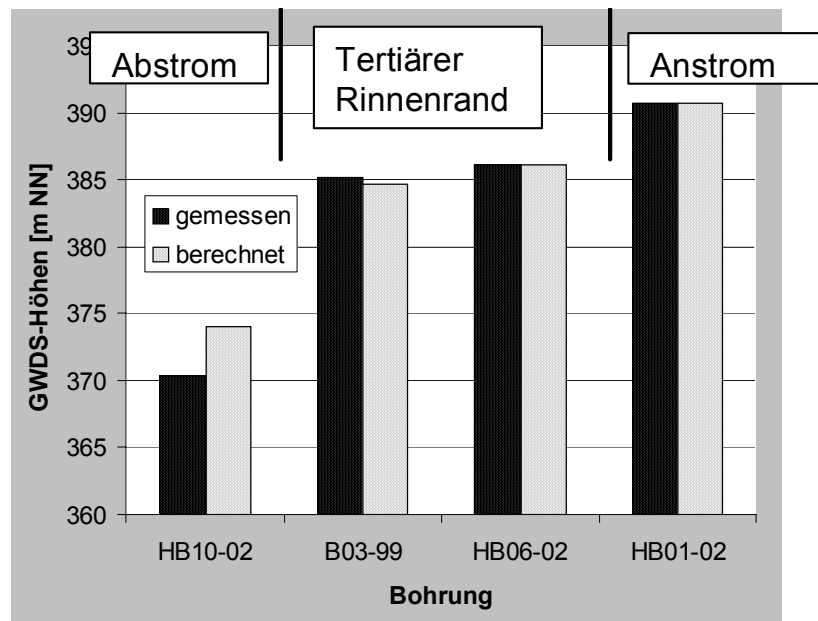
Fig. 85:   Opposing of measured (black columns) and calculated (white columns) water heads as basis for calibration of the flow models (by means of GWDS- measurements on 23rd January, 2003)

After calibration the model presents the natural conditions of the boreholes in the upstream and Tertiary rim edge adequately. Calculated and measured GW-levels of borehole B03-99 vary in cm, of boreholes HB01-02 and HB06-02 only in a mm range.

In contrast, in the downstream area (borehole HB10-02) the measured GW-levels are below the calculated values by several metres. At the same time it must be pointed out that the model represents a situation prior to open-cast mining. Today however a large part of the former coal sediments is replaced by backfill material. In addition the newly formed lake Knappensee represents a receiving stream. In comparison to the modelled undisturbed conditions prior to mining activities, today a higher hydraulic gradient is existent in the downstream flow which explains the recent low water levels of the borehole HB10-02.

After calibration a check of the model is carried out by means of recorded GW-levels of the time dependent measurements at the points HB01-02 and HB06-02 that were available for the period from March to September 2003. In Fig. 86 the calculated modelling results are compared with actual registered GW-levels at the measuring point HB06-02.
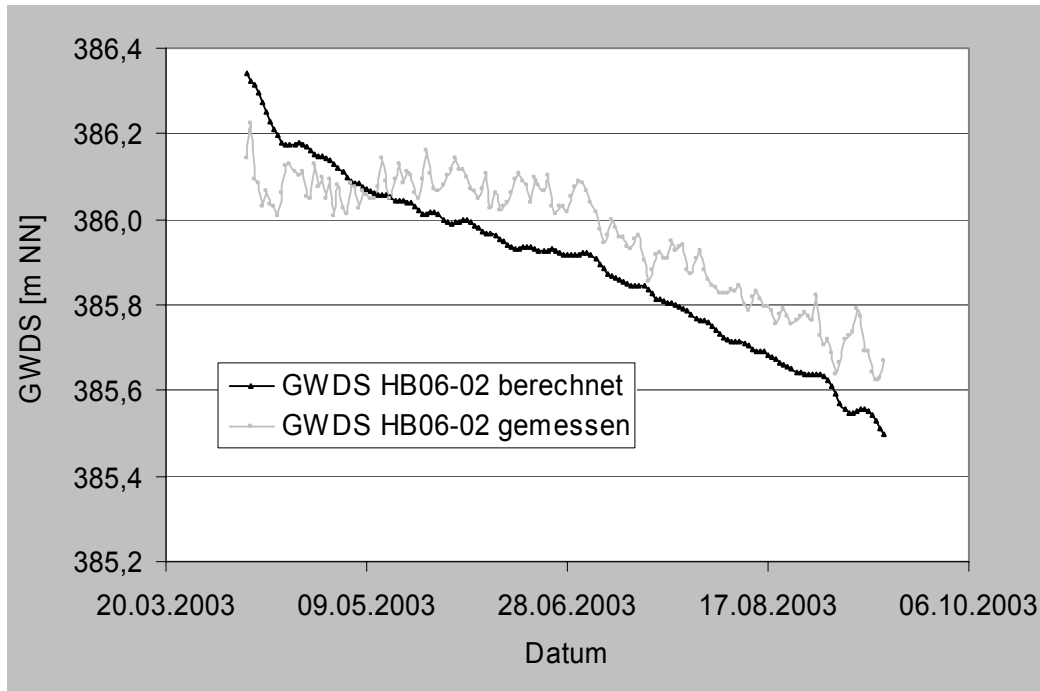
Fig. 86: Comparison of calculated (black) and daily measured (grey) water heads in well HB06-02

Slight variations of the measured data compared with the calculated data exist. On average the modelling results are 10-15 cm below the GW-levels observed. The variations and differences can be put down to the effect that recharge by precipitation is not considered in the model. For calculation of the uranium input into the Tertiary rim over a period of several hundred thousand years, these variations are not relevant.

The results of the flow modelling under moderate upstream conditions (Scenario 1) are presented in Fig. 87 and Fig. 88. In Fig. 87 the flow of the Keuper groundwater into the Tertiary rim is demonstrated. It becomes clear that the uranium bearing layer of the lignite horizon area is permanently below the ground water table.

The maximum ground water flow velocity is achieved by 14 m/a in the Keuper below the Tertiary rim. A similar velocity of the groundwater is reached in the overlying Tertiary directly at the border to the Keuper sandstone. In the course of the overlying

Tertiary the flow velocity of the groundwater decreases rapidly. In the rear part of this horizon flow velocities of only a few meters per year are achieved. The ground water in the lignite horizon has a maximum flow velocity of 1.5 m/a; in the clay horizon in contrast only a few cm/a. The results are in accordance with the site experiments showing almost stagnating water within the Tertiary rim.
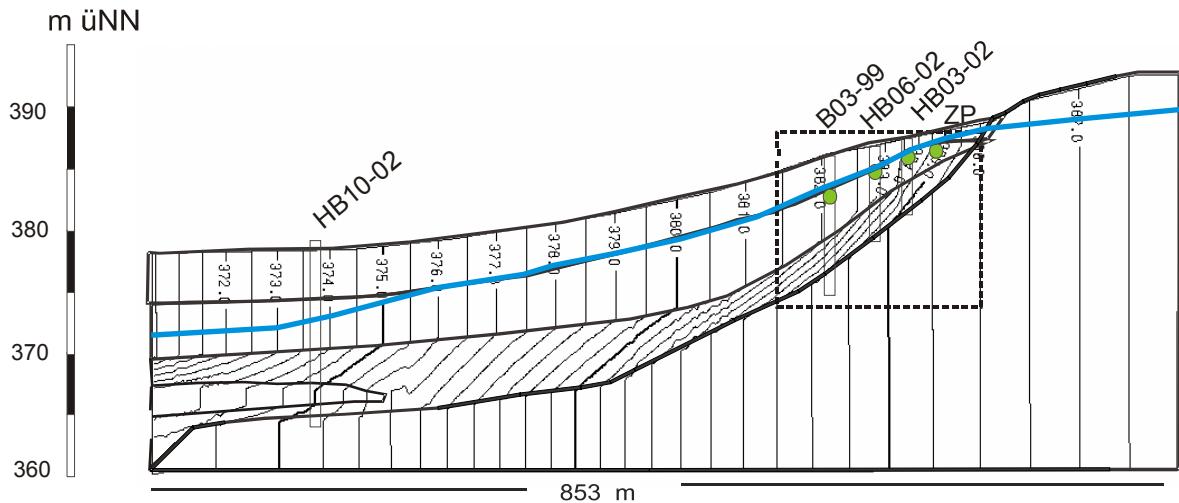
Fig. 87: Isolines of the calculated ground water pressure level for a moderate upstream down to the present day [390 m a.s.l., vertical exaggeration: 10x]; blue= ground water pressure level
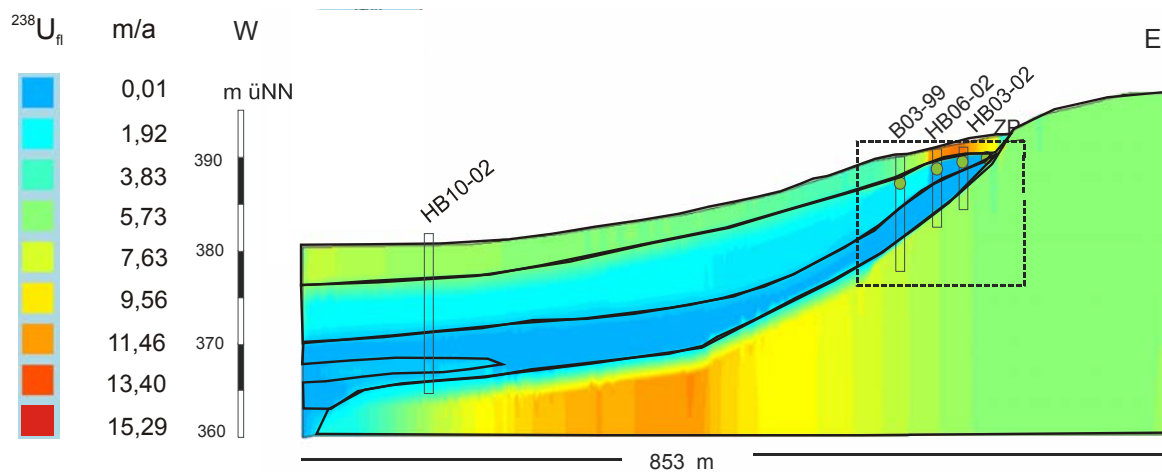
Fig. 88: Calculated groundwater velocity for a moderate upstream under present conditions [390 m a.s.l., vertical exaggeration: 10x].

The flow modelling does not show considerable changes of the flow field under increased upstream flow conditions (Scenario 2). Only an adjustment of the isolines to the set levelling can be noticed.

7.3.4.2 Transport modeling

Calculation of the Uranium enrichment

Scenario 1

Calculations based on the first run (RL 1) with adopted, more realistic maximum concentration C_{max} of 1.0 ppb in the Tertiary rim, in combination with slightly increased uranium concentrations in the inflow of 1.5 ppb, show a continuous uranium fixation in the sediment. In this case, after 800 ky max. 1557 ppm ^{238}U is enriched in the sediments of the Tertiary rim. In the four observation points the concentrations of the irreversible bound uranium phase vary between 509 and 910 ppm (Table 48).

The transport calculations of a continuous uranium input with today's uranium concentration of 1 ppb in the groundwater only makes sense if the adopted maximum concentration C_{max} of 1,0 ppb in the Tertiary rim is brought down to a value below 1 (in this case to 0,6 ppb). Otherwise, the C_{max}-concentration will never be achieved and a formation of the solid uranium phase would not occur. Based on this fact the transport calculations RL 2 show maximum $^{238}U_s$-concentrations in the sediment of 720 ppm. The values at the observation points vary between 208 and 365°ppm $^{238}U_s$.

Table 48: Concentrations of the irreversibly bound uranium $^{238}U_s$ [ppm] and sorbed uranium phase ($^{238}U_{ad}$) [ppm] in the observation points for the different runs (RL) after a continuous uranium input over 800 ky

Observation Point RL	B03-99 $^{238}U_s$	$^{238}U_{ad}$	HB06-02 $^{238}U_s$	$^{238}U_{ad}$	HB03-02 $^{238}U_s$	$^{238}U_{ad}$	ZB $^{238}U_s$	$^{238}U_{ad}$
RL 1	509	0.17	650	0.18	820	0.19	910	0.20
RL 2	208	0.07	264	0.09	333	0.11	365	0.12

The model results in Table 48 show that uranium predominantly exists as irreversibly bound uranium. The concentration of the equilibrium sorbed, hence easy to remobilise uranium U_{ad} varies between 0.07 ppm in RL and 0.20 ppm in RL 1 and amounts to a maximum of 0.04 % of the uranium fixation.
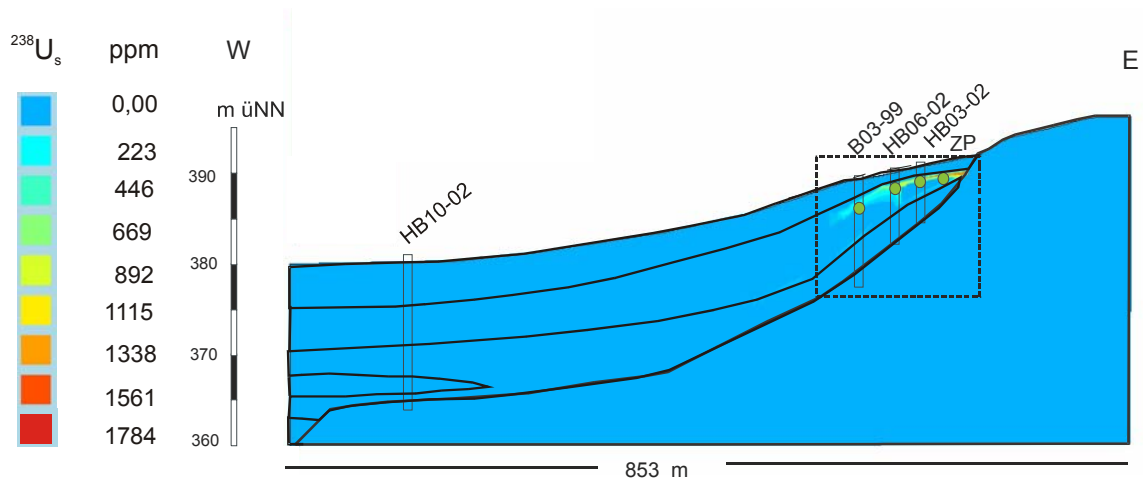
Fig. 89: Concentration of the irreversibly bound uranium $^{238}U_s$ (RL 1) after a continuous uranium input over 800 ky (vertical exaggeration: 10x)

Fig. 89 shows that the main proportion of the irreversibly-bound uranium in the Tertiary rim is narrowly distributed alongside the interface of the overlying Tertiary / lignite horizon. The ground water inflow and consequently the uranium transport within the overlying Tertiary, is limited to the first 150 m of the Tertiary rim edge.

The model calculations show a formation up to 389 ppm of irreversibly bound ^{238}U in the lower part of the lignite horizon. This is due to - beside the main input via the overlying Tertiary - uranium diffusion via the clay horizon leading ot concentrations higher than C_{max} and thereby uranium fixation at the basement of the lignite layer.

The calculated concentrations of the irreversible bound uranium phase in RL 1 are in the range of the actual verified uranium enrichment in the sediment. The model calculations of RL 2 do not achieve these concentrations. In this case the calculations result in a reduced uranium concentration of 500 ppm in average.

In order to accumulate a sufficient extent of uranium over time, an input concentration of 1.0 ppb, as it is observed in Keuper-ground water at present, is not sufficient. Among the selected model parameters, a slightly increased uranium concentration in the inflow water of 1.5 ppb is required, to reach the actual uranium enrichment by this scenario.

Scenario 2

The calculated concentrations of the irreversibly bound uranium phases [ppm] for the four observation points of all runs (RL) of Scenario 2, are listed in Table 49.

140

The results show that groundwater containing dissolved uranium over the first 1'000 years leads to uranium concentrations in the sediment that correspond with present conditions. This model option (as highlighted in Tab 6) is referred to in the following as a reference and presented in detail.

The uranium upstream concentration of 30 ppb corresponds with values observed in natural oxidising groundwaters. Investigations on groundwater samples e.g. from Marocco /HAK 01/ show uranium concentrations of up to 25 ppb.

For the reference case, Fig. 90 shows the dissolved $^{238}U_{fl}$ concentration in the groundwater at different points in time during the interglacial period of 20'000 y. The scaling of the colours in various pictures was adjusted to the relevant concentrations, in order to illustrate smaller concentrations.

Table 49: Concentration of the irreversibly bound uranium $^{238}U_s$ and sorbed uranium phase $^{238}U_{ad}$ [ppm] at the observatiuon points for Scenario 2 after five melt water inputs

Observation point / RL	B03-99		HB06-02		HB03-02		ZB	
	$^{238}U_s$	$^{238}U_{ad}$	$^{238}U_s$	$^{238}U_{ad}$	$^{238}U_s$	$^{238}U_{ad}$	$^{238}U_s$	$^{238}U_{ad}$
RL 3: 5 ppb	98	0.13	157	0.15	249	0.15	322	0.13
RL 4: 10 ppb	175	0.13	294	0.15	475	0.15	698	0.13
RL 5: 20 ppb	369	0.13	557	0.15	903	0.15	1382	0.13
RL 6: 30 ppb	**511**	0.13	**778**	0.15	**1307**	0.15	**1925**	0.13
RL 7: 50 ppb	877	0.13	1404	0.15	2319	0.15	3247	0.13
RL 8: C_{max} decreased	570	0.06	898	0.08	1930	0.09	2867	0.09
RL 9: C_{max}increased	518	1.19	830	0.18	1333	0.18	1826	0.16
RL 10: Precipitation rate decreased	672	0.13	204	0.15	224	0.16	286	0.17

RL = Run; marked red= Reference

After the phase with increased uranium inflow concentration ended (after 1'000 y), in addition to the Keuper-sandstone also parts of the overlying Tertiary at the Tertiary rim show an uranium concentration of 30 ppb $^{238}U_{fl}$. The uranium input is limited to the first 150 m of the Tertiary rim, according to the flow field. A rapid transport of the

groundwater with increased uranium concentrations via the overlying Tertiary beyond the left model edge is not observed.
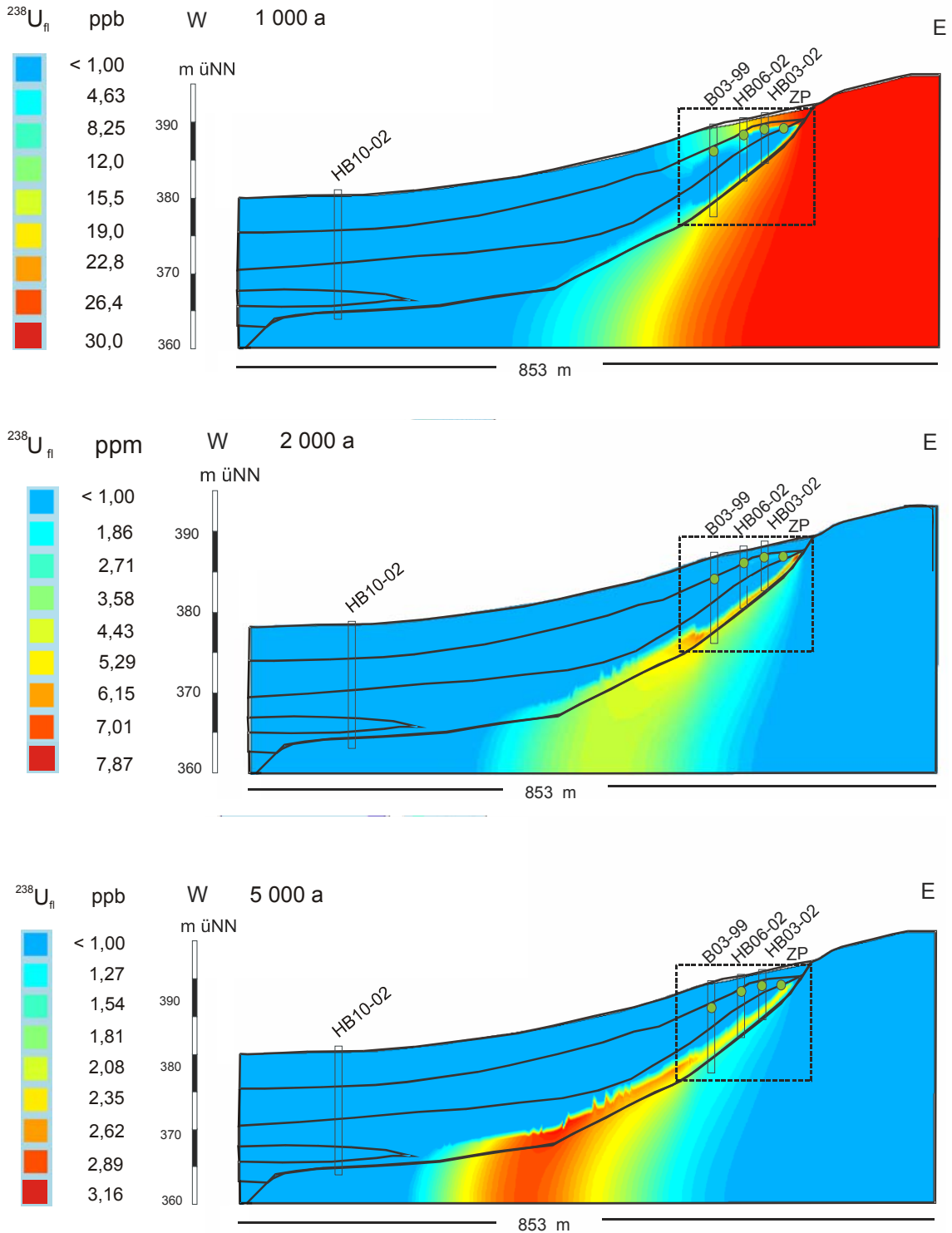
Fig. 90: The $^{238}U_{fl}$-phase of the reference (RL 7) at different points in time during an interglacial period (vertical exaggeration: 10x) [follow up next page]
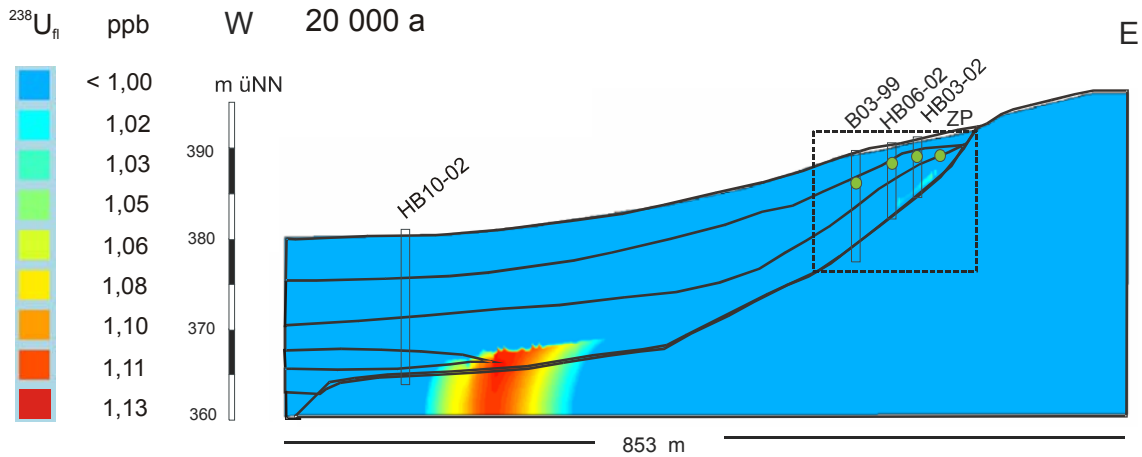
Fig. 90 (cont.): The $238U_{fl}$-phase of the reference (RL 7) at different points in time during an interglacial period (vertical exaggeration: 10x)

After 2'000 years the uranium concentration in the groundwater of the overlying Tertiary and the upper area of the lignite horizon is decreased to a maximum of 1.8 ppb, due to the dilution by the groundwater with the background concentration of 1 ppb. After 5'000 y, no increased uranium concentrations in these ground waters are to be found any longer.

Within the subordinated clay horizon uranium concentrations are elevated for a longer time due to its very low permeability. After 2'000 years 7 ppb, after 5'000 years still 2-3 ppb $^{238}U_{fl}$ exist there. By the end of an interglacial period after 20'000 years only small increase in the order of up to 1.1 ppb is found.

The calculated irreversibly bound uranium phase $^{238}U_s$ is formed as in Scenario 1, narrow shaped along the interface of the overlying Tertiary / lignite horizon and varies at the Tertiary rim with max. 743 ppm per melt water inflow, which corresponds to maximum accumulated immobile uranium concentration of 3'715 ppm, assuming 5 interglacial inputs into the sediment (Fig. 91).

While modelling the shorter periods of 20'000 years in Scenario 2, no irreversibly bound uranium phase at the lower lignite horizon area is formed compared with Scenario 1.

Assuming five interglacials the values of the uranium concentrations at the observation points as well as the shape of the uranium enriched zone correspond with the

143

conditions found at the site. However, a comparison of the uranium concentrations calculated at the observation points with the analytically determined uranium concentrations of single sediment samples (Table 50) results in slight discrepancies.
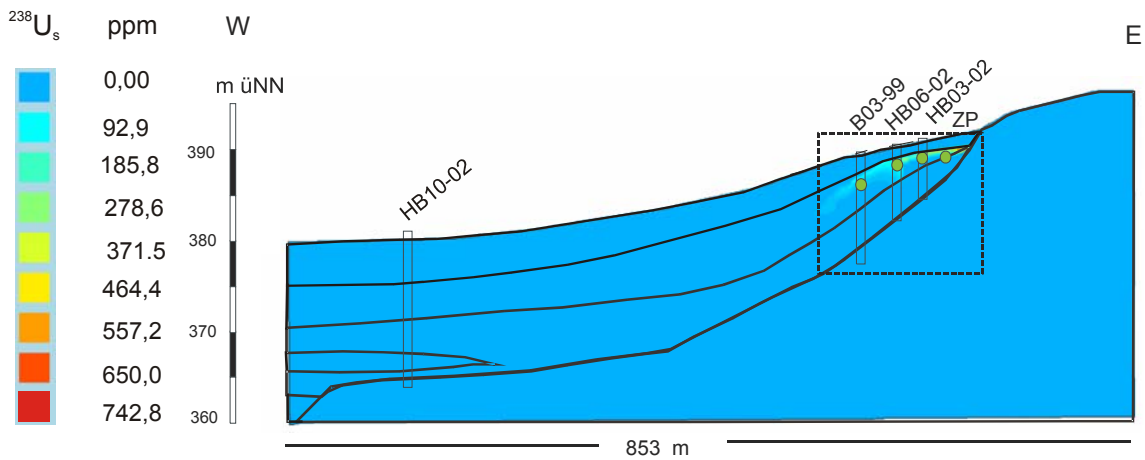
Fig. 91: $^{238}U_s$-phase of the reference (RL 6) after an uranium input over 20'000 y (vertical exaggeration: 10x)

Table 50: Comparison of the maximum analytically determined uranium concentrations [ppm] in sediment samples with calculated uranium concentrations in the observation points for the reference case

	B03-99	HB06-02	HB03-02
Calculated	511	778	1307
Observed	292	767	738

Borehole B03-99 shows signifcant lower uranium concentrations in the sediment than were calculated in the transport calculation (Table 50). Whilst in the reference case the uranium concentrations of borehole HB06-02 is in good agreement, the calculated uranium concentrations in borehole HB06-02 seem too high by some 100 ppm.

It is to be noted, that the highest uranium concentration within the sediments was not observed directly at the Tertiary rim, but in a sample from borehole HB11-03. This borehole is some 10 meters away from the actual rim and shows a higher uranium concentration in the sediment by more than 300 ppm, compared with borehole HB03-02, which is localised further from the rim edge.

144

A linear dip of the uranium content towards the rim centre, as calculated in the model is not realistic. Possibly the high uranium content within the rim area is due to groundwater and uranium input from different directions. An additional ground water flow into the Tertiary rim from the southerly Keupersporn would be possible in this regard.

Ground water inflow from different directions cannot be considered in a 2D-modelling. Therefore detailed knowledge of the side flow pathways in the vicinity of the model area and a 3D-modelling of the rim system would be necessary.

Sensitivity analysis

The effects regarding the calculation results of the variations of the upstream flow concentrations of the maximum uranium concentration C_{max} and the precipitation rate are demonstrated in Fig. 92 for every observation point. As basis, the calculated results from the reference are defined. Variations from the reference case are shown respectively by means of calculated uranium concentration as differences in ppm.
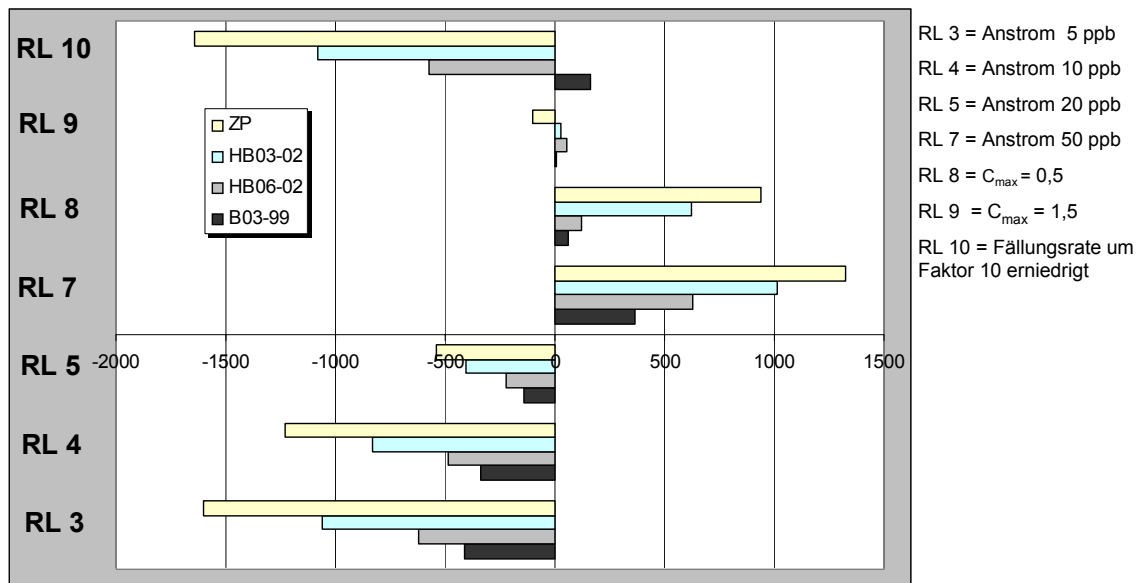
Fig. 92: Deviations of the calculated uranium concentration [ppm] from the reference

Compared with the calculated uranium contents of the reference, much lower uranium concentrations result with variations between 142 and 1'603 ppm (28-83 %), with an uranium upstream flow concentration of 5, 10 and 20 ppb (RL 3 to RL 5), respectively. Assuming an uranium upstream flow concentration of 50 ppb (RL 7) much higher uranium contents of up to 1'322 ppm (69%) compared to the reference occur.

These high variations between the single runs demonstrate the strong influence of the uranium concentration as a fixed boundary condition, on the extent of the irreversible bound uranium phase. With a decrease in the maximum uranium concentration C_{max} (RL 8) the calculated results differ from the reference especially in the area of the Tertiary rim. While the uranium concentrations in the observation points HB03-02 and ZP are 48 respectively 49 % above the values calculated in the reference, the variation in the further basin area is only at max. + 15 %. The majority of the uranium input is determined at an early stage and does not reach far downstream sediments.

Relatively low variations in percent from the reference case (-5 to +6.7 %) occur for the increase of the maximum uranium concentration C_{max} in the Tertiary by + 0.5 ppb to 1.5 ppb. The irreversibly bound uranium concentration calculated in RL 9 lies, as expected, below the values calculated in the reference, at the observation point ZP.

In the gradient of the flow direction the model calcuations for the three remaining observation points show a slightly increased $^{238}U_s$-concentration compared with the reference. This effect could be due to the dissolved uranium concentration in the groundwater reaching the uranium concentration C_{max} at the Tertiary rim at a later stage and the dissolved uranium reaches into rear areas before it is detracted from the groundwater.

From Fig. 92 and Fig. 93 it becomes apparent that the decrease of precipitation rate by factor 10 (RL 10) also exerts an influence as well on the extent as on the expansion of the uranium concentration. While up to 85 % less uranium is fixed at the direct Tertiary rim edge, an increased uranium input at the rear rim section (observation point B03-99) is noticed. Analogous to RL 9 this example shows that by the slowed reaction, a migration of the mobile uranium phase $^{238}U_{fl}$ according to the flow field in the rear rim section, is possible.
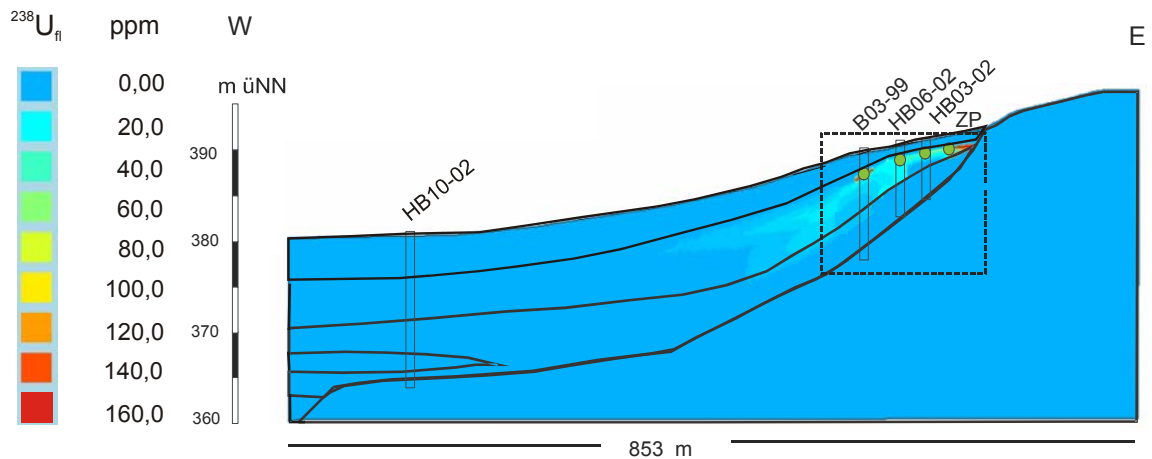
Fig. 93: $^{238}U_s$-phase (RL 10) after an uranium input over 20'000 y (vertical exaggeration: 10x).

Per melt water input, the irreversibly bound uranium phase in this run reaches concentrations of max. 570 ppm. This corresponds with an over 5 interglacial periods accumulated $^{238}U_s$-phase of 2'850 ppm, compared with the 3'715 ppm as in the reference. Furthermore, in comparison to the reference, the irreversibly bound uranium phase extends almost constantly along a profile of up to a length of approximately 300 m. Thus, the uranium enrichment reaches twice as much the expansion of the reference case.

In conclusion it can be summarised that changes in the upstream flow concentrations have a significant influence on the extent of the uranium accumulation. Changes in the precipitation rate affect especially the shape of the uranium distribution. Changes of the maximum uranium concentration in the Tertiary sediments C_{max} mainly cause changes in uranium content at the Tertiary rim edge.

7.3.5   Summary of the model results

Main objective of the modelling was to check whether the assumed scenarios can explain the amount and shape of the uranium enrichment at Heselbach site. Even if great uncertainties regarding the boundary conditions exist, the location as well as topology and the concentration of the identified uranium enrichment could be followed under consideration of plausible parameters and by means of 2D vertical models.

Both uranium transport scenarios reached dimension of uranium concentration within the Tertiary rim which are consistent with the recent observed contents in these sediments. The model calculations confirm the idea that uranium could have reached the Tertiary rim epigenetically either continuously or periodically over several interglacial events.

The transport calculations show, that the main part of the uranium dissolved in the Keuper-groundwater is transported below the Tertiary rim. A small part reaches the Tertiary rim via the overlying Tertiary and is distributed from there along a length of about 150 m. The transported uranium is effectively enriched by the Tertiary lignite horizon. This can be noted from the rapid decrease of the uranium content in the sediment within the first 150 m apart from the rim edge.

Furthermore the model calculations for Scenario 1 prove that beside the dominant advective transport via the overlying Tertiary, in case of a continuous uranium inflow also diffusion processes via the "Liegendton" into the lignite horizon can be responsible for the formation of irreversible bound uranium at the bottom lignite horizon area. However, altogether the calculated uranium concentrations lie below the actual proven uranium concentrations in the sediment, in the case of today's inflow concentrations. That means, that a continuous input based on the requirements from today can not explain the proven uranium enrichment. Therefore an increase of the uranium inflow by 0.5 ppb to continuous 1.5 ppb is necessary.

In the transport calculations the interglacial periods that consider a period of 20'000 years, the advective transport via the overlying Tertiary is dominant and significant for the distribution of the immobile uranium concentration. The back-diffusion of the input uranium from the clay into the Keuper-sandstone in combination with the rapid, advective evacuation, does not lead to an irreversible uranium phase in the bottom lignite area.

The calculated uranium concentrations and distributions for Scenario 2 reflect the conditions of the examined area quite well. The best conformity of the actual measurement data is achieved by the model of a periodical uranium inflow concentration of 30 ppb, which corresponds with an actual uranium concentration in the groundwater under strongly oxidized milieu conditions.

In connection with the analyses of the experimentally calculated data, the transport calculation presented in Scenario 2 is to be seen as the more probable scenario. A periodical uranium input is consistent with the analysed $^{234}U/^{238}U$-activity ratios within the Keuper-sediments. This input considers the variations of the chemical conditions within the Quaternary caused by climatic changes, in form of the increased uranium contents in the groundwater.

A constant concentration of the mobile uranium in the groundwater over a longer period as assumed in Scenario 1, only reaches a realistic high uranium input under the assumption that a higher uranium background concentration was present in the past. In addition to the fact, that increased uranium concentration is less likely in periods of moderate upstream, it also cannot be assumed that a continuous groundwater flow and therefore an advective transport during permafrost periods took place.

8   Summarised results

The investigation of the Heselbach site (Bavaria) described in this report has been performed by Gesellschaft für Anlagen- und Reaktorsicherheit (GRS) mbH in co-operation with the Technical University of Braunschweig. The aim of the investigations was to verify the suitability of the site, assumed so far, as "natural analogue for radionuclide migration in the far field of a repository" and to assess the suitability after site evaluation. For this purpose, geology, hydrology, hydrogeology and radiochemistry of the location, in particular of the uranium-containing Tertiary layers, were investigated in detail. After integration of all data, Heselbach site can be characterised as follows:

The investigation area is divided into two subbasins. Distinction is to be made between the branches of the Tertiary basin located south and north of the interstate road B85 that are separated by a Keuper spur extending into the investigation area. While in the southern part uranium-containing sediments ceased to exist due to anthropogenic excavation and backfill, near-surface uranium-containing sediments were drilled in the northern part. In this N subbasin, the 'main interbedded clay' (at the margins) or backfill material from surface mining (apart from the margins) seal the structure of the Tertiary basin towards the deeper basement. The upper seam deposited in the Upper Miocene and locally conserved at some outermost parts of the Tertiary rim (e.g. Heselbach), is covered by sandy/silty sediments of the overlying Tertiary.

The double-peak distribution of the uranium within the Tertiary rim sediments, already known from previous exploration drills, was confirmed by means of new drillings. Altogether maximum uranium concentrations of 1'128 ppm in the lignitic horizon and 724 ppm in the underlying interbedded clay were determined. But due to strong heterogeneity of the sediments, the uranium content varies significantly within single horizons with only few centimetres thickness.

The highest uranium values were measured in well HB11-03. This well is located at the transition from the Keuper to the Tertiary basin and characterised by a strongly argillised residual seam with a thickness of 0.9 m. Altogether, the uranium concentrations in the sediments decrease towards the centre of the basin. According to the location of the uranium enrichments, transport by groundwater from the Keuper into the Tertiary basin from E or S has to be considered.

For the Keuper aquifer, hydrogeological investigations at the site showed a hydraulic conductivity of about $1.54 \cdot 10^{-5}$ m/s. Thus, Keuper sediments represent the geological formation with the highest hydraulic conductivity in the investigation area. The sediments of the Tertiary basin and the relocated backfill material are less permeable (k_f-values between $3.15 \cdot 10^{-06}$ to $2.9 \cdot 10^{-9}$ m/s). This also becomes evident by the extremely low flow velocities within the Tertiary basin. A tracer test even showed stagnant groundwater conditions for the lignite horizon of the Tertiary basin. Tritium data of the drillings (20.6 TU) are evidence that a large part of the water originates from the 1970's. The assumption of lignite horizon being a second groundwater aquifer supplied by the Keuper sandstone can thus not be confirmed. Further, the evaluations of stable isotope analyses show a clear signature difference between waters of the Keuper and the Tertiary rim. In groundwater samples of the downstream area, however, admixture with Keuper isotope signature was identified which indicates a connection of the upstream and downstream area below the Tertiary.

The uranium phases were characterised by different methods. Evaluations of autoradiographies show an evenly fine distribution within the sediment. Analyses with a scanning electron microscope did not reveal any particular uranium enrichment or uranium minerals.

The results of the sequential extractions from sediments argue against adsorption as main enrichment process for uranium. Further, it was not confirmed that uranium was bound to iron and manganese oxide hydroxides, which first was considered as significant bond form. The results of the sequential extraction rather indicate an association of the major uranium fraction with organic phase.

A clear result was achieved by analyses on the uranium valence within the sediments: uranium occurs to more than 99 % in the form of U(VI). This result is also confirmed by the spectroscopic investigations. Typical uranium-oxygen bond lengths, as they normally exist in uranyl ions, were identified. For Heselbach, this result implies that a reduction of U(VI) to U(IV) and formation of secondary tetravalent uranium minerals can be excluded as enrichment process. Further, thermodynamic calculations showed no existence range in which secondary, crystalline U(VI) phases are stable. For these reasons, an association of the uranium with organic matter (see above), in particular humic acids, is regarded as most probable bond form. In literature, a positioning of the uranyl ions onto ion exchange sites of humic acids is known for quite a long time. In early diagenetic sediments, such as peat and lignite, von Borstel /VBO 84/ verified

correlations of U(VI) with functional groups of the humic acids with, in the course of diagenesis, increasingly lose importance. For a slightly acid environment, as it exists in the Heselbach sediments, is to be assumed that uranyl ions are bound to carboxylate groups of the humic acids.

Conceptual model for uranium transport

The $^{234}U/^{238}U$ and $^{230}Th/^{23}4U$ activity ratios indicate that the uranium input into the Tertiary basin is a more or less recent process. The dating of uranium enrichment by means of activity disequilibria proved an uranium deposition in the lignite and clay layers during the past 40'000 to 300'000 years. In this respect, the possibility is to be taken into account that this result may also be achieved by a combination of older uranium with very young uranium input.

Low $^{234}U/^{238}U$ activity ratios of 0.75 in the Keuper sandstone show that uranium was only remobilised from the Keuper sandstone and transported away after a long fixation time. In light of this finding, the previous assumption that uranium was continuously transported into the Tertiary basin, seems not to be correct. In fact, special "events" are necessary for the release of uranium from the Keuper sandstone. In this context, a sudden change of the chemical environment and, as a consequence, oxidation and transport of uranium due to the influence of Quaternary meltwaters may be possible. The formation of enormous water masses during the warm periods of the ice age cycles might have caused an increased groundwater level and would have led, as model calculations show, to uranium input into the Tertiary basin via the overlying Tertiary. It is possible that during the warm periods uranium was transported into basin as uranyl ion $[UO2^{2+}]$ and formed uranyl humate complexes with the humic acids that are present there. Since it was verified for the Bodenwöhr basin that there were four to five ice ages within the last 800'000 years /TIL 56/, it can be assumed that there were also four to five phases of uranium input into the Tertiary basin. According to this theory, the episodically recurring uranium inputs into the Tertiary basin would have taken place between 10'000 and 800'000 years ago which is in good agreement with the activity ratios determined in the sediments.

The low groundwater level today does not lead to a dilution of Tertiary basin water via the overlying Tertiary but allows discharge of the Keuper groundwater below the basin. Further, due to low oxygen contents of 0.1 to 2 mg/l only small amounts of uranium (1 ppb) are in the groundwater. Thus, recent uranium input is not to be assumed.

Site assessment

For the assessment of the Heselbach site regarding its suitability as "natural analogue" for radionuclide migration in the far field of a repository, positive and negative aspects have to be weighed against each other.

The geological succession of the stratigraphic layers argues for an applicability of the results for performance assessment (PA) purposes. The Tertiary at the site consists of clayey and sandy sediments with interbedded lignite horizons. This succession is also found in the overburden layers of potential repositories (e. g. Gorleben). Further, the uranium enrichment is in the time range of 1 ma which is relevant for long-term safety analyses. The measured uranium content of the groundwaters also corresponds with the concentration generally assumed for the far field of a repository.

However, the investigations on the geological and, in particular, the hydrological conditions at the site showed that uranium enrichment had massively been superimposed and disturbed by anthropogenic influences. On the one hand, open pit mining over several decades influenced and changed landscape and groundwater conditions such that today's groundwater levels cannot simply be applied to earlier periods. On the other hand, the recently performed pavement work directly at the margin of the Tertiary basin leads to a change of the chemical environment. The surface water percolating through the overlying lime gravel increases the pH value of the groundwater and leads to a recent dissolution of the fixed uranium. Due to these recent changes caused by the nearness to the surface, the Heselbach site itself seems to be rather unsuitable as potential natural analogue in future but similar geological situations might exist in the vicinity (along the Tertiary basin's margin) which have not yet been detected or surveyed.

Investigations that yield new findings on the bond form of naturally bound uranium in lignite-rich sediments could make a valuable contribution to the research on radionuclide migration and enrichment processes. In this respect, the development of a sequential extraction method especially for uranium in lignites would be possible. Further, the identification and quantification of diffusion processes within the clay layers is an interesting area of research which could provide new findings about diffusion processes of uranium in natural sediments.

9 References

/AMT 01/ Amthauer, G., Pavicevic, M.K.(2001): Physikalisch-chemische Unter-suchungsmethoden in den Geowissenschaften, Band 2.- 262 pp.; Stuttgart, E. Schweizerbart'sche Verlagsbuchhandlung.

/BRA 02/ Brasser, Th., Noseck, U., Schönwiese, D. (2002): Uranium Migration in Argillaceous Sediments as Analogue for Transport Processes in the Far Field of Repositories (Heselbach Site, Germany).- in: Merkel, B.J., Planer-Friedrich, B, Wolkersdorfer, Ch (eds.): Uranium in the aquatic environment., pp. 139-146; Berlin, Springer.

/CHE 71/ Cherdynstev, V.V. (1971): Uranium-234.- Israel program for scientific translations [zitiert in /GER 00/].

/CLA 97/ Clark, I., Fritz, P. (1997): Environmental Isotopes in Hydrogeology.- 328 pp.; CRC Press LLC.

/DAR 04/ Dardenne, K., Denecke, M.A. (2004): Speciation of uranium in samples originating from uranium-rich horizons near Ruprechtov and Heselbach.- ANKA-Jahresbericht 2004, Karlsruhe.

/DIE 05/ Diersch, H.-J.G.: Reference Manual and White Papers, Vol. 1-3.- Feflow-Handbuch der Firma Wasy mbH, Berlin.

/DVW 96a/ Deutscher Verband für Wasserwirtschaft und Kulturbau DVWK (Ed.) (1996): Hydrochemische Stoffsysteme Teil I.- Schriftenreihe des Deutschen Verbandes für Wasserwirtschaft und Kulturbau e.V., Heft 110, 324 pp.; Bonn, Wirtschafts- und Verlagsgesellschaft Gas und Wasser mbH.

/DVW 96b/ Deutscher Verband für Wasserwirtschaft und Kulturbau DVWK (Ed.) (1996): Ermittlung der Verdunstung von Land- und Wasserflächen.- DVWK-Merkblätter, Heft 238, 134 pp.; Bonn, Wirtschafts- und Verlagsgesellschaft Gas und Wasser mbH.

/DYC 95/ Dyck, S., Peschke, G. (1995): Grundlagen der Hydrologie.- 3. Auflg., 536 pp.; Berlin, Verlag für Bauwesen.

/GEC 05/   Geckeis, H. (2005): Personal Communication (FZK-Institut für Nukleare Entsorgung), September 2005.

/HAK 01/   Hakam, O.K., Choukri, A., Reyss, J.L., Lferde, M. (2001): Determination and comparison of uranium and radium isotopes activities and activity ratios in samples from some natural water sources in Morocco.- J. of Env. Radioactivity 57, pp. 175-189.

/HEI 90/   Heim, D. (1990): Tone und Tonminerale: Grundlagen der Sedimentologie und Mineralogie.- 157 pp; Stuttgart, Enke.

/HOE 96/   Hölting, B. (1996): Hydrogeologie - Einführung in die Allgemeine und Angewandte Hydrogeologie.- 5 Aufl., 441 pp.; Stuttgart, Enke.

/HUE 94/   Hüttner, L. (1994): Wasser und Wasseruntersuchungen: Methodik, Theorie und Praxis chemisch-physikalischer, biologischer und bakteriologischer Untersuchungsverfahren.- 512 pp.; Frankfurt a.M., Salle.

/IVA 94/   Ivanovich, M. (1994): Uranium Series Disequilibrium: Concepts and Applications.- Radiochimica Acta, 64, pp. 81-84.

/KIN 87/   Kinzelbach, W. (1987): Numerische Methoden zur Modellierung des Transportes von Schadstoffen im Grundwasser.- Schriftenreihe gfw Wasser/Abwasser, Band 21, 317 pp., München et al., R. Oldenbourg.

/KIN 92/   Kinzelbach, W. (1992): Numerische Methoden zur Modellierung des Transportes von Schadstoffen im Grundwasser.- 343 pp.; München et al., Oldenbourg.

/KOR 94/   Korn, H. (1994): Geschichte der Wackersdorfer Braunkohle 1800-1982.- Heimatkundliche Schriftenreihe, Nr.1, 112 pp.; Amberg, Flierl-Druck.

/LAN 80/   Langguth, H.R., Voigt, R. (1980): Hydrogeologische Methoden.- 486 pp.; Heidelberg, Springer Verlag.

/MAT 03/   Matthess, G., Ubell, K. (2003): Lehrbuch der Hydrogeologie, Band 1: Allgemeine Hydrogeologie, Grundwasserhaushalt.- 2nd edition; 575 pp; Berlin-Stuttgart, Gebrüder Bornträger.

/MAT 94/   Matthes, G. (1994): Lehrbuch der Hydrogeologie, Band 2: Die Beschaffenheit des Grundwassers.- 3rd edition; 498 pp; Berlin-Stuttgart, Gebrüder Bornträger.

/MAZ 04/   Mazor, E. (2004): Chemical Isotopic Groundwater Hydrology.- 3rd edition, 453 pp.; New York, Marcel Dekker.

/MER 97/   Merkel, B., Hartsch, J., Pinka, F., Peters, H. (1997): Chemische Veränderungen nach Auflassen von Uranbergwerken unter besonderer Berücksichtigung von Radionukliden.- www.geo.tu-freiberg.de/~merkel/ gruflu.pdf.

/MEY 93/   Meyer, R.K.F., Mielke, H. (1993): Geologische Karte von Bayern 1:25'000 - Erläuterungen zum Blatt Nr. 6639 Wackersdorf.- 194 pp.; München, Bayerisches Geologisches Landesamt.

/MEY 98/   Meyer, R.K.F., Bauberger, W. (1998): Geologische Karte von Bayern 1:25'000 - Erläuterungen zum Blatt Nr. 6739 Bruck i. d. OPf.- 164 pp.; München, Bayerisches Geologisches Landesamt.

/MOS 80/   Moser, H., Rauert, W. (1980): Isotopenmethoden in der Hydrogeologie.- Lehrbuch der Hydrogeologie, Band 8, 400 pp.; Berlin-Stuttgart, Gebrüder Bornträger.

/NOS 02/   Noseck, U., Brasser, Th., Pohl, W. (2002): Tertiäre Sedimente als Barriere für die U-/Th-Migration im Fernfeld von Endlagern.- GRS 176, 295 pp.; Köln.

/OSM 83/   Osmond, J.K., Cowart, J.B., Ivanovich, M. (1983): Uranium Isotopic Disequilibrium in Ground water as an Indicator of Anomalies.- Int. J. Appl. Radiat. Isot., 34/1, pp. 283-308.

/PER 90/ Percival, J.B. (1990): Clay mineralogy, geochemistry and partitioning of uranium within the alteration halo of the Cigar Lake Uranium Deposit, Saskatchewan.- Dissertation; Ottawa, Carleton University.

/REE 96/ Reed, S.J.B. (1996): Electron microprobe analysis and scanning electron microscopy in geology.- 201 pp.; Cambridge University Press.

/REN 90/ Renger, M., Wessolek, G. (1990): Auswirkungen von Grundwasserabsenkung und Nutzungsänderung auf die Grundwasserneubildung.- Mitt. Inst. Für Wasserwesen, Universität der Bundeswehr München, Vol. 386, pp. 295-307.

/SCH 02/ Schönbuchner, H. (2002). Untersuchungen zu Mobilität und Boden-Pflanze-Transfer von Schwermetallen auf/in uranhaltigen Haldenböden.- Dissertation, 169 pp; Friedrich-Schiller-Universität Jena.

/SHE 06/ Shewchuk, J.R. (2006): http://www.cs.cmu.edu/~quake/triangle.html (11.09. 2006)

/SUK 05/ Suksi, J. (2005): Personal communication.- University of Helsinki, July 2005.

/TIL 54/ Tillmann, H., Kirschhock, E. (1954): Neuere Untersuchungen im Braunkohlen-Tertiär der Oberpfalz. 1.Teil Nord-, Ost- und Westfeld der Bayer. Braunkohlen- Industrie AG. Schwandorf.- Geologica Bavarica, Nr. 21; München, Bayer. Geologisches Landesamt.

/TIL 56/ Tillmann, H. (1956): Zur Geologie des Oberpfälzer Tertiärs und seiner Lagerstätten.- In: 50 Jahre BBI. Bayrische Braunkohlen Industrie AG, Schwandorf, pp. 109-127.

/VBO 84/ Von Borstel, D. (1984): Bindungsformen von Uran in kohligen Ablagerungen von Sedimenten unterschiedlicher Diagenesegrades.- 156 pp.; Dissertation TU-Clausthal.

/VOI 90/ Voigt, H.-J. (1990): Hydrogeochemie.- 310 pp. ; Berlin-Heidelberg, Springer.

/WEN 91/   Wendling, U., Schellin, H.-G., Thomä, M. (1991): Bereitstellung von täglichen Informationen zum Wasserhaushalt des Bodens für die Zwecke der agrar-meteorologischen Beratung.- Z. Meteorol. 41, pp. 468-475.

/ZEI 89/   Zeien, H., Brümmer, G.W. (1989): Chemische Extraktion zur Bestimmung von Schwermetallbindungsformen in Böden.- Mitteilgn. Dtsch. Bodenkundl. Gesellsch. 59 (1), pp. 505-509.

/ZIE 57/   Ziehr, H. (1957): Uranvorkommen in Bayern.- Die Atomwirtschaft 6, pp. 193-196.

/ZIE 61/   Ziehr, H. (1961): Uranhaltige Kohlen in Europa.- Glückauf, 97, pp. 1370-1383.

List of figures

162

164

List of tables